Misfolded cytosolic proteins are trafficked through the endoplasmic reticulum for degradation: the molecular and cellular mechanisms for the turnover of human NAT1 R64W and parkin R42P

A DISSERTATION
SUBMITTED TO THE FACULTY OF THE GRADUATE SCHOOL
OF THE UNIVERSITY OF MINNESOTA
BY

Fen Liu

IN PARTIAL FULFILLMENT OF THE REQUIREMENTS
FOR THE DEGREE OF
DOCTOR OF PHILOSOPHY

Kylie J. Walters, PhD
Advisor

April 2009

ACKNOWLEDGEMENTS

I owe sincere thanks to all those who offered me support and assistance during my graduate study. I would like to convey my deep gratitude and appreciation to my advisor, Dr. Kylie J. Walters, for her understanding and support in my efforts to pursue scientific goals and meanwhile enjoy the happiness of being a Mom. Her continuous encouragement and expert guidance are the major driving force to accomplish my study. Our novel finding on the mechanism of cytosolic protein quality control was inspired by her critical thinking and deep perception on biological sciences. Her infectious enthusiasm to science, scientific attitude and energetic working style will have great influence on my future scientific career.

A special thank you to my friend Dr. Naixia Zhang, who was not only helping me with the NMR spectroscopy and structure modeling, but also looking after my son when I had to work after hours. I really appreciate the conversation between us that cheered me up when I was down. I am grateful to Dr. Deanna M. Koepp for her instruction and help with the cellular experiments and the use of her cell culture facilities. I also want to extend my gratitude to Dr. Mark A. Sanders for his tremendous work on electron microscopy, Dr. Deborah A. Ferrington and Dr. Cheryl M. Ethen for their work on the Mass spectrometry, Dr. Patrick E. Hanna, Dr. Carston R. Wagner and Xin Zhou for the help with NAT kinetics assays, and Dr. Bala Medicherla and Dr. Yang Kang for the collaboration in some experiments.

I thank the members of my thesis committee, Dr. David D. Thomas, Dr. Anja-Katrin Bielinsky, Dr. Deanna M. Koepp and Dr. Sharon E. Murphy for their guidance, expertise and patience throughout my graduate study, especially for their valuable feedbacks and encouragement after each of my student seminar presentation, and for their time to review and comment on my dissertation.

I would like to thank all the members of the Walters Lab and other friends at the U, Dr. Naixia Zhang, Dr. Kang Yang, Dr. Xiang Chen, Dr. Qinghua Wang, Leah A. Randles, Aaron C. Ehlinger, Wei Zhang, Li Liu, to name only a few, who share all these days with me and make me feel less lonely in a foreign country. I am also indebted to Dr. Sean Conner at the U to provide the tet-off system, Dr. Edith Sim at the Oxford University for NAT1 antibody, and Dr. Paul Henning Jensen at the University of Aarhus, Denmark, for the neuroblastoma cell line stably expressing parkin. I would also like to express my gratitude to Dr. Carol H. and Wayne A. Pletcher who established the Pletcher Fellowship that supports female graduate students with financial need.

Dedication

This dissertation is dedicated to my grandparents, my husband and my lovely son George for their endless love and support.

ABSTRACT

Misfolded proteins are routinely produced in cells due to faulty protein synthesis or folding, or to environmental damage such as oxidative stress. Maintaining protein structural integrity is critical to cell viability and human health, as misfolded proteins often aggregate and disrupt vital cellular processes. Protein aggregation and the resulting cytotoxity are hallmarks of neurodegenerative diseases**.** To provide mechanistic insights into how aberrant cytoplasmic proteins are recognized and eliminated in mammalian cells, the proteolysis of naturally occurring human variants of arylamine N-acetyltransferase 1 (NAT1) and parkin were studied. NAT and parkin variants are associated with cancer and parkinsonism, respectively.

Initially, biophysical and biochemical characterization was done to unravel the unique properties that lead to the ubiquitination of NAT1 R64W variant. Data from multiple techniques including 2-dimensional nuclear magnetic resonance (NMR) spectroscopy, circular dichorism spectroscopy, dynamic light scattering, sedimentation velocity experiments, and enzyme kinetics analysis indicated that the arginine to tryptophan mutation does not disrupt NAT1 protein structure, thermal stability or enzymatic activity, but rather makes it aggregation prone. Indirect immunofluorescence indicated this NAT1 protein variant to form microaggegrates in cells that co-localize with ubiquitin. Altogether, these findings suggest an interplay between NAT1 R64W aggregation and its constitutive ubiquitination.

Studies were expanded to define the cellular pathway for the ubiquitination and degradation of misfolded cytosolic proteins. Human NAT1 R64W and parkin R42P were used as model substrates and studied via a variety of techniques, including confocal microscopy, cell fractionation, co-immunoprecipitation, mass spectrometry, protease protection, and immunogold electron microscopy. A novel pathway of protein quality control was revealed that involves the routing of

aberrant cytosolic proteins through the endoplasmic reticulum (ER). ER-associated protein degradation (ERAD) is typically used for the quality control of ER proteins. However, the data presented in this dissertation suggest that two unrelated structurally compromised cytosolic protein variants, human NAT1 R64W and parkin R42P, are recognized by the molecular chaperone Hsc70 in the cytosol, trafficked to the ER, where they are translocated into the lumen and later retro-translocated out of the ER for ubiquitination. Knockdown of a key ERAD component, p97, by RNAi results in inefficient degradation of ubiquitinated NAT1 R64W and the activation of autophagy and degradation by the lysosome. These observations indicate that the ER plays a broader role in protein quality control than previously anticipated and this study is expected to have significant impact in areas including protein quality control and ER transportation.

TABLE OF CONTENTS

	page
Acknowledgements	**i**
Dedication	**iii**
Abstract	**iv**
Table of Contents	**vi**
Lists of Table	**ix**
Lists of Figures	**x**
Introduction	**1**
Protein misfolding disorders	**1**
Overview of protein degradation	**4**
The ubiquitin-proteasome system (UPS)	**5**
Degradation by the proteasome at the endoplasmic reticulum (ERAD)	**9**
Degradation by the proteasome in the cytosol	**12**
Degradation by the autophagy / lysosomal pathway	**13**
Overview and novelty of the thesis research	**20**
Chapter 1. Human arylamine N-acetyltransferase 1 (NAT1) aggregation and constitutive ubiquitination	
Introduction	**22**
Although human NAT1 can be isolated from *E. coli*, its R64W variant is insoluble	**24**
Hamster NAT2 R64W retains its secondary structure but aggregates	**27**
Cooperative unfolding is lost for the hamster NAT2 R64W variant	**31**
Kinetic data reveals that the hamster NAT2 R64W variant is not catalytically compromised *in vitro*	**33**
Human NAT1 R64W forms microaggregates *in vivo*	**34**
A structural model of human NAT1 reveals R64 to reside at a peripheral location	**36**
Summary and Discussion	**38**

page

Chapter 2. Human NAT1 R64W is trafficked through the ER for degradation

Introduction 40

Constitutively ubiquitinated NAT1 is routed to the endoplasmic reticulum 41

NAT1 R64W enters the ER lumen, where it interacts with Bip 49

NAT1 R64W is retrotranslocated back to the cytosolic surface of the ER where it is ubiquitinated 60

Knock-down of p97, a key component of ERAD, interferes with the degradation of ubiquitinated NAT1 R64W 63

Human NAT1 R64W is recognized by Hsc70 69

Summary 74

Chapter 3. Like NAT1 R64W, parkin R42P is trafficked through ER for its degradation

Introduction 75

Parkin R42P is routed to the ER 76

Parkin R42P enters the ER lumen 79

Hsc70 recognizes aberrant parkin R42P protein, but not its truncated form 83

Summary 85

Summary and Discussion

The aggregation of human NAT1 R64W and its ubiquitination 86

A novel pathway of cytosolic protein quality control that involves trafficking through the ER lumen 87

ER, the hub coordinating autophagy and ubiquitin-proteasome system? 90

Protein misfolding is required for ER translocation and recognition by cytosolic molecular chaperones 92

How are misfolded cytosolic proteins transported into the ER lumen? 93

Conclusions 95

page

Materials and Methods

Preparation of recombinant human and hamster NAT variant proteins from *E.Coli* **96**

Spectroscopy **96**

Dynamic light scattering analysis **96**

Sedimentation velocity analysis **97**

Steady state kinetics analysis **97**

Cell culture, drug treatment and plasmid transfection **98**

Western blot and immunoprecipitation assays **99**

Indirect immunofluorescence microscopy **100**

ER enrichment by calcium chloride precipitation **102**

Protease protection assay **103**

Glycosylation assay **103**

RNA interference assay **103**

Mass spectrometry **104**

Immunogold electron microscopy **104**

Quantitation of probe density and analysis **105**

Colocalization analysis **106**

References **108**

LIST OF TABLES

	page
Table 1: Steady state kinetics data for acetylation of wild-type and R64W hamster NAT2 at 25°C, pH 7.0	**33**
Table 2. Summary of quantitative morphometric analysis of immunogold labeled NAT1 R64W and Bip in HeLa cells transfected with FLAG-NAT1	**55**
Table 3. Summary of mass spectrometry identification of proteins	**73**
Table 4. Summary of quantitative morphometric analysis of immunogold labeled parkin R42P and Bip in SH-SY5Y cells	**82**
Table 5. Antibody dilutions used in the experiments	**101**

LIST OF FIGURES

page

Figure 1. A. Schematic representation of protein ubiquitination cascade **7**

Figure 2. The schematic representation of protein quality control in the endoplasmic reticulum of yeast **11**

Figure 3. Schematic representation of three types of autophagy **15**

Figure 4. The schematic representation of the molecular events in autophagosome formation in mammals **18**

Figure 5. Hamster NAT2 variants mimic human NAT1 in the properties leading to their ubiquitination **26**

Figure 6. Hamster NAT2 R64W retains its secondary structure but aggregates **29**

Figure 7. Whereas wild-type hamster NAT2 unfolds cooperatively, the thermal denaturation profile of the R64W variant reflects that of an aggregated protein **32**

Figure 8. The R64W mutation causes human NAT1 (A) and hamster NAT 2 (B) to form microaggregates *in vivo* **35**

Figure 9. A model structure of human NAT1 illustrates the structural implications of the R64W mutation **37**

Figure 10. Over-expressed NAT1 R64W forms ubiquitinated aggregates and upon MG132 treatment accumulates at a perinuclear structure **43**

Figure 11. NAT1 R64W is ubiquitinated at the endoplasmic reticulum **47**

Figure 12. Proteasome interacts with human NAT1 R64W at both the ER membrane and the cytosol **48**

Figure 13. Protease protection assay indicates that NAT1 R64W is translocated into the ER lumen and ubiquitinated at the cytosolic surface of the ER **50**

page

Figure 14. Immunogold electron microscopy suggests that NAT1 R64W enters the ER lumen **52**

Figure 15. Quantitative morphometric analysis of HeLa cells transfected with NAT1 R64W demonstrated that this protein enters the ER lumen **54**

Figure 16. NAT1 R64W interacts with the ER luminal Hsp70 protein Bip **57**

Figure 17. Human NAT1 R64W is glycosylated in the ER when glycosylation sites were incorporated into its sequence **58**

Figure 18. NAT1 R64W is not shuttled to the ER through the autophagy pathway **59**

Figure 19. NAT1 R64W is trafficked into (A) and out of (B) the ER lumen **61**

Figure 20. Knockdown of p97 compromises the degradation of ubiquitinated NAT1 R64W **63**

Figure 21. p97 knockdown causes NAT1 R64W to accumulate in puncta that colocalizes with ubiquitin (upper panel), but not calnexin (lower panel) **64**

Figure 22. p97 knockdown causes NAT1 R64W to colocalize with autophagy marker LC3B **66**

Figure 23. p97 knockdown causes NAT1 R64W to partially colocalize with lysosome marker LAMP1 when treated with lysosome specific inhibitor chloroquine **67**

Figure 24. With normal p97 activity, NAT1 R64W puncta does not co-localize with the lysosomal marker LAMP1 or autophagy marker LC3B when lysosome activity is inhibited with chloroquine **68**

Figure 25. Hsc70 recognizes non-ubiquitinated NAT1 R64W in the cytosol **70**

Figure 26. Other molecular chaperons may play redundant role as Hsc70 **72**

Figure 27. A schematic model of how human NAT1 R64W is removed from cells **73**

page

Figure 28. The schematic representation of the domains in protein parkin **76**

Figure 29. parkin R42P is partially co-localized with ER marker calnexin **77**

Figure 30. Parkin R42P is ubiquitinated at the endoplasmic reticulum **78**

Figure 31. Parkin R42P is transported into the lumen of the endoplasmic reticulum **80**

Figure 32. Parkin R42P interacts with the ER luminal Hsp70 protein Bip in the ER **83**

Figure 33. Hsc70 recognizes parkin R42P that has a misfolded N-terminal domain **84**

Figure 34. Schematic model of how NAT1 R64W and parkin R42P are removed from cells **85**

Figure 35. Flowchart of the ER enrichment by calcium precipitation **102**

INTRODUCTION

Maintaining structural integrity is critical for proper protein function. Proteins lose their native structure as a consequence of production errors, inherited gene variations or environmental damage such as oxidative modifications[1], with an estimated 30% of all newly synthesized proteins recognized as non-productive and eliminated from cells within 30 minutes[2]. Even correctly synthesized proteins can fail to assemble properly when they are part of a larger protein complex or contain multiple transmembrane domains. Misfolded proteins usually have hydrophobic regions or inappropriate reactive elements exposed, which invite non-specific interactions with other proteins or the formation of protein aggregates that convey cytotoxicity.

The folding status of proteins is under strict surveillance by protein quality control (PQC) systems in cells, which include molecular chaperones and protein degradation machineries[3,4]. Molecular chaperones assist newly synthesized peptides in forming and maintaining functional structures. When proteins are trapped in misfolded conformations, they are recognized by molecular chaperones, which unfold the misfolded state or disassemble aggregates to promote refolding into the correct conformation[5]. Terminally misfolded proteins are eliminated through protein degradation mechanisms when refolding fails. In healthy cells, protein folding, aggregation and degradation are tightly regulated and strike a delicate balance, which is usually lost in malignant cells[6].

Protein misfolding disorders

Uncontrolled aggregation resulting from misfolding of a specific protein disrupts vital cellular processes such as transcription, microtubule transport, energy metabolism, or general folding homeostasis and hallmarks many neurodegenerative diseases. Such neurodegenerative diseases and other ailments that are associated with aberrant protein folding, aggregation or

unregulated degradation of a particular protein are collectively called protein misfolding disorders or protein conformational disorders[7,8].

The proper identification and removal of proteins with inappropriate structural and surface properties, which promote chronic aggregation, is critical to human health. Failure to eliminate such proteins can lead to overloading of molecular chaperones and formation of cytotoxic protein aggregates. These effects result in cell dysfunction and contribute to the gain-of-function pathogenesis of many protein misfolding diseases[7]. On the other hand, loss-of-function pathogenesis can arise from unregulated degradation of a particular protein[7] that is physiologically important. Many protein misfolding disorders show both loss- and gain-of-function pathogenesis, leading to diverse cellular and clinical consequences.

Some protein misfolding diseases, like cystic fibrosis and Fabry disease, are characterized by the elimination of an important protein due to its misfolding, which usually stems from intrinsic gene variations. For instance, cystic fibrosis (CF) is an autosomal recessive disease that is caused by mutations in the cystic fibrosis transmembrane-conductance regulator (CFTR)[9]. CFTR protein is a chloride ion channel important in mucus production. Deficiency in CFTR disturbs electrolyte transport across epithelial membranes, resulting in improper mucus buildup in the airway. CF is life-threatening usually due to lung failure. ΔF508 CFTR is the most common mutation among the thousands associated with CF[10]. This mutation produces a protein that fails to fold normally and therefore is degraded from cells prematurely[11].

Another class of protein misfolding diseases is characterized by the deposition of insoluble protein aggregates inside or outside of the cellular environment; Alzheimer's, Huntington's, Parkinson's, and prion diseases as well as amyotrophic lateral sclerosis fall into this category. Alzheimer's disease is associated with abnormal aggregation of β-amyloid and tau proteins in the brain[12], whereas Huntington's disease arises from aggregation of huntingtin

protein, which has a polyglutamine stretch at its N-terminus. The length of the N-terminal polyglutamine stretch decides the fate of this protein[13] as huntingtin with less than 36 glutamine expansions is competent for degradation by proteasome, whereas species with more accumulate as aggregates predominately in the cell nuclei[14]. Extended polyglutamine stretches are characteristic to at least ten other neurologic disorders[15]. Although the pathogenesis of Parkinson's disease is not yet fully understood, patients manifest accumulated α-synuclein in the cytosol of affected neuron cells[16]. α-synuclein is an unstable, aggregation-prone protein, and is naturally unfolded in its resting state, which is controlled by a protein quality control pathway[7]. Patients with inherited Parkinson's diseases usually have mutations that cause defects in the cell's ability to degrade α-synuclein.

Therefore, defects in protein quality control are most likely responsible for the pathogenesis of protein misfolding diseases. Many such diseases appear to arise from mutations that destabilize a particular protein and/or promote its aggregation, or mutations in the protein quality control pathways that disrupt the correct folding or clearance of proteins. However, for many patients, genetic mutations are not identified, but rather disease progression appears to associate with age and stress. A lot of neurodegenerative diseases are common in elderly people because the cells' abilities to cope with misfolded proteins decreases dramatically with age[7].

Besides protein misfolding disorders, other diseases, such as certain cancers and heart diseases, can also be a consequence of malfunction of protein degradation pathways. Protein function is highly regulated by synthesis and degradation at the appropriate time. Protein degradation, especially through the ubiquitin-proteasome pathway, plays a major role in regulating important cellular processes[17], such as gene transcription, cell cycle progression, cell signaling and apoptosis. In conclusion, protein quality control systems are physiologically important to human health and studies on the mechanisms of protein degradation might provide insights into new treatments for life-threatening diseases.

Overview of protein degradation

Protein degradation or proteolysis is the digestion of protein molecules into amino acids or smaller fragments through hydrolysis at peptide bonds by enzymes collectively called proteases. Depending on where the proteolysis events occur, protein degradation can be divided into three major categories, proteasomal degradation, lysosomal degradation, and other proteolysis events.

The ubiquitin-proteasomal system (UPS) is a major targeted protein degradation pathway that regulates various key cellular processes[17]. In eukaryotic cells, most proteins destined for degradation are first labeled with a polyubiquitin chain, which serves as a signal for recruitment to the 26S proteasome, which degrades protein substrates into small peptides. The 26S proteasome is a large protein complex that has three different protease activities.

The lysosome is a membrane bound organelle that contains digestive enzymes in its lumen, including various proteases, carbohydrases, lipases and nucleases. These hydrolases are only functional at acidic pH. The membrane of lysosome separates the acidic luminal environment from the rest of the cell, protecting cytosolic molecules from being digested. The acidic environment of lysosome can also help unfold the substrates and therefore promote their digestion. Lysosome can digest not only simple macromolecules like proteins, but also excess or worn-out organelles and engulfed viruses or bacteria through fusion with vacuoles.

Besides these two large protein degradation machineries, there are hundreds of other proteases inside or outside cells, performing important functions by degrading protein substrates. For example, proteases in the intestine digest proteins from food so that they can be absorbed and utilized. A lot of proteases play important regulatory roles by cleaving off a portion of pre-proteins to yield mature functioning conformations. For instance, insulin is initially produced as a proinsulin precursor. The central portion of proinsulin is cut off and

the C- and N-terminal ends of proinsulin are joined by a disulfide bond to yield the final insulin molecule[18]. Similar scenarios exist for the activation of the caspase cascade in apoptosis[19], cytokine maturation[20], and the activation of coagulation factors in coagulation.

The ubiquitin-proteasome and lysosome pathways are major components of protein quality control systems. Misfolded proteins are usually degraded through the ubiquitin-proteasome pathway. However, when this pathway becomes overloaded, large protein aggregates start to form, which are largely cleared from cells by the autophagy / lysosomal pathway.

The ubiquitin-proteasome system (UPS)

Ubiquitin is a small protein composed of 76 amino acids. It is highly conserved and ubiquitously expressed in all eukaryotes, probably because it plays very important functional roles through its conjugation to a wide range of protein targets, of which it modifies function and fate.

Protein ubiquitination is the post-translational modification of a protein by covalently attaching one ubiquitin moiety or a polyubiquitin chain to a lysine residue on the protein. As schematically shown in Figure 1A, the ubiquitination of a protein involves three sequential reactions catalyzed by a ubiquitin-activating enzyme (E1), a ubiquitin-conjugating enzyme (E2) and a ubiquitin-protein ligase (E3) (reviewed in [21]). E1 activates free ubiquitin by forming a thiol-ester bond between a cysteine on the E1 and the carbonyl group of ubiquitin's C-terminal glycine; this step requires ATP. The ubiquitin moiety is then transferred to E2, with which it forms a thiol-ester bond. E3 ligases bind both ubiquitin-conjugated E2s and cognate protein substrates to facilitate the transfer of ubiquitin from E2 enzymes to the protein substrate. Ubiquitin is attached to protein substrates via an isopeptide bond between ubiquitin's C-terminal carbonyl group and a lysine residue on the substrate. Depending on the specific E2/E3 pair, the ubiquitin will either form a thiol-ester bond with the E3 ligase before its transfer to the

substrate, as described for HECT domain containing E3s, or be transferred directly from the E2 conjugating enzyme to the substrate, as observed for RING and U-box domain containing E3s. The enzymatic cascade can be repeated to add an additional ubiquitin subunit to a lysine residue of the substrate-attached ubiquitin, leading to the formation of a polyubiquitin chain on the protein substrate. It is worth noting that ubiquitin belongs to a family of regulatory proteins that can be conjugated to other proteins to in turn modify their function. These include SUMO (sumoylation) and Nedd8 (neddylation)[22].

Proteins can be modified by ubiquitination in a variety ways for different physiological consequences[23]. Mono- or multiple-ubiquitination is the attachment of a single ubiquitin moiety to one or multiple lysine residues on the substrate; this modification regulates DNA repair and receptor endocytosis[24]. Polyubiquitination usually refers to the conjugation of a polyubiquitin chain variable in length or linkage type[23,25]. Ubiquitin has seven lysine residues and an N-terminus, each of which could potentially be used for chain elongation. The chain could be homotypic, using the same lysine in each ubiquitin for elongation of a linear chain, or of mixed-linkage, using different ubiquitin lysines to connect the subunits to yield either linear or branched chains[25]. Lysine-48 linked ubiquitin chains were the first identified and they direct protein substrates to the 26S proteasome for degradation. Other types of chain are collectively called atypical ubiquitin chains and distinct roles for chains of varying linkage are still being elucidated[23,26].

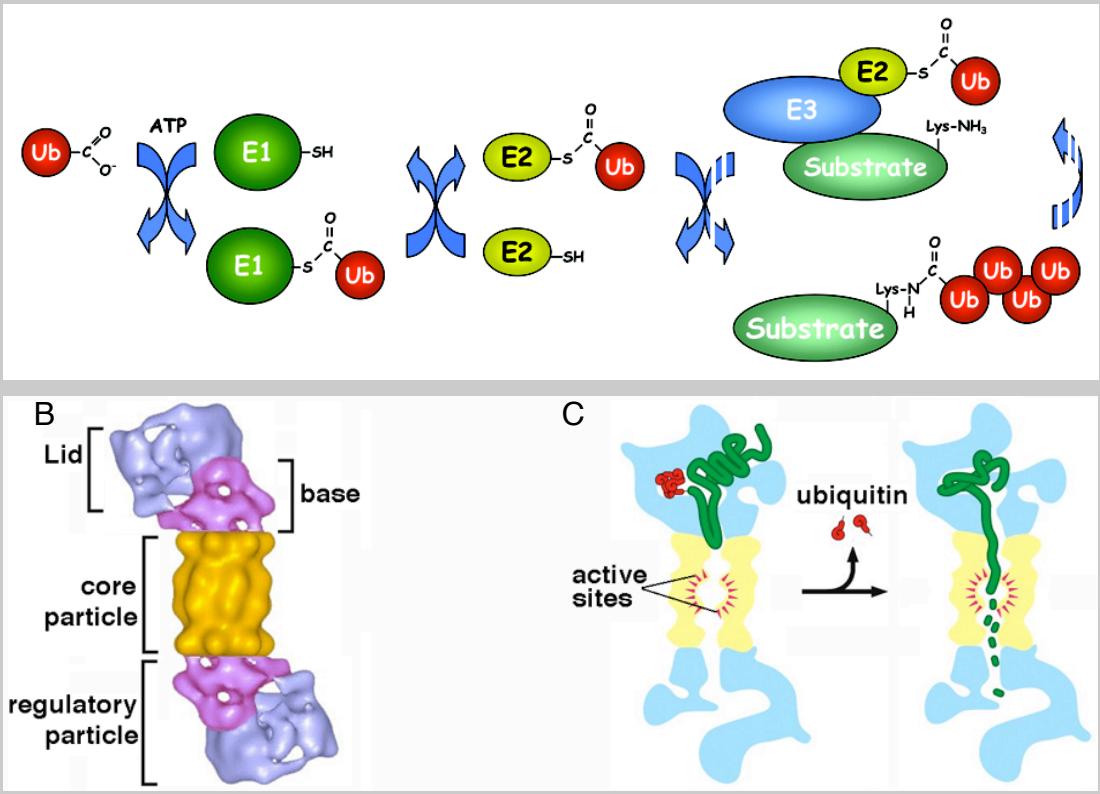

Figure 1. A. Schematic representation of protein ubiquitination cascade. Free ubiquitin (Ub) is activated by the ubiquitin-activating enzyme (E1), and then transferred to ubiquitin-conjugating enzyme (E2). Ubiquitin ligase (E3) can bind both the Ub-conjugated E2 and the protein substrate, transfering the ubiquitin moiety from E2 to the protein substrate. An active cysteine in the E1 or E2 forms a thiol-ester bond with the C-terminal carbonyl group of the ubiquitin in the first two steps, whereas an isopeptide bond is formed between this group and a lysine residue in the substrate. This process repeats to add additional ubiquitin to the lysine residue of the attached ubiquitin moiety, forming a polyubiquitin chain on the protein substrate, which serves as a signal to target the protein substrate to 26S proteasome for degradation. **B. Three-dimentional electron microscopy reconstruction of a yeast proteasome complex.** (Adapted from www.biw.kuleuven.be/dtp/cmpg/pgprb.htm). **C. Schematic representation of degradation by proteasome.** Polyubiquitin chain (red objects) is recognized by the regulatory particle of the 26S proteasome, which cleaves off the ubiquitin for recycle, unfolds the substrate and threads it into the core particle which harbors the active sites for cleavage of the peptide. (Adapted from Molecular Biology of the Cell 5/e © Garland Science 2008)

Degradation by the proteasome is a major degradation pathway in cells for removing misfolded proteins, and regulates key cellular processes from gene transcription to cell death through the regulated digestion of particular proteins[17]. The proteasome is composed of a core particle in which proteolysis occurs that is capped with one or more regulatory particles (Figure 1B). The most well known and studied regulatory particle is that with ubiquitin-binding activity, namely the 19S regulatory particles (RP)[27]. The RP contains ubiquitin receptors that recognize ubiquitin chains, deubiquitinating enzymes that disassemble and release ubiquitin chains into cytosol for recycling[28], and AAA-ATPases that unfold and passage the protein substrate into the core particle for proteolysis[29] (Figure 1C). In eukaryotes, the core particle consists of four stacked ring structures formed by 7 distinct subunits respectively[29]. The two inner rings form an interior chamber that harbors the protease active sites. The two outer rings serve as docking sites for 19S particles and form a gate that only allows unfolded peptide to enter. Unfolded proteins are digested into small peptides of about 7-8 amino acids long processively as they pass through the core particle[29] (Figure 1C); the peptides can be further digested into amino acids in the cytosol and used in protein synthesis.

The ubiquitin-mediated proteasomal degradation of a particular protein is highly regulated through controlled protein ubiquitination, which is largely determined by interactions between E2, E3 and the protein substrate[30]. Moreover, the type of linkage used for the chain may be largely determined by E2 and E3 pairs. An E3 ligase could be activated for a specific substrate through the formation of a correct complex[31], or through post-translational modification including phosphorylation, ubiquitination or neddylation[32], which might only occur under particular physiological conditions. On the other hand, a protein substrate may only be recognized by its E3 ligase after itself is modified by phosphorylation, oxidation or acetylation[30]. Alternatively, compromised protein structure may lead to recognition by molecular chaperones[33] before its

ubiquitination. Some proteins are ubiquitinated and degraded after the exposure of an unstable motif that is otherwise hiden, through the dissociation of a shielding subunit or the cleavage of one portion by a protease[34].

Degradation by the proteasome at the endoplasmic reticulum (ERAD)

Mechanistically, degradation by the proteasome is best understood for proteins that are naturally targeted to the endoplasmic reticulum (ER), and the pathway used for such proteins is called ER-associated degradation (ERAD). Briefly, the ERAD pathway represents a quality control process operating in the endoplasmic reticulum, where unfolded or unassembled proteins are selectively ubiquitinated at the ER membrane and degraded by the proteasome in the cytosol (reviewed in [35] and [36]). In principle, newly synthesized secretory or membrane proteins are transported into the ER through a protein channel named the translocon. Nascent polypeptides begin to fold with the assistance of chaperones residing in the ER lumen during import, and undergo glycosylation if glycosylation sites exist and are correctly recognized. Polypeptides that cannot properly fold in the ER lumen are identified, probably by specific chaperones, inserted into a transport channel, and then transported back into the cytosol through a process termed retrotranslocation or protein dislocation. During the dislocation of ERAD substrates, a polyubiquitin chain is attached onto the protein at the cytosolic surface of the ER membrane, a step requiring the action of membrane-bound E2 and E3 enzymes. In the final step of this process, the polyubiquitinated protein is degraded by proteasome either at the cytosolic surface of the ER membrane or in the cytosol (Figure 2).

It has been shown that in yeast, the participating molecular chaperones, ubiquitin conjugating enzymes and ubiquitin ligases of a particular ERAD substrate are determined by where the misfolded region of the protein substrate resides[37,38]. Luminal proteins and transmembrane proteins with a misfolded luminal domain are degraded by ERAD-L[38], which requires the E3 ligase Hrd1p

and its cofactors Hrd3p, Der1p, and Usa1p. Proteins with a misfolded transmembrane domain are degraded by ERAD-M[38], which is independent of Der1p and Usa1p. Membrane proteins with misfolded cytosolic domains are degraded by the ERAD-C pathway[38], which uses Doa10 as the ubiquitin ligase and needs the assistance from cytosolic chaprones.

The misfolded ERAD substrate has to be retro-translocated back into the cytosol for degradation since the components of the ubiquitin-proteasome system are located in the cytoplasm. N-glycan is the key determinant element to sort the glycosylated proteins to ERAD[39]. However, for non-glycosylated luminal proteins and integral membrane substrates, it is less clear how misfolded proteins are recognized and sorted to ERAD, except through the involvement of various chaperones[37,40]. Ubiquitination is important for retro-translocation since a minimal ubiquitin chain length is required for the export of substrates[41]. After the substrate is ubiquitinated at the cytosolic surface of the ER, retro-translocation is facilitated by the Cdc48/p97 complex[42]. Cdc48/p97 is a multi-functional, hexameric AAA-ATPase, which together with its cofactors binds to the ubiquitinated ERAD substrates and hydrolyzes ATP to provide the driving force to pull a peptide out of the lipid bilayer. ERAD substrates can however also be dislocated in a ubiquitin- and cdc48-independent manner[43], by use of the proteasome's 19S regulatory particles[43-46]. Since the 19S regulatory particle is composed of ubiquitin receptors and AAA-ATPases[47] and is abundant at the ER membrane[48], the proteasome may play a general role in extracting ERAD substrates. However, our current understanding of this role remains obscure. Some evidence suggests that retro-translocation and degradation of ERAD substrates may be uncoupled[46]; however, for some substrates functional proteasome is required for efficient extraction[45], as misfolded secretory proteins accumulate in the ER lumen due to the proteasome inhibition by specific inhibitors or proteasome mutants with deficient proteolytic subunits[45].

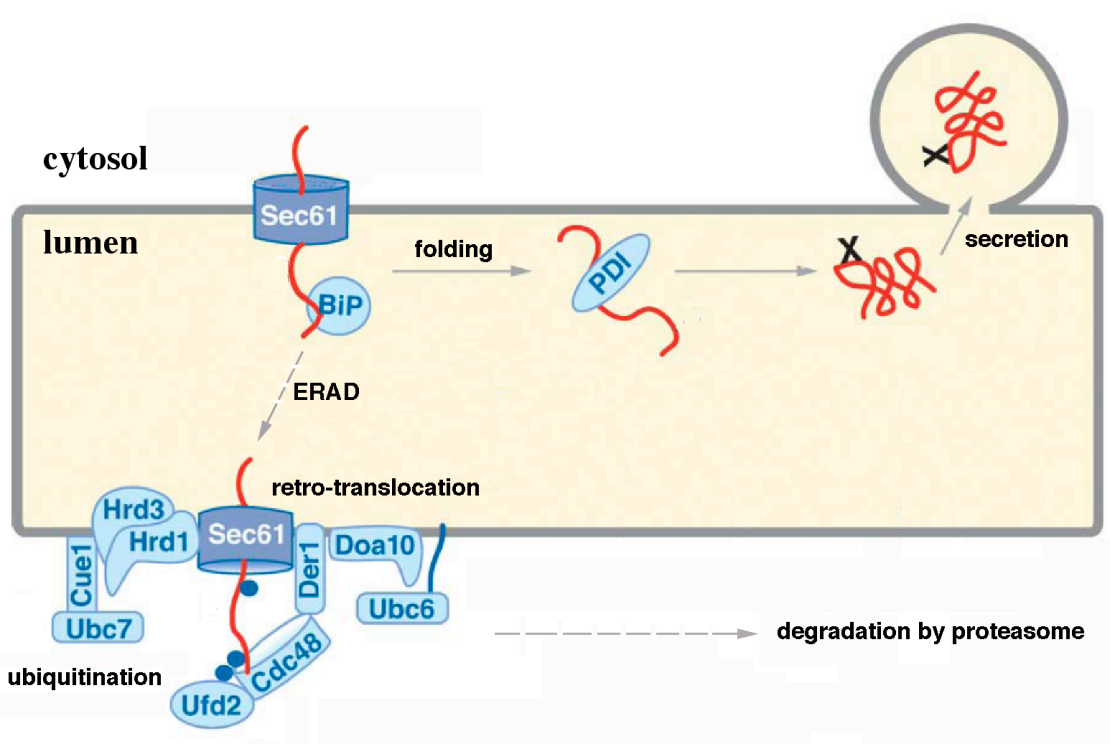

Figure 2. The schematic representation of protein quality control in the endoplasmic reticulum of yeast. Newly synthesized proteins are transported into ER lumen through the translocon composed of Sec61 complex. Proteins are either properly folded in the ER lumen with the help of molecular chaperones (Bip, PDI, etc.) and go through the secretory pathway, or remain improper folding and eliminated through the ERAD pathway. During ERAD, misfolded peptides are transported back into the cytosol through retrotranslocon (probably Sec61 complex), ubiquitinated at the cytosolic surface of the ER by ER associated E2s (ubc6/7) and E3s (Hrd1/3 complex or Doa10). Cdc48-ufd2 complex recognizes the polyubiquitinated substrate and pull it out of ER. Ubiquitin receptors in the cytosol may escort ERAD substrates to the proteasome for degradation. In some cases, ubiquitinated or un-modified ERAD substrates are dislocated and digested directly at the cytosolic surface by the ER-associated protesomes. The model is simplified by omitting the integral membrane substrates. (Figure modified from [36])

Degradation by the proteasome in the cytosol

Compared to ERAD, the mechanisms for quality control and proteasomal degradation of misfolded proteins in the cytosol are poorly defined. Recently, studies in budding yeast have made some progress in revealing how proteasomal degradation occurs for certain structurally compromised cytosolic proteins, but a general picture of cytosolic quality control remains obscure.

Cytosolic quality control relies on molecular chaperones. There are distinct molecular chaperone pathways in the cytosol that promote the proper folding of different proteins[49]. Chaperones aid protein folding by repeatedly binding and releasing from substrates with the consumption of ATP, holding the substrate in solution and preventing its aggregation. It is therefore easy to speculate that molecular chaperones participate in the triage decision and direct terminally misfolded protein to the ubiquitin-proteasome pathway for degradation. Recent studies support this hypothesis and find that molecular chaperones play an active and specific role in protein destruction that extends beyond a simple extension of their primary role in protein folding[50]. For example, some chaperones interact directly with components of the ubiquitin-proteasome pathway. Hsp70 and Hsp90 interact specifically with the U-box containing E3 ligase CHIP[33]. Moreover, chaperones that support protein folding are often distinct from those used for its destruction[50]. Hsp70 is required for both the folding and degradation of the von Hippel-Lindau (VHL) tumor suppressor protein, whereas the chaperonin TRiC is essential only for its folding and Hsp90 is required only for degradation[50]. It is worth mentioning that different protein substrates may require different chaperone machineries for folding or degradation and the rules defining the requirements are not yet understood.

Carboxypeptidase yscY (CPY) has served as a model substrate for studying ERAD and derivatives of this protein that lack an ER signaling sequence (ΔssCPY* and ΔssCPY*-GFP) have been useful for studying the degradation of misfolded cytosolic proteins. ΔssCPY* is defective for ER import and

accumulates as a misfolded cytosolic protein. Sae-Hun Park et.al. demonstrated that the cytosolic Hsp70 Ssa chaperone machinery and its co-chaperone Ydj1p are involved in the degradation of ΔssCPY* derivatives[51]. By contrast, Hsp90, Hsp104 and the small heat shock proteins Hsp26 and Hsp42 were found not to be involved in the degradation of these ER import-incompetent substrates[51]. This study also showed that the degradation was dependent on cytosolic E2s, Ubc4p and Ubc5p, but not the ER-associated E3 ligases Doa10p and Der3p[51].

However, the involvement of ER-localized ubiquitination machinery including Ubc6p, Ubc7p-Cue1p and Doa10p was demonstrated in the degradation of several cytosolic degron-protein fusions[52,53]. A degron is a specific peptide sequence that directs a protein for degradation. Those works have lead to a model in which these proteins are directed to the cytoplasmic surface of the ER membrane for ubiquitination prior to their degradation by the proteasome. These findings suggest that ER may serve as a platform for protein quality control.

Degradation by the autophagy / lysosome pathway

The lysosome is a dynamic digestive compartment in eukaryotic cells that consists of a heterogeneous group of acidic vesicles, which undergo constant fusion and division[54]. The lysosome can digest materials that are outside or inside of cells through endocytosis/phagocytosis or autophagy, respectively. The digestive enzymes in the lumen of the lysosome are produced in the endoplasmic reticulum and mature in the Golgi apparatus. They are transported from the Golgi network in the form of tiny transport vesicles, which fuse with other intracellular vacuolar structures, like late endosomes and autophagic vesicles (also called autophagosomes), and digest their contents[55]. After fusion with late endosomes, lysosomal hydrolases become activated and the lysosome lumen becomes acidic through the ATP-dependent action of membrane-associated proton pumps, which continuously passage protons from cytosol to the lumen.

Autophagy (self-eating) is the lysosomal pathway that degrades and recycles intracellular components including bulk cytoplasm, long-lived proteins and worn out organelles in all eukaryotes. Under starvation, autophagy is greatly enhanced to provide materials and energies that are necessary to maintain cell functions. Autophagy also serves as a mechanism to degrade aberrant and aggregated proteins when cells are overloaded with misfolded proteins[56]. It can also trigger apoptosis, and participates in cytosolic rearrangements that are essential for cell differentiation, proliferation or death during development[57]. Recent data suggest additional roles for autophagy in antigen processing and presentation[58].

Mechanistically, autophagy can be divided into three main forms: microautophagy, chaperone-mediated autophagy (CMA) and macroautophagy, (Figure 3). During microautophagy, cytosolic components are transferred into the lysosome lumen for degradation by direct invagination of a highly specialized part of lysosomal membrane[59,60] (Figure 3A). Microautophay is triggered by nutrition limitation and also used for maintaining organelle size and membrane composition as it is the direct uptake and degradation of boundary membrane. Topologically, microautophagy is different from other budding processes like endocytosis and the formation of transport vesicles between ER, Golgi apparatus and endosomes, which bud toward the cytosol[59], as the autophagic vesicles bud into the lysosomal lumen and away from the cytosolic environment. The molecular pathways controlling microautophagy remain elusive and hard to work on largely because it can only be characterized under electron microscope.

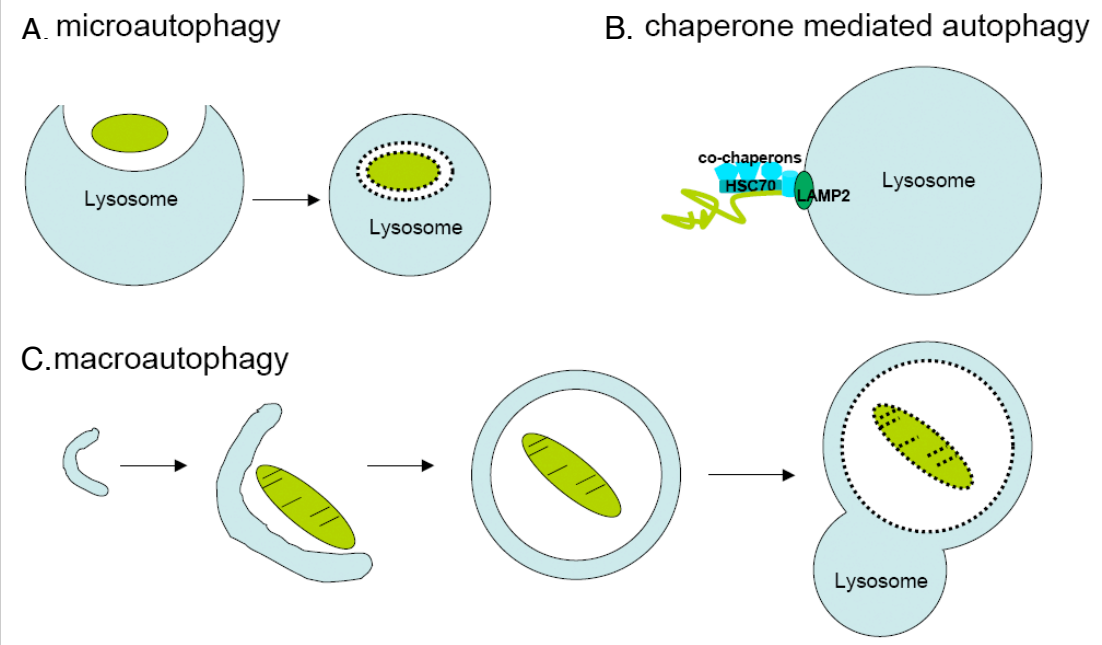

Figure 3. Schematic representation of three types of autophagy. A. Microautophagy is the direct invagination of lysosome membrane and the uptake of cytoplasm into the lumen. **B.** Chaperone mediated autophagy (CMA) is the recognition and transportation of specific proteins from the cytosol by molecular chaperone Hsc70 and its co-chaperones into the lysosome lumen. LAMP2 is the receptor on the lysosome membrane that forms the channel for protein translocation. **C.** Macroautophagy starts from the *de novo* formation of isolation membranes that wrap around the targets until the ends fuse together to form a double-membrane bounded vesicles called autophagosome. The outer membrane of the autophagosome fuses with lysosome, which digests the inner membrane and the content.

Chaperone-mediated autophagy (CMA) is the lysosomal degradation of specific cytosolic proteins without the involvement of vesicular trafficking (Figure 3B). Briefly, CMA substrates are recognized in the cytosol by a chaperone complex containing Hsc70 and its co-chaperones including Hop, Hsp40, Hip and Bag-1[61]. The chaperone complex next associates with the homo-multimer LAMP-2A[62], a lysosome-localized membrane protein with transmembrane segments that form a putative translocon. The chaperone complex unfolds CMA substrates and inserts them into the translocon. A lysosome luminal Hsc70 protein (lys-hsc70) then pulls unfolded substrates into the lysosome lumen for degradation[63]. The cytosolic substrates of CMA usually contain a KFERQ-like motif, which consists of glutamine flanked on either side by the sequence K/R, D/E, F/I/L/V, and K/R/F/I/L/V[63]. About 30% of cytosolic proteins contain this motif. CMA becomes activated during nutrient limitation and oxidative stress.

In most literature, the term autophagy is used in reference to macroautophagy, which is the most well understood form of the three autophagy / lysosome pathways. During macroautophagy, portions of cytosol or large organelles are sequestered into double-membrane bound vesicles called autophagosomes. Autophagosomes then fuse with lysosomes to form large membrane-bounded vesicles called autolysosomes, in which the inner membrane and contents of autophagosomes are digested by lysosome enzymes (Figure 3C).

A unique feature of autophagy is the involvement of a dynamic membrane biogenesis process. The double membrane of autophagosomes are believed to be assembled *de novo* by the expansion of a small isolation membrane (phagophore), which elongates until the ends fuse, wrapping around portions of cytosol or organelles[64]. Largely by using yeast genetics, more than 30 evolutionarily conserved Atg (autophagy-related) proteins have been identified to control the membrane biogenesis in autophagy, including two ubiquitin-like conjugation systems that mediate the initiation and elongation of the isolation

membrane[65]. In mammals, one such conjugation system catalyzes the lipidation of LC3[66] (Figure 4, upper panel), a mammalian homolog of Atg8. Atg7 and Atg3 are E1 and E2 enzymes respectively for the conjugation of free LC3-I to phosphatidylethanolamine (PE) to in turn produce the membrane-associated form LC3-II[67]. The other conjugation system uses Atg7 and Atg10 as E1 and E2 enzymes respectively to conjugate Atg12 to Atg5 (Figure 4). The Atg12-Atg5 conjugate associates with Atg16L and oligomerizes to form a large complex (Atg16L complex)[68,69]. Both LC3-II and the Atg16L complex localize to the isolation membrane and regulate its elongation. After the ends merge, the Atg16L complex falls off whereas LC3-II remains on the autophagosome (Figure 4, lower panel). Therefore, the localization of LC3-II on vesicular structures is used as a marker for autophagy activation. Recent data indicate that the Atg16L complex probably determines where the LC3-I lipidation occurs[70], but the exact role for LC3-II in autophagosome formation is not known.

A class III PI3 kinase complex containing the catalytic subunit Vps34 and the regulatory subunit p150 (Vps15) and Beclin-1 (Atg6) is important for the initial nucleation and assembly of the isolation membrane[71,72]. Several proteins can regulate autophagy by associating with Beclin-1 and the phosphorylation product of this PI3 kinase complex, PI3P, is required for autophagosome formation, although the underlying mechanism for this requirement is not yet known[70]. One possibility is that proteins may regulate autophagy by binding to PI3P, which is a constituent of autophagosomal membrane[70].

A remaining question in the autophagy field is how the autophagosomal membrane originates. There are two general models that are actively debated[73]. The maturation model proposes that the isolation membrane is derived from the ER or other pre-existing membranes. For example, part of the ER membrane may fold onto itself, or ER-derived vesicles may fuse together to form the isolation membrane[73]. Although there are lots of observations in agreement with this model, a lack of direct evidence to implicate the ER in autophagosome

biogenesis has motivated the assembly model. This model posits the *de novo* nucleation, assembly and elongation of the isolation membrane either by local synthesis or non-vesicular transport of lipid materials[73].

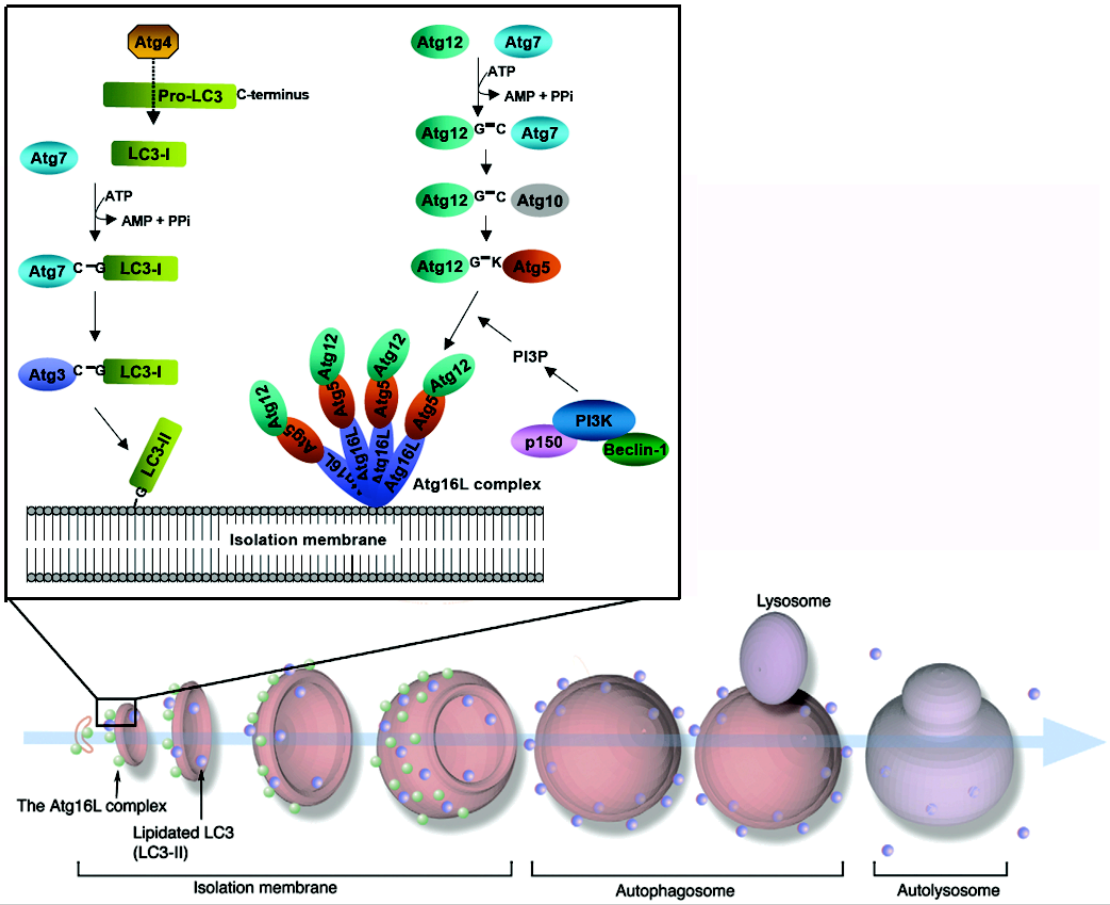

Figure 4. The schematic representation of the molecular events in autophagosome formation in mammals. The bottom panel illustrates the dynamic biogenesis and maturation from isolation membrane to autophagosome and to autolysosome. The green and purple dots indicate Atg16L complex and LC3-II respectively. **The upper panel** depicts the current knowledge of Atg proteins involved in the membrane biogenesis of autophagy. In brief, LC3-II and Atg5-Atg12 conjugates are formed via two ubiquitin-like conjugation systems. The formation of Atg16L complex and LC3-II at the isolation membrane labels it for further elongation. A class III PI3 kinase complex composed of Vps34, p150 and Beclin-1 and the product of this kinase complex, PI3P, are required for the membrane biogenesis, probably through regulation of other proteins binding to the isolation membrane. (Figure modified from [70])

Currently, the role of the autophagy / lysosomal pathway in the degradation of misfolded proteins is largely assigned to its ability to engulf and digest protein aggregates that are refractory to proteasomal degradation, or to remove subcellular structures like protein inclusions. The ubiquitin-binding protein p62/SQSTM1 binds both Agt8/LC3 and ubiquitinated protein aggregates and therefore may facilitate their clearance through autophagy[74]. Protein inclusions are large, detergent-insoluble protein aggregates that form intracellular foci which are visible by microscopy[75]. Protein inclusions entrap not only misfolded protein aggregates but also other structurally intact proteins. Their formation is a hallmark of many neurodegenerative disorders. It is still debated, however, whether the inclusions play a protective or toxic role. In mammalian cells, the formation of cytoplasmic inclusions requires active, dynein-dependent retrograde transport of misfolded proteins along microtubules from the cell periphery to the microtubule organizing centers. These microtubule-dependent inclusions are termed aggresomes[76]. Under an electron microscope, aggresomes are either juxtanuclear, surround or adjacent to a centriole. They are electron dense and membrane-free[75]. In addition to the aggregated protein, which may be ubiquitinated, aggresomes contain chaperones, proteasome components, dynein, vimentin, and γ-tubulin[75].

In a recently published paper, cytosolic misfolded or amyloidogenic proteins were reported to be actively sequestered and partitioned into two distinct inclusions, which were named insoluble protein deposit (IPOD) and juxtanuclear quality control (JUNQ)[77]. This sorting into each of these compartments depended upon protein ubiquitination state and solubility[77]. The JUNQ compartment was found to contain soluble, globular, misfolded proteins and exchange was observed between JUNQ-allocated proteins and the cytoplasm. Deconvolution microscopy revealed that JUNQ is located at an indentation of the nucleus, and in close proximity to an ER region that participates in ERAD[77]. In contrast, the IPOD localized to a perivacuolar peripheral compartment and harbors mostly

non-diffusing, aggregated proteins, which were not ubiquitinated. Proteasomes are re-distributed to the JUNQ but not the IPOD, whereas the autophagy marker Atg8 co-localized with the IPOD but not the JUNQ. Interestingly, amyloidogenic proteins were preferentially targeted to IPODs[77]. The JUNQ shares some features with aggresomes, but it does not co- localize with the microtubule organizing center.

Overview and novelty of the thesis research

As noted previously, the mechanisms of cytosolic protein quality control is poorly defined. Moreover, most of our current understanding of the degradation of misfolded cytosolic proteins comes from yeast, which may or may not reflect what happens in higher eukaryotes. Proper quality control for cytosolic proteins has significant physiologic and pathologic impact, since a large number of proteins are synthesized and function in cytoplasm. Many of the conformational disorders are associated with cytosolic proteins that are not properly cleared. Therefore, to provide mechanistic insights into how aberrant cytoplasmic proteins are recognized and eliminated in mammalian cells, I studied the proteolysis of naturally occurring human variants of two cytosolic proteins, arylamine N-acetyltransferase 1 (NAT1) and parkin. NAT1 and parkin variants are associated with cancer[78,79] and parkinsonism[80,81], respectively.

Some polymorphisms of human NAT1 lead to unregulated degradation of the protein in mammalian cells through the ubiquitin-proteasome pathway[82]. One such variant is human NAT1 R64W in which R64 is replaced with tryptophan. To unravel the biochemical properties that trigger the ubiquitination of this NAT1 variant, multiple biophysical techniques were used to analyze the protein purified from *E.coli*, including nuclear magnetic resonance (NMR) spectroscopy, circular dichorism (CD) spectroscopy, dynamic light scattering, and analytical ultracentrifugation. My data revealed that the arginine to tryptophan mutation does not disrupt the NAT1 protein structure or thermal stability, but rather makes

it aggregation prone. Kinetic data suggest that the protein remains enzymatically active. It is therefore highly likely that the hydrophobic patch created by the mutation causes the protein to be recognized as an aggregation-prone substrate by a cytosolic quality control system.

These studies were therefore expanded to use human NAT1 R64W as a model molecule to identify the cellular components that ubiquitinate and degrade misfolded cytosolic proteins. By using techniques including confocal microscopy, cell fractionation, co-immunoprecipitation, mass spectrometry, protease protection, and immunogold electron microscopy, a novel pathway of cytosolic protein quality control was revealed that involves the routing of aberrant cytosolic proteins through the endoplasmic reticulum. ER-associated protein degradation (ERAD) is typically used for the quality control of ER resident proteins. However, my results suggest that human NAT1 R64W is recognized by the molecular chaperone Hsc70, trafficked to the ER, where it is translocated into the lumen and later retro-translocated out of the ER for ubiquitination. Knockdown of a key ERAD component, p97, by RNAi results in inefficient degradation of ubiquitinated NAT1 R64W and the activation of the autophagy / lysosome pathway.

To test whether the pathway uncovered for NAT1 R64W is general, the studies were expanded to parkin R42P, which contains an unfolded UBL domain. This cytosolic protein variant is processed in an identical manner compared to NAT1 R64W. These two unrelated proteins therefore use a common pathway for degradation that surprisingly involves passage through the ER lumen. These observations indicate that the ER plays a broader role in protein quality control than previously anticipated and have significant impact in areas including protein quality control and ER transportation.

CHAPTER 1

Human arylamine N-acetyltransferase 1 (NAT1) aggregation and constitutive ubiquitination[*]

Introduction

Humans possess two arylamine N-acetyltransferases (NAT1 and NAT2), which catalyze the acetylation of arylamines, arylhydrazines and N-hydroxylated metabolites through the transfer of an acetyl group from acetyl-CoA[83-85]. The medical importance of NATs' N-acetylation capabilities was first realized by its inactivation of the antitubercular drug isoniazid[86]. Although human NAT1 catalyzes the acetylation of the folic acid catabolite *p*-aminobenzoylglutamic acid, no endogenous substrate has been identified for NAT2[87,88]. Both of the human NAT enzymes have attracted attention because of their roles in either activating or detoxifying arylamines and arylhydroxylamine carcinogens[89,90]. For example, the NATs acetylate the bladder carcinogen 4-aminobiphenyl, which is present in tobacco smoke[79,91,92], a process which prevents its bioactivation by p450s.

Humans possess two NAT homologues, however genetic variations exist between individuals that result in proteins with altered enzymatic activity and cellular abundance. Epidemiological studies have made connections between the slow acetylator phenotype, in which NAT function is compromised by genetic polymorphisms, and certain cancer types, the most well-established being for urinary bladder cancer[93-97]. For human NAT1, dramatic reductions in N- and O-acetyltransferase catalytic activities are observed for recombinant NAT1 allozymes encoded by NAT1*14B (R187Q), NAT1*15 (R187Stop), NAT1*17 (R64W), NAT1*19 (R33Stop) and NAT1*22 (D251V)[98]. The observed reduction in

[*] Reproduced with permission from Liu, F., Zhang N., Zhou, X., Hanna, P.E., Wagner, C.R., Koepp, D.M., and Walters, K.J., (2006) *J. Mol. Biol.* 361(3):482-492. ©2006 Elsevier Ltd.

enzymatic activities correlate with reduced protein levels[98]; however, no change is observed for their rate of gene transcription[98]. Instead, the reduced cellular activity of these NAT variants has been suggested to be due to their constitutive ubiquitination, which leads to their degradation by the 26S proteasome[82].

NAT1*14B (R187Q), NAT1*15 (R187Stop), NAT1*17 (R64W), and NAT1*22 (D251V) are reported to be constitutively ubiquitinated in cultured cells[82]. Such ubiquitination is not observed for the protein product of NAT1*4[82], which is designated as the wild-type (wt) species and does not suffer from reduced enzymatic activity[98]. The ubiquitin-proteasome pathway is well renowned for its role in targeted protein degradation, which includes identifying and removing improperly folded proteins. Indeed, the severely truncated protein product of NAT1*15 is expected to be highly misfolded, as crystal structures of prokaryotic NATs indicate that they are not composed of structurally independent domains[99,100]. A rationale for the constitutive ubiquitination of the protein products of NAT1*14, NAT1*17, and NAT1*22, however, is less obvious and the mechanistic pathways that target NAT1 variants for constitutive ubiquitination are not known. An understanding of such would have implications for future therapeutic approaches in NAT1-associated carcinogenesis.

I hypothesized that the point mutations in these variants lead to a change in their biochemical properties, which causes the protein to be recognized and sorted to the ubiquitin-proteasome pathway for degradation. Therefore, to identify the unique features that cause constitutive ubiquitination of NAT1, I focused on the R64W mutation. A variety of biophysical and kinetic assays were performed with protein purified from *E. coli,* which demonstrated a link between protein aggregation and constitutive ubiquitination for the R64W NAT variant. In contrast to human NAT1 wild-type protein, the R64W variant was found to form insoluble inclusion bodies when expressed in *Escherichia coli*. Therefore, I established a model system for the biophysical and biochemical study of this mutation in hamster. The human NAT1 ortholog in hamster is

unfortunately named hamster NAT2. Hamster NAT2 shares 82% sequence identity and analogous substrate specificity and kinetic profiles with human NAT1[101,102]. This protein is an appropriate model system for studying how human NAT1 R64W becomes constitutively ubiquitinated because, as I demonstrate, like human NAT1, hamster NAT2 harboring the R64W mutation is constitutively ubiquitinated, whereas the hamster NAT2 wild-type protein is not[82]. Biophysical and kinetic experiments performed on the hamster NAT2 model system to reveal that the R64W mutation does not perturb NAT thermostability, overall protein structure, or catalytic activity. Instead, it causes local surface changes that cause NAT to aggregate *in vitro*. Such aggregation persists *in vivo*, as demonstrated through cellular experiments that reveal wild-type NAT1 to have a diffused cytoplasmic distribution, whereas the R64W mutant microaggregates. This research demonstrates the important interplay between protein aggregation and ubiquitination and provides insights into why certain NAT isozymes exhibit dramatically different cellular activities.

Although human NAT1 can be isolated from *E. coli*, its R64W variant is insoluble

The ubiquitin-proteasome pathway is a well-established mechanism by which improperly folded proteins are removed from cells. I hypothesized that certain NAT1 variants are constitutively ubiquitinated in cells[82] due to changes in their structural or surface properties, which result from amino acid substitutions. To determine the structural implications of the R64W mutation in human NAT1, I attempted to express and purify human NAT1 R64W and the wild-type protein from *E. coli* by using a previously described method[101] with the goal of comparing their biophysical and biochemical properties. Although the wild-type protein could be isolated and is amenable to *in vitro* analysis[101], the R64W variant becomes insoluble following cellular lysis (Figure 5B). Such insolubility suggests severe aggregation resulting from the mutation, but prohibits direct study.

The hamster ortholog of human NAT1 (hamster NAT2) can also be expressed and purified from *E. coli*[103]. Hamster NAT2 shares 82% sequence identity (Figure 5A) and analogous substrate specificity and kinetic profiles[101,102] compared to human NAT1. I therefore tested whether hamster NAT2 with the R64W mutation incorporated can be purified from *E. coli*. This mutation was introduced into an established *E. coli* expression system for hamster NAT2[103]. Although the hamster NAT2 R64W variant could not be solubilized at the level of the wild-type protein it could be isolated at levels sufficient for biophysical and kinetics experiments (Figure 5B).

To establish whether hamster NAT2 is an appropriate model system to study why certain human NAT1 variants are constitutively ubiquitinated, I tested whether hamster NAT2 mutants become constitutively ubiquitinated. A human embryonic kidney cell line (293T) transfected with HA-tagged ubiquitin[104] and either hamster NAT2 wild-type or variant proteins was treated for eight hours with proteasome and lysosome inhibitor MG132 or DMSO (as a control). As expected, Western blot analyses performed on the cell lysates revealed the formation of higher molecular weight species for the R64W, R187Q and D251V variants, but not for wild-type hamster NAT2. An increased accumulation of such higher molecular weight species occurs when cells are treated with MG132 (Figure 5C). When immunoprecipitated with EZview Red ANTI-FLAG M2 Affinity Gel and probed with anti-HA antibody, cell lysates containing NAT variants exhibit polyubiquitinated species that are absent in cells transfected with empty vector or wild-type hamster NAT2 (Figure 5D). These results demonstrated that hamster NAT2 variants are ubiquitinated when those mutations are introduced, consistent with observations of the corresponding human NAT1 proteins[82]. Therefore, the properties that cause the R64W variant to be ubiquitinated are conserved between hamster and human.

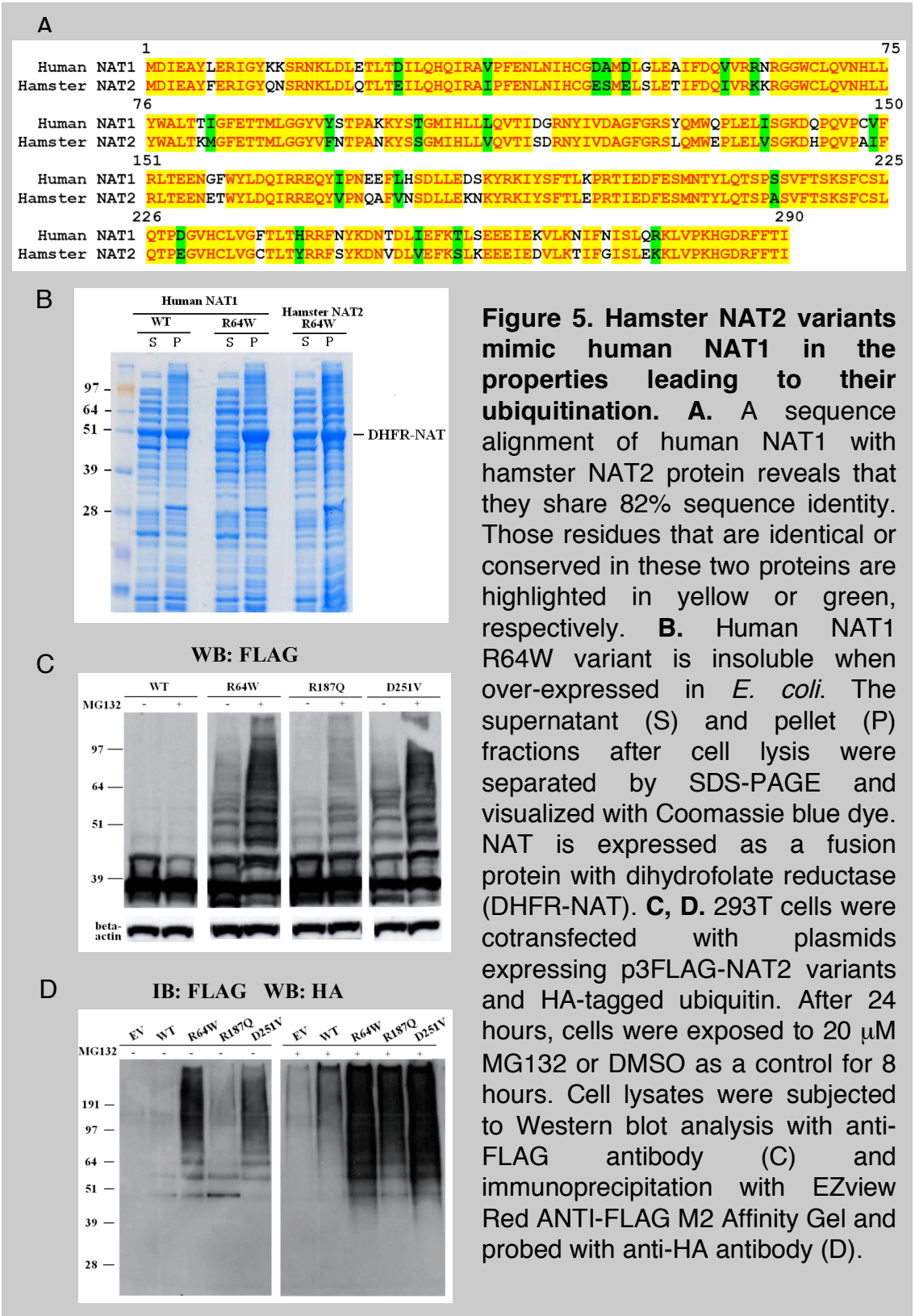

Figure 5. Hamster NAT2 variants mimic human NAT1 in the properties leading to their ubiquitination. A. A sequence alignment of human NAT1 with hamster NAT2 protein reveals that they share 82% sequence identity. Those residues that are identical or conserved in these two proteins are highlighted in yellow or green, respectively. **B.** Human NAT1 R64W variant is insoluble when over-expressed in *E. coli*. The supernatant (S) and pellet (P) fractions after cell lysis were separated by SDS-PAGE and visualized with Coomassie blue dye. NAT is expressed as a fusion protein with dihydrofolate reductase (DHFR-NAT). **C, D.** 293T cells were cotransfected with plasmids expressing p3FLAG-NAT2 variants and HA-tagged ubiquitin. After 24 hours, cells were exposed to 20 μM MG132 or DMSO as a control for 8 hours. Cell lysates were subjected to Western blot analysis with anti-FLAG antibody (C) and immunoprecipitation with EZview Red ANTI-FLAG M2 Affinity Gel and probed with anti-HA antibody (D).

Hamster NAT2 R64W retains its secondary structure but aggregates

Two different methodologies were used to evaluate the structural effect of the R64W mutation: circular dichroism (CD) and NMR spectroscopy. CD spectroscopy is sensitive to the composition of secondary structural elements within a protein and spectra recorded on hamster NAT2 wild-type and R64W proteins were almost identical (Figure 6A). This result suggests that the R64W mutation does not significantly disrupt NAT secondary structure.

To complement this analysis I recorded [^{1}H,^{15}N] HSQC experiments on ^{15}N labeled wild-type or R64W hamster NAT2 protein (Figure 6B). HSQC spectrum correlates the nitrogen atom of an NH_x group with the directly attached proton. Each cross peak in a HSQC spectrum represents a proton that is bound to a nitrogen atom, and therefore the whole spectrum is a fingerprint for the protein structure. The [^{1}H,^{15}N] HSQC spectrum of hamster NAT2 R64W was strikingly similar to the wt protein, as its resonance cross peaks broaden but do not shift dramatically (Figure 6B). This comparison suggests that the overall fold of hamster NAT2 is largely maintained despite the R64W mutation. Resonance broadening arises in proteins undergoing chemical exchange or slower tumbling, which leads to their having large rotational correlation times[105]. Aggregation causes each of these phenomena and was suggested by the insolubility of human NAT1 R64W protein (Figure 5B).

To provide direct information on how the R64W mutation affects the oligomerization state of hamster NAT2, I used dynamic light scattering to measure the rate at which each of these proteins diffuse. This method yields a distribution of hydrodynamic radius, which is a measurement of the molecular weight and the oligomerization state of proteins in the solution. The hydrodynamic radius calculated by this method revealed ~98% of wt hamster NAT2 to have an average hydrodynamic radius of 2.5 nm (Figure 6C, black), corresponding to a molecular weight of 29 kDa. This value is close to its monomeric molecular weight of 34 kDa. In contrast, 71% of the R64W hamster

NAT2 R64W displayed an average hydrodynamic radius of 3.6 nm (Figure 6C, red), corresponding to a molecular weight of 68 kDa. In addition the remaining population of hamster NAT2 R64W protein was represented in larger non-specific aggregates, as suggested by the broadened peak at the larger hydrodynamic radius value (Figure 6C, red). These results provide direct evidence that the R64W mutation causes NAT to aggregate.

To further characterize the aggregation state of hamster NAT2 R64W protein, sedimentation velocity analysis was performed to reveal the size distribution of protein samples of 1.67, 0.58, and 0.25 mg/ml (Figure 6D). The data were analyzed by using a continuous distribution model of the sedimenting species and integrated to estimate of the amount of material between 1S to 3S, where monomeric protein would sediment, and 3S to 40S. The results of the integration demonstrate that hamster NAT2 R64W exists as a non-interacting mixture of ~37% monomeric and 63% aggregated protein. The aggregated species are distributed over a wide size range that exceeds 500 kDa's. Furthermore, the observed distribution was nearly identical for all three dilutions. Hence, hamster NAT2 R64W forms irreversible aggregates that do not dissociate upon dilution, at least within the time frame of the experiment.

A

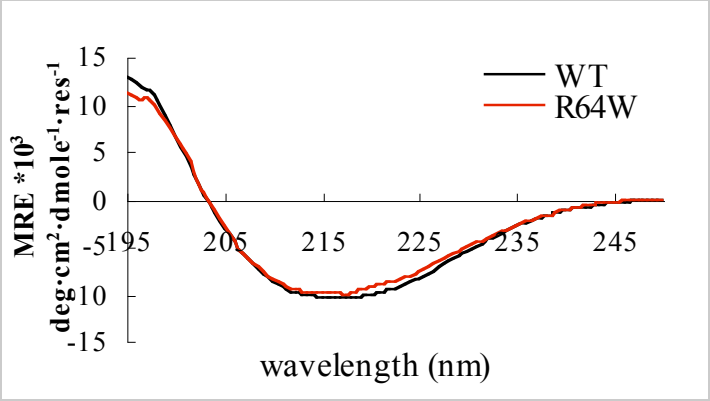
15
10
5
0
-5
-10
-15
195
205
215
225
235
245
MRE *10^3
deg·cm^2·dmole^-1·res^-1
WT
R64W
wavelength (nm)

B

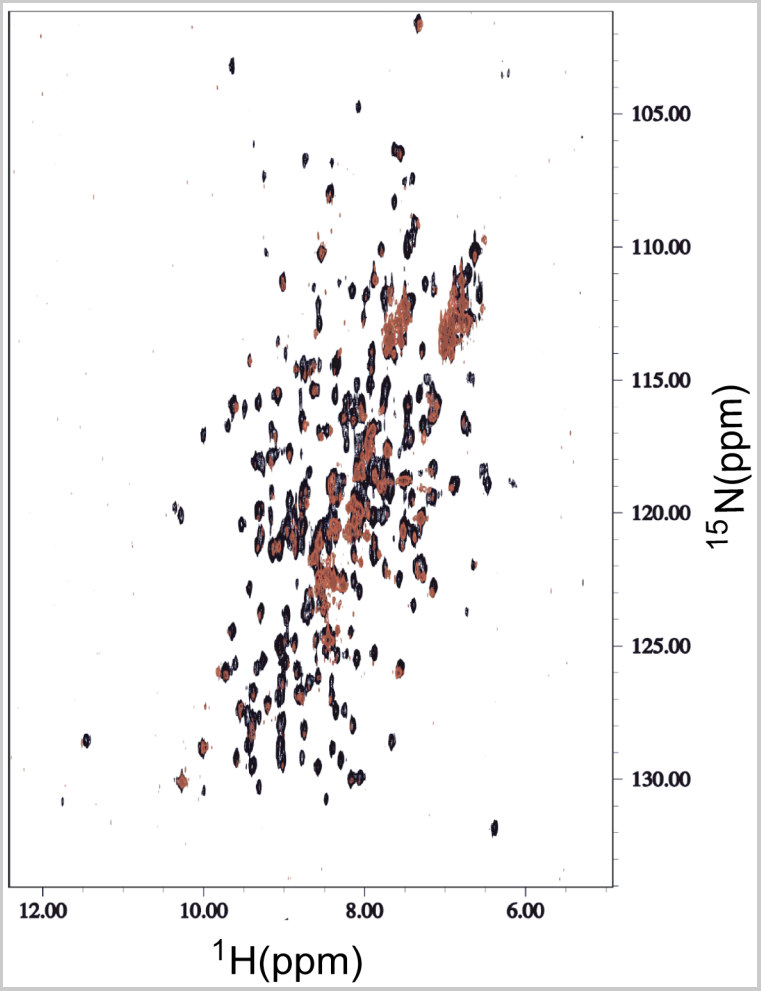
105.00
110.00
115.00
120.00
125.00
130.00
15N(ppm)
12.00
10.00
8.00
6.00
1H(ppm)

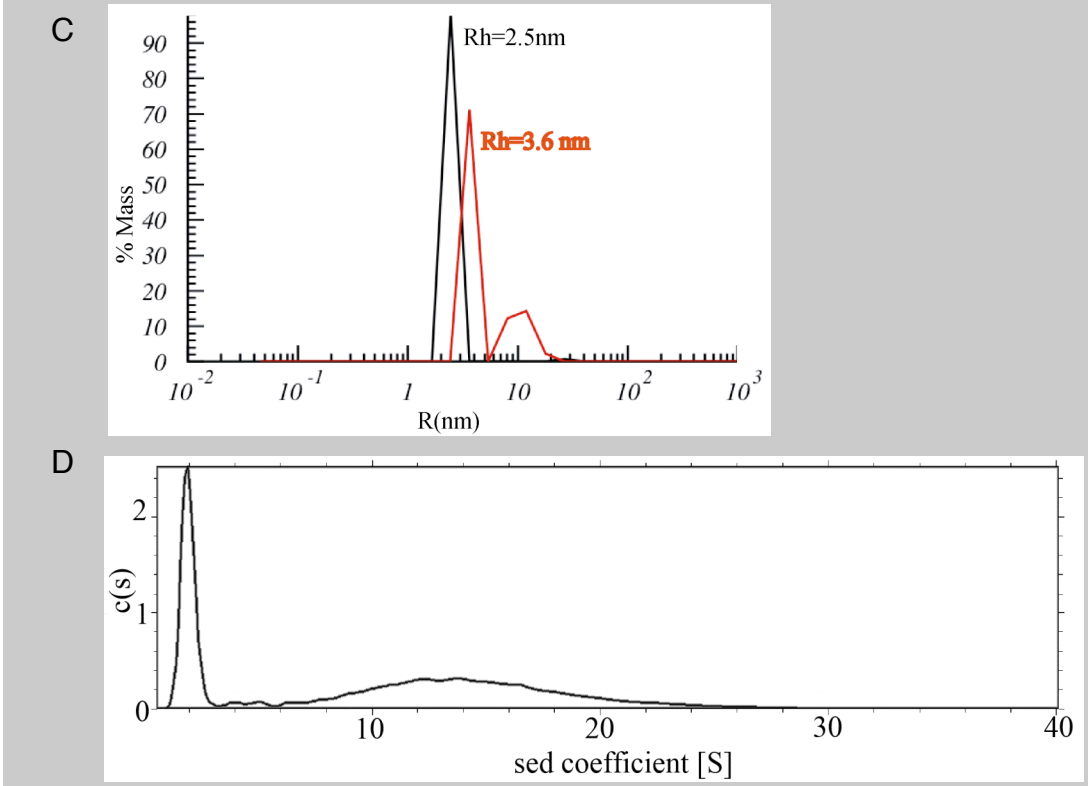

Figure 6. Hamster NAT2 R64W retains its secondary structure but aggregates. A. Superimposed circular dichroism (CD) spectra reveal hamster NAT2 wt (black) and R64W (red) proteins to have similar secondary structural characteristics. These spectra were recorded at room temperature with protein concentrations of 3.0 and 2.9 μM for hamster NAT2 wt and R64W protein, respectively. **B.** Superimposed [^{1}H,^{15}N] HSQC spectra of wt (black) and R64W (red) hamster NAT2 protein reveal overlapping resonance cross peaks. Resonance cross peaks of hamster NAT2 R64W protein was recorded at 10°C and 800 MHz on a 0.1 mM protein sample dissolved in75 mM phosphate buffer, pH 6.8. **C.** Dynamic light scattering experiments were performed at 10°C on samples of 0.2 mg/ml of purified wt (black) and R64W (red) hamster NAT2. 98% of wt hamster NAT2 has an average hydrodynamic radius of 2.5 nm, corresponding to a molecular weight of 29 kDa. The R64W mutation causes this value to be significantly increased as 71% of the R64W NAT2 protein population has an average hydrodynamic radius of 3.6 nm and the remaining 29% has an even higher value. **D.** Sedimentation velocity analysis was performed at 10°C and 50,000 rpm. The c(s) plot is included for hamster NAT2 R64W protein at 1.67 mg/ml. Integration of the material between 1S to 3S and 3S to 40S reveal that hamster NAT2 R64W exists as a non-interacting mixture of ~37% monomeric and 63% aggregated protein.

Cooperative unfolding is lost for the hamster NAT2 R64W variant

To test how the R64W mutation affects NAT protein stability, I used CD spectroscopy to monitor the effect of temperature on the structural integrity of hamster NAT2 wt and R64W protein. The entire spectrum in the far-UV region is monitored across temperatures ranging from 20 to 80 °C (Figure 7A, 7B). The changes of mean residue ellipticity at 208 nm and 215 nm over temperature were re-plotted to directly show the thermal unfolding transition curves (Figure 7C). These experiments reveal that hamster NAT2 wt protein loses its structural fold in a highly cooperative manner (Figure 7A and 7C). This result is consistent with published data indicating that it unfolds cooperatively and loses its structural integrity between 45 and 50°C[106]. Such a thermal denaturation profile supports a model in which it forms a single structural fold that is not aggregated.

The R64W mutation significantly disrupts the thermal denaturation profile of hamster NAT2 (Figure 7B and 7C). In contrast with the wild-type protein, this variant unfolds gradually and non-cooperatively, and with no unfolding transition. Hence, the thermal denaturation profile of this variant suggests it to form a non-homogenous population of oligomers. It is worth noting that the R64W mutation results in a protein that maintains its secondary structure over a greater temperature range. Taken together with the comparisons provided in Figure 6A and 6B these results provide strong evidence that this NAT variant forms folded, rather than unfolded, protein aggregates. It is therefore not likely that unfolding or inherent instability causes the R64W variant to be rapidly ubiquitinated in cells.

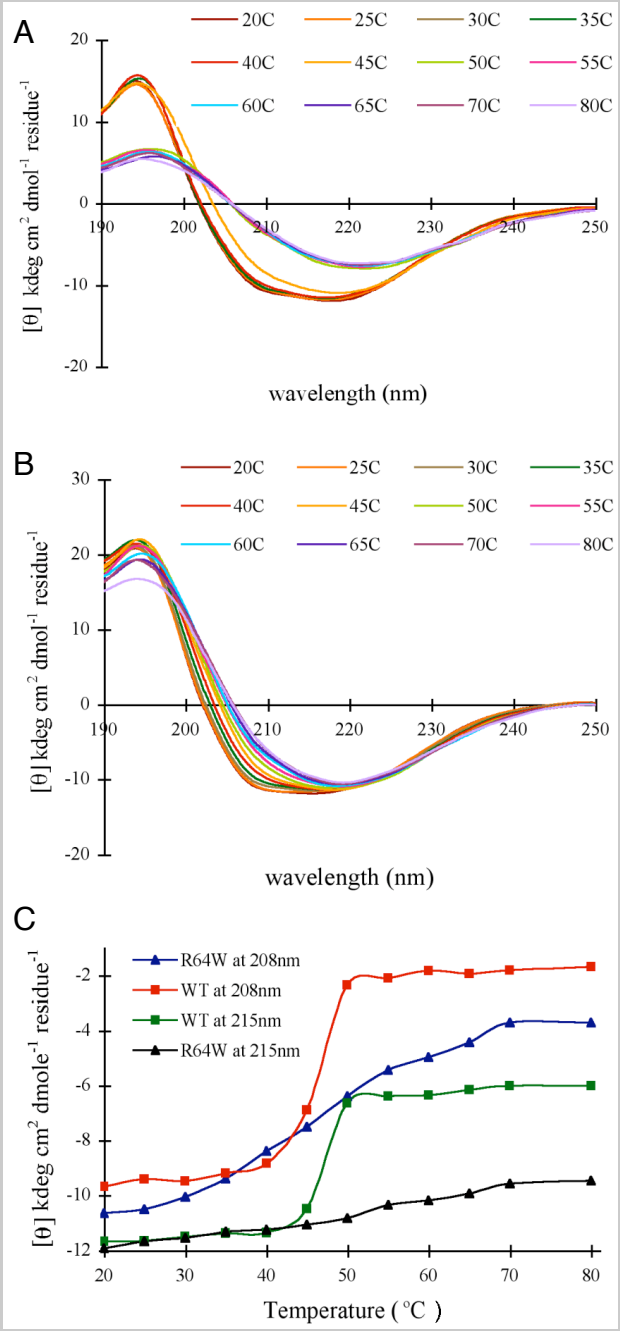

Figure 7. Whereas wild-type hamster NAT2 unfolds cooperatively, the thermal denaturation profile of the R64W variant reflects that of an aggregated protein. CD spectra in the far-UV region are monitored at several temperatures spanning from 20 to 80 ºC on hamster NAT2 wt (**A**), and hamster NAT2 R64W (**B**), by using a spectropolarimeter equipped with a water circulation temperature control. **C.** Thermal unfolding transition curves are provided by plotting the change in ellipticity at 208 and 215 nm from (A) and (B) across temperature. The wt protein exhibits a cooperative unfolding process, whereas no melting transition is observed for the hamster NAT2 R64W variant.

Kinetic data reveals that the hamster NAT2 R64W variant is not catalytically compromised *in vitro*

To test whether the R64W mutation prohibits either the acetylation of hamster NAT2 or its ability to transfer the acetyl group to substrate, I performed steady state kinetics experiments analogous to those published for wt hamster NAT[102]. The results of these experiments along with the previously published results for the wild-type protein[102,107], are provided in Table 1 and indicate that the R64W mutation does not affect NAT acetylation by PNPA. In particular, the values of the second order rate constant for acetylation of R64W and wild-type hamster NAT2 by PNPA are similar, as are the rates of hydrolysis of the acetyl group from the acetyl-cysteinyl-NAT enzyme (Table 1[*]). These results suggest that the constitutive ubiquitination of NAT is not coupled to acetylation or catalytic deficiencies.

Table 1: Steady state kinetics data for acetylation of wild-type and R64W hamster NAT2 at 25°C, pH 7.0

NAT2	K_{PNPA} (mM)	K_{PABA} (mM)	k_{cat} (s^{-1})	k_{cat}/K_{PNPA} ($s^{-1}mM^{-1}$)	k_{cat}/K_{PABA} ($s^{-1}mM^{-1}$)	$t_{1/2}$ (s) [a]
WT	10±1 [b]	0.23±0.02 [b]	620±40 [b]	62±9 [b]	2700±400 [b]	88.3±8.3 [c]
R64W	4.81±0.89	0.37±0.06	265±27	55±16	717±194	56.3±8.4

[a] The $t_{1/2}$ value is the half-life of the acetylated state of NAT at 25°C, pH 7.0.

[b] Values are taken from Wang et al[102]

[c] Values are taken from Wang et al[107]

[*] Table 1 was generated with the help from Xin Zhou.

Human NAT1 R64W forms microaggregates *in vivo*

The biophysical and kinetic experiments described above demonstrate that R64W mutation in hamster NAT2 does not significantly disrupt its overall fold, thermostability, or intrinsic catalytic capabilities, but rather changes its surface properties to favor protein aggregation. Since human NAT1 R64W protein cannot be studied *in vitro*, I used an *in vivo* system to directly test whether it also aggregates. For this purpose, I performed immunofluorescence experiment on HeLa cells transfected with either FLAG-tagged human NAT1 wild-type or R64W expression vector. The cellular distribution of NAT protein was visualized 40 hours after transfection by indirect immunofluorescence. Interestingly, whereas the wild-type protein exhibits diffused cytoplasmic staining (Figure 8A, top panel), the R64W variant forms microaggregates in a subset of transfected cells (Figure 8A, bottom panel). These experiments were paralleled with hamster NAT2 to reveal an analogous effect (Figure 8B). It is worth noting that a significantly greater number of such microaggregates are observed for human NAT1 R64W protein than hamster NAT2 R64W, which is consistent with our *in vitro* data (Figure 5B), indicating that the hamster variant is less aggregated than the human one.

By comparing the acetyltransferase activity of NAT in lysates from transfected and non-transfected HeLa cells, I estimated the concentration of human NAT1 to be ~450-fold greater in transfected cells compared to endogenous protein levels. It is worth noting, however, that both the wild-type and R64W variant are over-expressed, and therefore, it is clear that the microaggregates observed in the R64W transfected cells are not due to over-expression, but rather a result of the mutation itself.

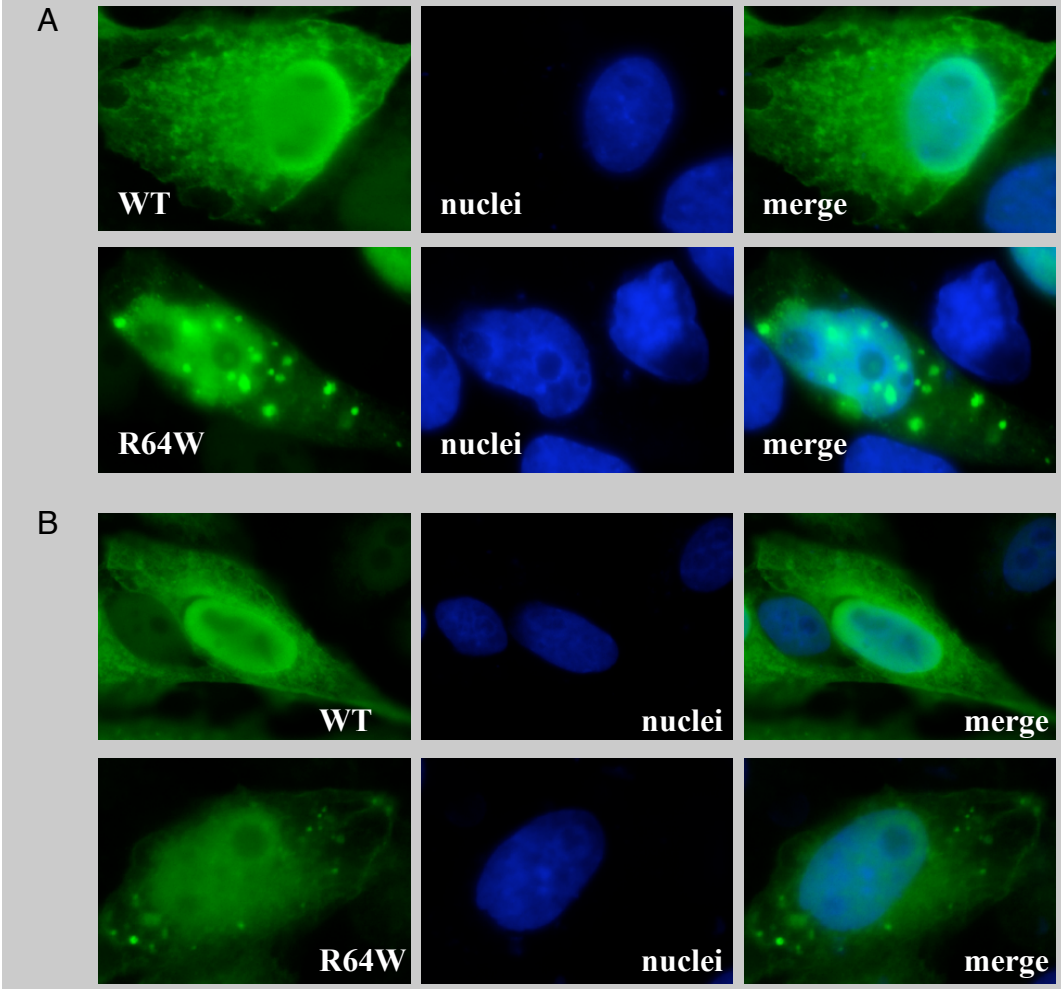

Figure 8. The R64W mutation causes human NAT1 (A) and hamster NAT 2 (B) to form microaggregates *in vivo*. Immunofluorescence microscopy on HeLa cells transfected with either FLAG-tagged NAT wild-type (top panels) or R64W variant (bottom panels) reveals the different distributions of these proteins in the cytoplasm. The wild-type protein shows a diffused cytoplasmic distribution (top panels) whereas the R64W variant forms microaggregates (bottom panels). The nuclei were stained with DAPI. The signals were observed under a Zeiss Axioscop 2 microscope equipped with a Zeiss Axiocam R2 digital camera and 100X objective. Images were captured using Zeiss Axiovision software release 3.1 (Carl Zeiss, Inc., Thornwood, NY) and processed with ImageJ.

A structural model of human NAT1 reveals R64 to reside at a peripheral location

The NMR and CD spectroscopy data demonstrated that the R64W mutation does not destroy NAT's overall protein structure (Figure 6A and 6B). A structural model for human NAT1 (Figure 9*) was then generated by using the Robetta structural prediction program[108]. The model generated was based on the crystal structure of *M. Smegmatis* NAT[100], in which R64 is conserved. This residue resides in a peripheral region of the human NAT1 structure, which provides an explanation for why its mutation to a tryptophan does not destroy the overall structural properties of NAT. The replacement of R64 wit h tryptophan causes steric clashes with the surrounding R62 and R277 residues in the model structure (Figure 9), and most likely an inability to shield this hydrophobic residue from solvent leads to the observed aggregation of human NAT1 R64W.

An analogous effect is observed in a structural model of hamster NAT2, in which R64 is similarly located at a peripheral region in the structure. Its replacement with tryptophan causes steric clashes with the surrounding Q58, K62 and K277 residues. These similarities stem from the high sequence identity between human NAT1 and hamster NAT2 and correlate well with the biophysical and cellular data.

Shortly after the publication of our data, the crystal structure of human NAT1 was resolved by Hong Wu et. al[109]. In agreement with our model structure, the R64 residue resides at a peripheral region. In the crystal structure, R64 forms hydrogen bond with Glu38 and Asn41 and substitution of R64 with tryptophan destroys these interactions[109]. R64W is located at a loop region between two helixes, therefore the substitution won't disrupt the overall fold, but the bulky side chain of tryptophan will change the local structure since it clashes with the surrounding residues[109]. The authors agree that the surface-exposed hydrophobic side chain of tryptophan will promote protein aggregation.

* The model structure for human NAT1 was generated by Dr. Naixia Zhang.

A

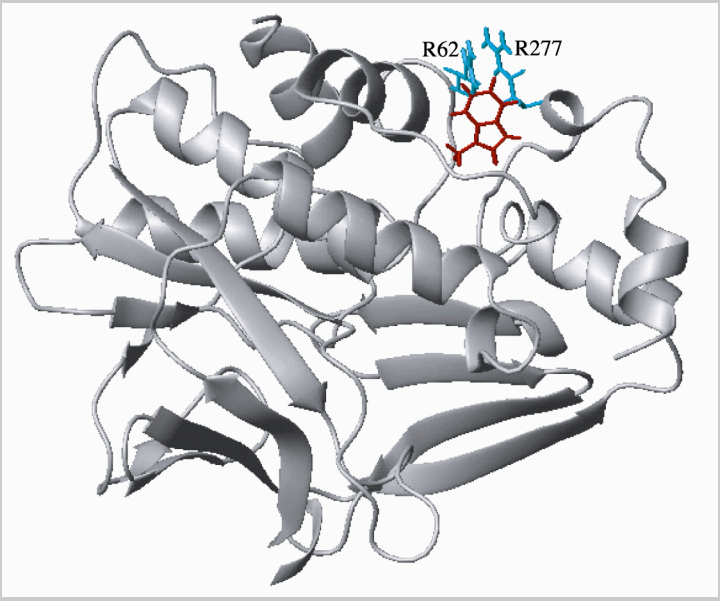

B

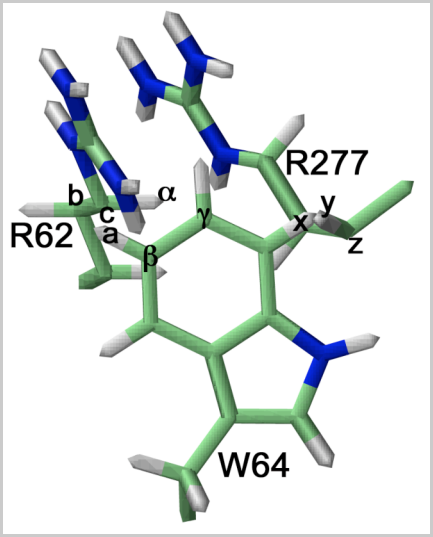

Figure 9. A model structure of human NAT1 illustrates the structural implications of the R64W mutation. A. A model structure is presented for human NAT1 in which R64 is replaced with a tryptophan residue (displayed in red). This replacement causes steric clashes with R62 and R277 (displayed in blue). The R64W variant likely maintains its protein fold due to the peripheral location of R64. **B.** Expanded view highlighting steric clashes. Atoms are colored by type (carbon: green, proton: white and nitrogen: blue). Three groups of clashing atoms are labeled as a-b-c, α-β-γ and x-y-z.

Summary and Discussion

The results of this study lead to a mechanistic model that attributes the reduced cellular activity of the human NAT1 R64W variant[98] to changes in its surface properties that favor protein aggregation. I reveal that hamster NAT2, like human NAT1, becomes constitutively ubiquitinated in cells with the introduction of the R64W mutation (Figure 5C and D). Interestingly, this protein exhibits no loss in its catalytic activity *in vitro* (Table 1) and its overall protein fold and thermostability are not compromised. Instead, the R64W mutation causes hamster NAT2 to aggregate both *in vitro* and *in vivo*. I tested and confirmed that an analogous effect occurs for human NAT1 *in vivo*. These data provide strong evidence that the reduced level of cellular enzymatic activity of the R64W variant is not caused by an intrinsic loss of catalytic activity, but rather originates from surface property changes, which leads to its aggregation and recognition as an ubiquitination target. Our results are consistent with a study that reports the human NAT2 I114T variant to exhibit significantly reduced cellular activity, but no change in its apparent K_m or V_{max} compared to the wild-type protein[110]. I expect that this variant is also ubiquitinated and degraded by the proteasome.

Our kinetic data suggest that human NAT1 R64W does not lose its catalytic activity *in vitro*. Therefore, the observed reduction in cellular activity[98] could be the results of both the increased degradation through ubiquitin-proteasome pathway and the aggregation caused by the R64W mutation, both of which deplete the protein from soluble fractions. An intriguing possibility indicated by our results is that the cellular activity could potentially be rescued by abrogating protein aggregation or the interaction with cellular components that recognize it as an aberrant protein. For this purpose, a deeper understanding is required of the cellular mechanisms that recognize the human NAT1 R64W protein as aberrant, and how it comes to be constitutively ubiquitinated.

Altogether our biophysical and kinetic experiments link NAT protein aggregation to its constitutive ubiquitination; however, further studies are required

to distinguish whether ubiquitination is caused by the aggregation itself or by the properties that lead to the aggregation, namely an increased hydrophobic surface area. Mechanisms for degrading newly synthesized proteins that fail to fold or assemble properly at the endoplasmic reticulum are well characterized[35]; however, less is known on how cells recognize and target aberrantly folded proteins for degradation. For NAT, this function clearly involves the ubiquitin-proteasome pathway, but whether E2 or E3 enzymes differentiate misfolded from properly folded proteins remains elusive[1]. Indeed, molecular chaperones may make this distinction prior to association with E2s or E3s.

In conclusion, my data reveal that the single amino acid substitution associated with the NAT1*17 polymorphism (R64W) does not disrupt its overall fold, thermostablility or enzymatic activity, but rather causes changes in its surface properties that promote aggregation *in vitro* and *in vivo*. The peripheral location of R64 enables its catalytic activity, as its overall structure is maintained; however, the local changes are sufficient to trigger aggregation and constitutive ubiquitination. Furthermore, NAT1 R64W provides an ideal model molecule to study cytosolic protein quality control in human cells *in vivo* since it is a naturally occurring human variant of a cytosolic protein. In addition to potentially inspiring new therapeutic approaches in NAT1-associated carcinogenesis, the identification of a cellular pathway that constitutively ubiquitinates human NAT1 R64W may have general application to the degradation of other cytosolic proteins. In the next chapter, I reveal a novel cellular pathway for human NAT1 R64W degradation that unexpectedly involves its trafficking through the endoplasmic reticulum.

CHAPTER 2

Human NAT1 R64W is trafficked through ER for degradation

Introduction

The results of the previous chapter demonstrate that the mutation in human NAT1 R64W does not disrupt its protein structure, thermal stability or enzymatic activity, but rather makes it aggregation prone. It is therefore highly likely that the hydrophobic patch created by the mutation causes the protein to be recognized as an aggregation-prone substrate *in vivo* by a cytosolic quality control system. Identifying components in this quality control system that recognize, sort and dispose of misfolded cytosolic proteins will enrich our understanding of the pathogenesis of not only NAT1-associated cancers, but also other protein misfolding disorders.

Mechanistically, protein quality control via degradation is best understood for misfolded secretory and integral membrane proteins synthesized at the endoplasmic reticulum, which are degraded via ER-associated degradation (ERAD) pathways[35]. ERAD substrates are recognized and sorted in the ER lumen, but ubiquitinated at the cytosolic surface of ER and in turn degraded by proteasome in cytoplasm (reviewed in [35,111]).

Quality control for cytosolic proteins via the proteasome is less well understood. A study in yeast demonstrated misfolded cytosolic proteins to be ubiquitinated by membrane-bound ERAD enzymes[52,53]. The prevailing model is that these proteins are directed to the cytoplasmic face of the ER membrane for ubiquitination prior to degradation by the proteasome. Recently, misfolded cytosolic proteins were revealed to partition either proximal to the nucleus or to a perivacuolar inclusion[77] in yeast. Proteasome was observed to re-distribute to the perinuclear inclusion, suggesting that proteins partitioned to this region are cleared via the ubiquitin-proteasome system. Notably, however, disease-

associated amyloidogenic proteins preferentially locate to the perivacuolar compartment, which does not co-localize with proteasome, but instead with autophagy markers[77].

Autophagy is an alternative quality control process in which portions of the cytoplasm and cellular organelles are engulfed by intracellular membranes and trafficked to the lysosome for degradation, reviewed in [56,112]. Cytoplasmic inclusions like aggresomes are believed to be cleared from cells through the autophagy / lysosomal pathway[113]. Moreover, recent evidence indicates that ERAD substrates may also be targeted for autophagy[114-117]. ER stress can induce autophagy to ameliorate the accumulation of aberrant proteins in the ER lumen[118].

Most of our current understanding of cytoplasmic quality control is derived from experiments performed in yeast, which may or may not be transferable to mammals. The aggregation-prone human NAT1 R64W protein is constitutively ubiquitinated and degraded in a proteasome-dependent manner. Therefore, to provide mechanistic insights into how aberrant cytoplasmic proteins are recognized and processed in mammalian cells, I studied how this naturally occurring variant is recognized and degraded. The results indicate that NAT1 R64W is degraded through a pathway that surprisingly, involves trafficking through the lumen of the endoplasmic reticulum.

Constitutively ubiquitinated NAT1 is routed to the endoplasmic reticulum.

I investigated whether the cellular localization of constitutively ubiquitinated NAT1 R64W differs from that of the “wild-type” protein using immunofluorescence confocal microscopy in HeLa cells expressing HA-tagged ubiquitin and either FLAG-tagged human NAT1 “wild-type” or R64W protein. Whereas diffuse cytoplasmic staining was observed for the “wild-type” protein (Figure 10A, top panel), a subset of cells transfected with the R64W variant

formed punctated structures in the cytoplasm that co-localize with ubiquitin (Figure 10A, third panel).

NAT1 R64W protein aggregates *in vitro*[121] and subjecting the cell lysate of NAT1 R64W expressing cells to centrifugation at 12,000g pelleted a large fraction of the non-ubiquitinated protein as well as a ladder of higher molecular weight species (Figure 10B, left lane) characteristic of NAT1 ubiquitination observed previously[82,119]. Resuspending the pelleted fraction in denaturing buffer and immunoprecipitating with anti-FLAG antibody revealed a ubiquitin ladder recognized by anti-HA antibody when HA-tagged ubiquitin was co-expressed with FLAG-NAT1 R64W (Figure 10C). By contrast, significant levels of ubiquitinated NAT1 R64W in the cytosol was not observed without the treatment of proteasome inhibitor MG132 (Figure10B, right lane). Together with the immunofluorescence data (Figure 10A, third panel), these data indicate that overexpressed NAT1 R64W forms ubiquitinated aggregates that are resistant to proteasomal degradation, consistent with previous studies indicating that protein aggregates are resistant to proteasomal degradation[120].

Interestingly, treating the cells with proteasome and lysosome inhibitor MG132 demonstrated a perinuclear accumulation of NAT1 R64W besides the diffused cytoplasmic distribution, which was not observed in cells transfected with “wild-type” NAT1 that only diffused in the cytoplasm (Figure 10A, bottom and second panels). Moreover, NAT1 R64W and ubiquitin showed significant co-localization at this perinuclear region.

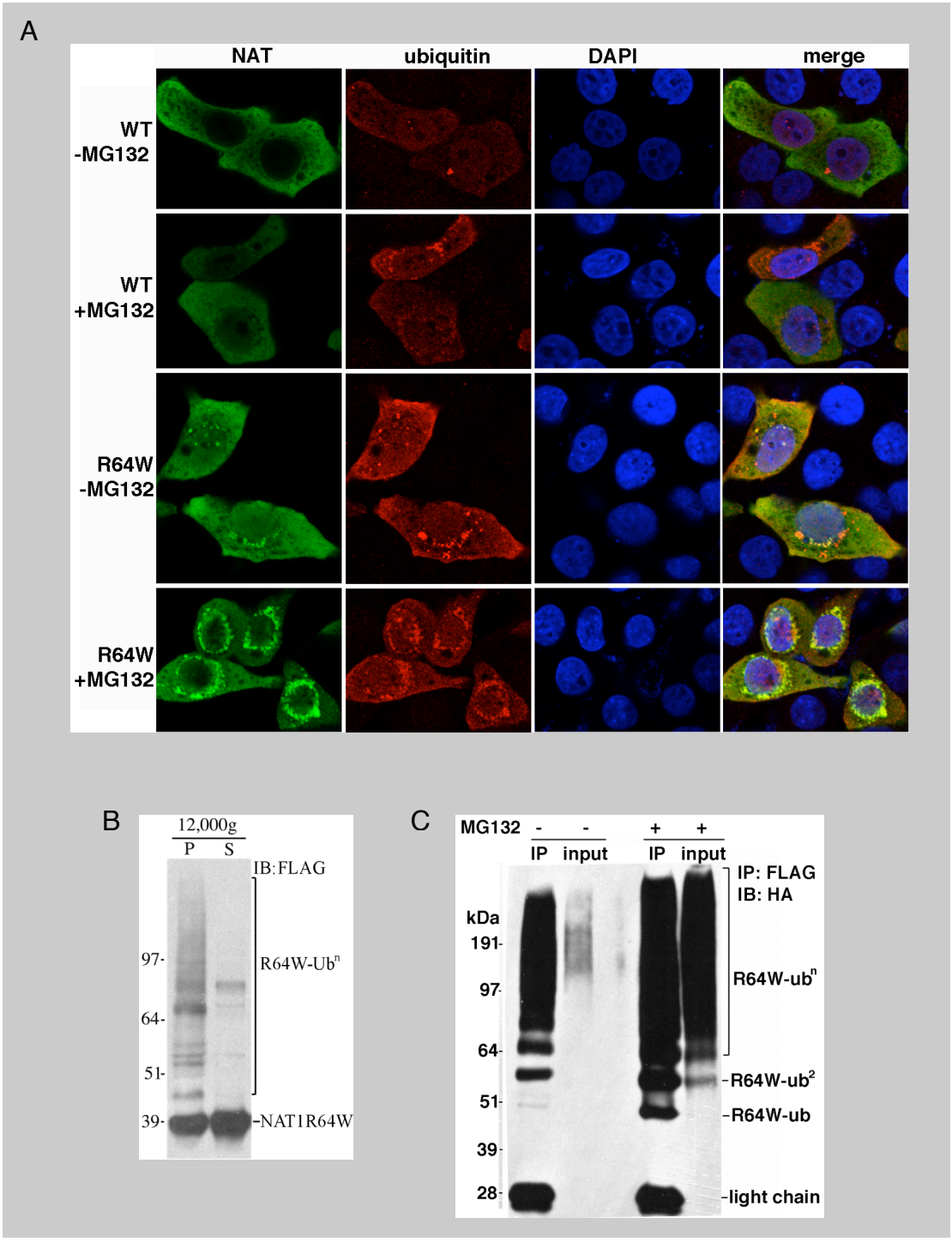
A
NAT
ubiquitin
DAPI
merge
WT
-MG132
WT
+MG132
R64W
-MG132
R64W
+MG132
B
12,000g
P
S
IB:FLAG
97-
64-
51-
39-
R64W-Ub^n
NAT1R64W
C
MG132 - - + +
IP input IP input
IP: FLAG
IB: HA
kDa
191-
97-
64-
51-
39-
28-
R64W-ub^n
R64W-ub^2
R64W-ub
light chain

Figure 10. Over-expressed NAT1 R64W forms ubiquitinated aggregates and upon MG132 treatment accumulates at a perinuclear structure. A. The human NAT1 R64W variant co-localizes with ubiquitin in both the presence (bottom panel) and absence (third panel) of proteasome inhibitor MG132, whereas the "wild-type" protein (WT) does not (top and second panels). Immunofluorescence microscopy was performed on HeLa cells co-transfected with HA-tagged ubiquitin (displayed with anti-HA antibody in red) and FLAG-tagged NAT1 "wild-type" or R64W protein (displayed with anti-FLAG antibody in green). Nuclei were stained with DAPI as shown in blue. Confocal optical section stacks with a Z-depth of 1 μm were collected and one optical section is displayed for each sample. **B.** Ubiquitinated and non-ubiquitinated species of over-expressed NAT1 R64W are pelleted by centrifugation at 12,000g. HeLa cells transfected with FLAG-tagged NAT1 R64W were homogenized and the lysate subjected to differential centrifugation at 1000g and 12,000g. The supernatant (S) and pelleted (P) fractions of the 12,000g centrifugation were probed by Western blot analysis using anti-FLAG antibody. Molecular weight markers are indicated. Polyubiquitinated NAT1 R64W species are labeled as R64W-Ub^n. **C.** Over-expressed NAT1 R64W forms ubiquitinated aggregates. HeLa cells co-transfected with HA-ubiquitin and FLAG-NAT1 R64W were homogenized and spun down at 12,000g. The pellet was dissolved in 1% SDS TBS buffer and diluted to 0.1% SDS for immunoprecipitation with anti-FLAG antibody and ubiquitin conjugates were detected by Western blot analysis with anti-HA antibody. Ubiquitin conjugates were observed even without MG132 treatment, indicating that NAT1 R64W forms ubiquitinated aggregates that resist degradation.

To establish the identity of the perinuclear structure where ubiquitin and NAT1 R64W co-localize upon proteasome inhibition, HeLa cells expressing FLAG-tagged human NAT1 R64W were co-stained with anti-FLAG antibody and markers for different cellular structures, including the Golgi apparatus, aggresomes and the ER. The Golgi apparatus was visualized with the Alexa Fluor® 488 conjugated wheat germ agglutinin, which selectively binds to N-acetylglucosamine and N-acetylneuraminic acid residues. No colocalization was observed between the perinuclear structure and Golgi in this circumstance. Aggresomes are perinuclear structures formed from aggregated proteins by dynein-dependent transport on microtubules to the microtubule organizing center and therefore contain dynein, vimentin, and γ-tubulin[121]. When the proteasome is inhibited, partial co-localization of NAT1 R64W with these proteins were observed. By contrast, confocal microscopy revealed strong co-localization between NAT1 R64W and the ER integral membrane protein calnexin in cells exposed to MG132 (Figure 11A, bottom panel), suggesting that NAT1 R64W localizes to the perinuclear ER when the proteasome was inhibited.

Altogether, the data presented in Figures 10A and 11A (bottom panels) indicate that proteasome inhibition leads to the accumulation of ubiquitinated NAT1 R64W protein at the ER. To test this model further, I determined whether NAT1 R64W co-localizes with the ER when cell lysates are fractionated by differential ultracentrifugation at 1,000g, 12,000g, and 100,000g. ER is pelleted at 100,000g but not at 1,000g or 12,000g[122]. As predicted, ubiquitinated NAT1 R64W protein accumulated in the fraction pelleted at 100,000g (Figure 11B). This methodology is not conclusive, however, as other cellular components, such as Golgi apparatus, endosomal membranes, or protein aggregates within the cytosol with the same sedimentation co-efficiency will also be pelleted. Therefore, I combined cell fractionation at lower speeds with specific $CaCl_2$ precipitation of rough ER to mitigate such contamination[123]. In brief, cells are homogenized and cellular debris, large vesicular structures like lysosomes and mitochondria and

large protein aggregates were removed by centrifugation at 1,000g and 12,000g respectively. Rough ER was subsequently precipitated by adding $CaCl_2$ to the supernatant and recovered by centrifugation at 8,000g. As controls, I examined the behavior of calnexin and Hsp70, a cytosolic protein, after the fractionation process. As shown in Figure 11C, the ER membrane protein calnexin precipitated with the $CaCl_2$ ER-enriched fraction, whereas Hsp70 did not. Moreover, I demonstrated that in HeLa cells, endogenous NAT1 protein is readily detectable in the cytosol, but not the ER (Figure 11C, bottom panel).

NAT1 R64W is observed both in the cytosolic and ER-enriched fractions of HeLa cells expressing FLAG-tagged NAT1 R64W regardless of proteasome inhibition (Figure 11D and 11E). Moreover, ubiquitinated NAT1 R64W is greatly enriched in the ER fraction. The fractionation procedure was not affected by the exogenous overexpression of NAT1 R64W as demonstrated by the efficient enrichment of calnexin by the addition of $CaCl_2$ (Figure 11E, bottom panel). To ensure that aggregated NAT1 R64W protein was excluded from this fractionation procedure, I performed the assay without $CaCl_2$ to demonstrate that NAT1 R64W protein is not present in the pellet without $CaCl_2$ (Figure 11E, lanes 4 and 5). The precipitation of ubiquitinated NAT1 R64W protein with the $CaCl_2$ ER-enriched fraction is consistent with what was observed by immunofluorescence (Figure 10A and 11A, bottom panels) and altogether, the data suggest a mechanism in which the cytosolic NAT1 R64W variant is delivered to the ER for ubiquitination and degradation.

Moreover, co-immunoprecipiation experiments offer evidence for the proteasome playing a direct role in degradation of NAT1 R64W both at the ER and cytosol, as the a7 subunit of the proteasome's 20S core particle associates with NAT1 R64W in both the ER-enriched and cytosolic fractions of cells treated with proteasome inhibitor LLNL (Figure 12).

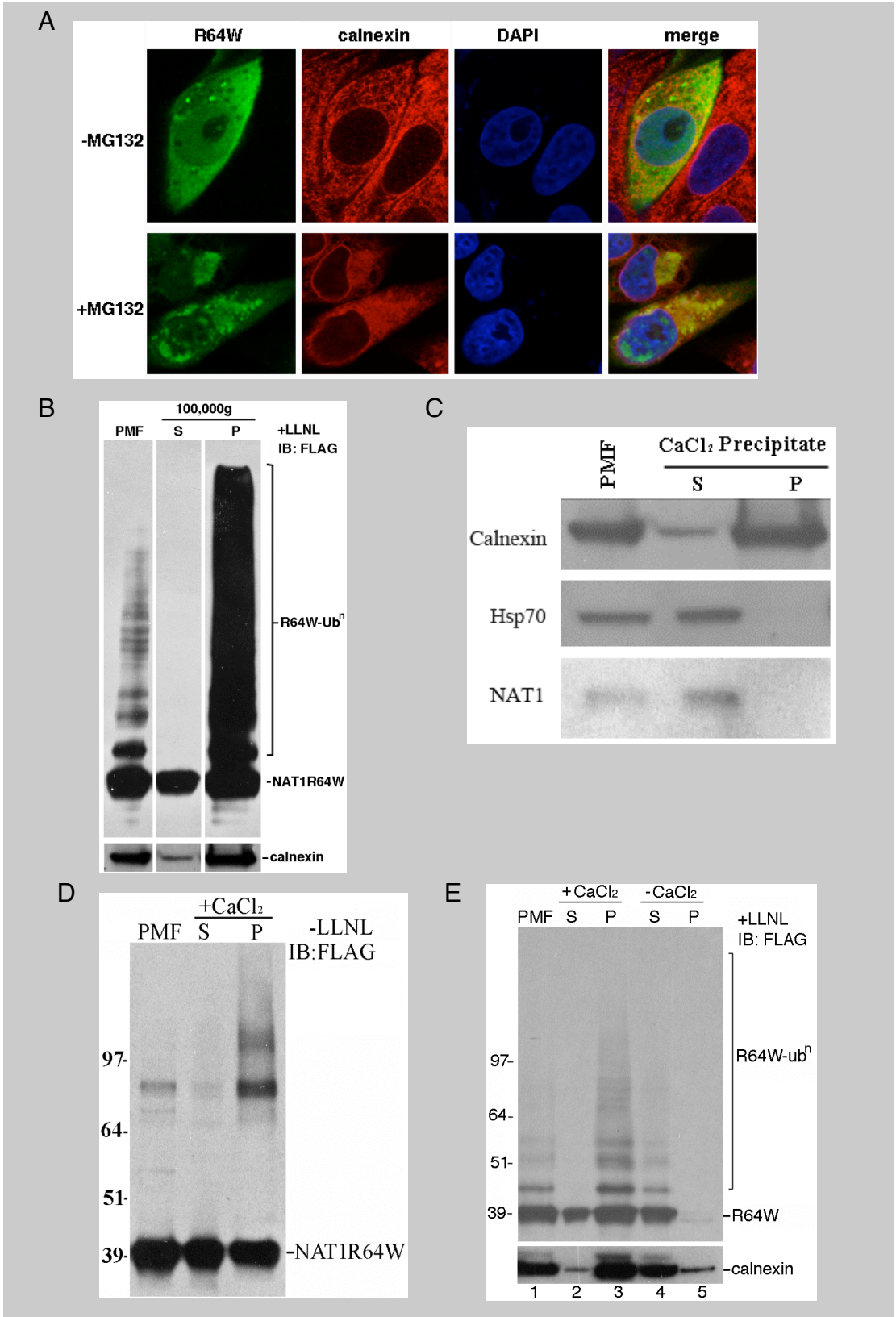
A
R64W
calnexin
DAPI
merge
-MG132
+MG132
B
100,000g
PMF
S
P
+LLNL
IB: FLAG
-R64W-Ubn
-NAT1R64W
-calnexin
C
PMF
CaCl2 Precipitate
S
P
Calnexin
Hsp70
NAT1
D
+CaCl2
PMF
S
P
-LLNL
IB:FLAG
97-
64-
51-
39-
-NAT1R64W
E
+CaCl2
-CaCl2
PMF
S
P
S
P
+LLNL
IB: FLAG
97-
64-
51-
39-
R64W-ubn
-R64W
-calnexin
1
2
3
4
5

Figure 11. NAT1 R64W is ubiquitinated at the endoplasmic reticulum. A. NAT1 R64W co-localizes with ER-marker calnexin after MG132 exposure. Immunofluorescence microscopy was performed on HeLa cells transfected with FLAG-tagged NAT1 R64W in the presence (bottom panel) and absence (upper panel) of 20 μM MG132 for 16 hours. Confocal optical section stacks with a Z-depth of 1 μm were collected and one optical section is displayed for each sample. **B.** Ubiquitinated human NAT1 R64W is enriched in an ER fraction prepared by ultracentrifugation. HeLa cells expressing NAT1 R64W were lysed by using glass homogenization and subjected to differential centrifugation at 1,000g, 12,000g and 100,000g, respectively. The supernatant fraction after 12,000g centrifugation (PMF) and the supernatant (S) and pelleted (P) fractions after an additional 100,000g centrifugation are displayed by Western blot with anti-FLAG antibody (upper panel). The ER marker calnexin is also displayed with anti-calnexin antibody (lower panel). Polyubiquitinated NAT1 R64W species are labeled as R64W-Ub^n. **C.** Endogenous NAT1 in HeLa cells is a cytosolic protein. Rough ER membrane was enriched by $CaCl_2$ precipitation of the post mitochondrial fraction (PMF) of HeLa cell lysate. Western blotting was used to detect proteins in the PMF as well as the supernatant (S) and pelleted ER-enriched (P) fractions after $CaCl_2$ precipitation. **D, E**. NAT1 R64W variant and its ubiquitin conjugates accumulate at the ER in the absence (D) or presence (E) of proteasomal inhibition. HeLa cells transfected with FLAG-tagged NAT1 R64W were treated with 50 μM proteasome inhibitor LLNL for 8 hours and the rough ER enriched by $CaCl_2$ precipitation. The post mitochondrial fraction (PMF), supernatant (S), and pelleted (P) fractions with or without $CaCl_2$ addition were separated by electrophoresis and NAT protein visualized by Western blot analysis with anti-FLAG antibody. The ER marker calnexin is also displayed with anti-calnexin antibody (E, lower panel).

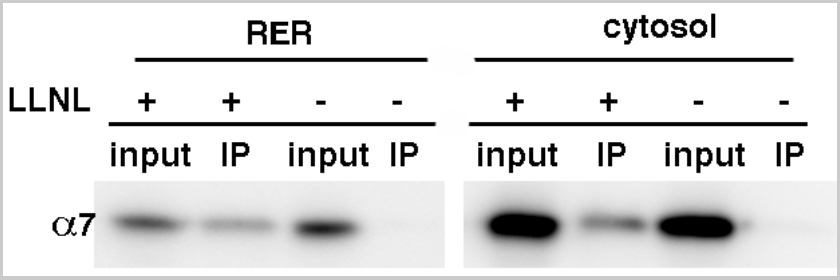

Figure 12. Proteasome interacts with human NAT1 R64W at both the ER membrane and the cytosol. HeLa cells transfected with FLAG-NAT1 R64W was lysed and fractionated with $CaCl_2$ precipitation as described in the text. The ER and cytosol fractions were then immunoprecipitated with anti-FLAG antibody and detected by Western blot with anti-α7, a subunit of the proteasome.

NAT1 R64W enters the ER lumen, where it interacts with Bip

To distinguish whether NAT1 R64W enters the ER lumen or just associates with the cytoplasmic surface of ER membrane, I performed a protease protection assay by exposing it to trypsin with and without the membrane disrupting detergent NP-40. Briefly, cellular debris and aggregated NAT1 R64W were removed by centrifugation at 12,000g after homogenization, and the remaining lysate, the post mitochondria fraction (PMF), exposed to trypsin with or without 0.5% NP-40. A population of fully intact non-ubiquitinated NAT1 R64W protein is protected from trypsin digestion in LLNL-treated cells (Figure 13A, left panel). This protection is markedly reduced by NP-40 (Figure 13A, right panel). The protease protection assay was validated with the cytosolic protein β-actin, the ER luminal protein Bip, and GAPDH, which forms amyloid-like aggregates in cells[124,125]. As expected, β-actin was readily digested; Bip was totally digested only with NP-40 addition; and GAPDH resisted to digestion even with NP-40 present (Figure 13D). Hence, the protection observed for NAT1 R64W is not a result of protein aggregation, but due to its shielding within the lumen of some membrane-bound structures, likely the ER.

Surprisingly, a significant population of NAT1 R64W is partially proteolyzed without LLNL treatment when NP-40 is not added (Figure 13B, left panel) indicating that part of the protein is exposed to trypsin while the remaining portion is protected in a membrane-bound compartment (see Figure 13C for a model for protease protection assay). This partially digested product was also observed at lower abundance in the LLNL-treated sample (Figure 13A), and apparently represents protein in the process of translocation or retrotranslocation, such that part of it is embedded in the membrane or on the luminal side of the ER (Figure 13C). No ubiquitinated NAT1 species are observed after two hours of trypsin treatment, even without NP-40, for cells treated or not with LLNL (Figure 13A and 13B, left panels). This finding is consistent with ubiquitination occurring at the cytosolic surface of the ER.

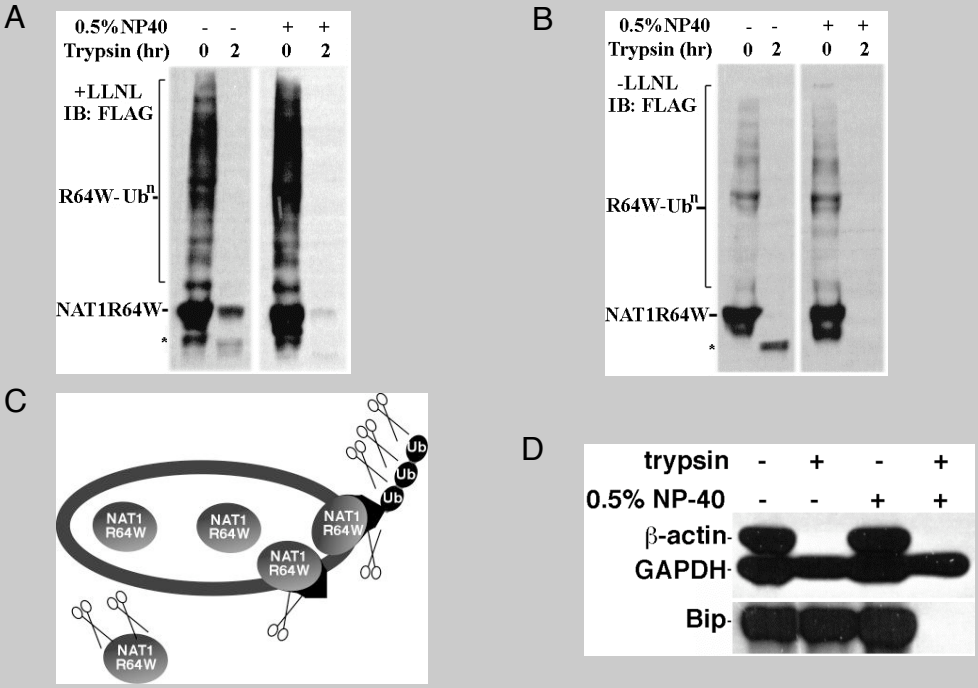

Figure 13. Protease protection assay indicates that NAT1 R64W is translocated into the ER lumen and ubiquitinated at the cytosolic surface of the ER. A, B. protease protection assay performed with HeLa cells transfected with FLAG-tagged human NAT1 R64W in the presence (A) or absence (B) of 50 μM proteasome inhibitor LLNL suggests that NAT1 R64W is translocated into the ER lumen. HeLa cells were lysed by homogenization and subjected to differential centrifugation at 1,000g and 12,000g respectively. The supernatant of the 12,000g centrifugation was incubated on ice with 50 μg/ml trypsin for 2 hours with or without the addition of 0.5% NP-40. Samples were resolved by SDS-PAGE and subjected to Western blot analysis using anti-FLAG antibodies. The star indicates a proteolytic product of NAT1 R64W. Polyubiquitinated NAT1 R64W species are labeled as R64W-Ub^n**. C.** An illustrative model for protease protection of different NAT1 R64W localizations. Protein in the cytosol and at the cytosolic surface of ER are digested by exogenously added trypsin (indicated with scissors) whereas protein in the lumen or embedded in the membrane is protected. **D**. Protease protection was observed for GAPDH aggregates and ER luminal protein Bip, but not for an abundant cytosolic protein β-actin. HeLa cells were homogenized and spun down at 12,000g. The supernatant was incubated with 50 μg/ml trypsin for digestion on ice for 2 hours in the presence or absence of the detergent NP-40. Western blotting was used to illustrate that Bip is protected from the protease only when NP-40 is absent. The cytosolic protein β-actin was not protected, whereas GAPDH aggregates were protected even when the detergent is present.

Since human NAT1 “wild-type” is a cytosolic protein, the R64W variant is speculated to locate in the cytosol too. However, to our surprise, the protease protection assay indicates that this variant is translocated into the ER lumen. Therefore, to provide another independent evidence for the ER luminal translocation of NAT1 R64W, immunogold labeling and electron microscopy was applied to visualize the ultrastructure of NAT1 R64W transfected HeLa cells. As shown in Figure 14, NAT1 R64W is largely localized at the membrane surface of ER cisternae in cells not treated with proteasome and lysosome inhibior MG132 (Figure 14A*). MG132 treatment leads to the vacuolation of ER and the dramatic increase of NAT1 R64W abundance in ER lumen (Figure 14B). These data are consistent with the protease protection assays, which demonstrate protection of the intact protein with LLNL (Figure 13A) and partial proteolysis without LLNL (Figure 13B). Morphologically, the vesicular structure depicted in Figure 14B are single-membrane bounded, which does not resemble double-membrane bounded autophagic vesicles. I propose those observed vesicular structures to be vacuolized ER, since it is single membrane bound and stained positive for ER chaperone protein Bip. This is consistent with the previous data indicating that NAT1 R64W localizes to the ER (Figure 11). Indeed, earlier reports have shown that over-expression of misfolded ER resident proteins leads to ER vacuolization[126,127]. It is worth noting that gold labeling at membranes is under-represented due to loss of membrane traces during sectioning[128]. This partially contributes to the lack of gold signals observed at the ER membrane in Figure 14B.

* Immunogold electron microscopy and quantitative morphometric analysis were performed by Dr. Mark A. Sanders.

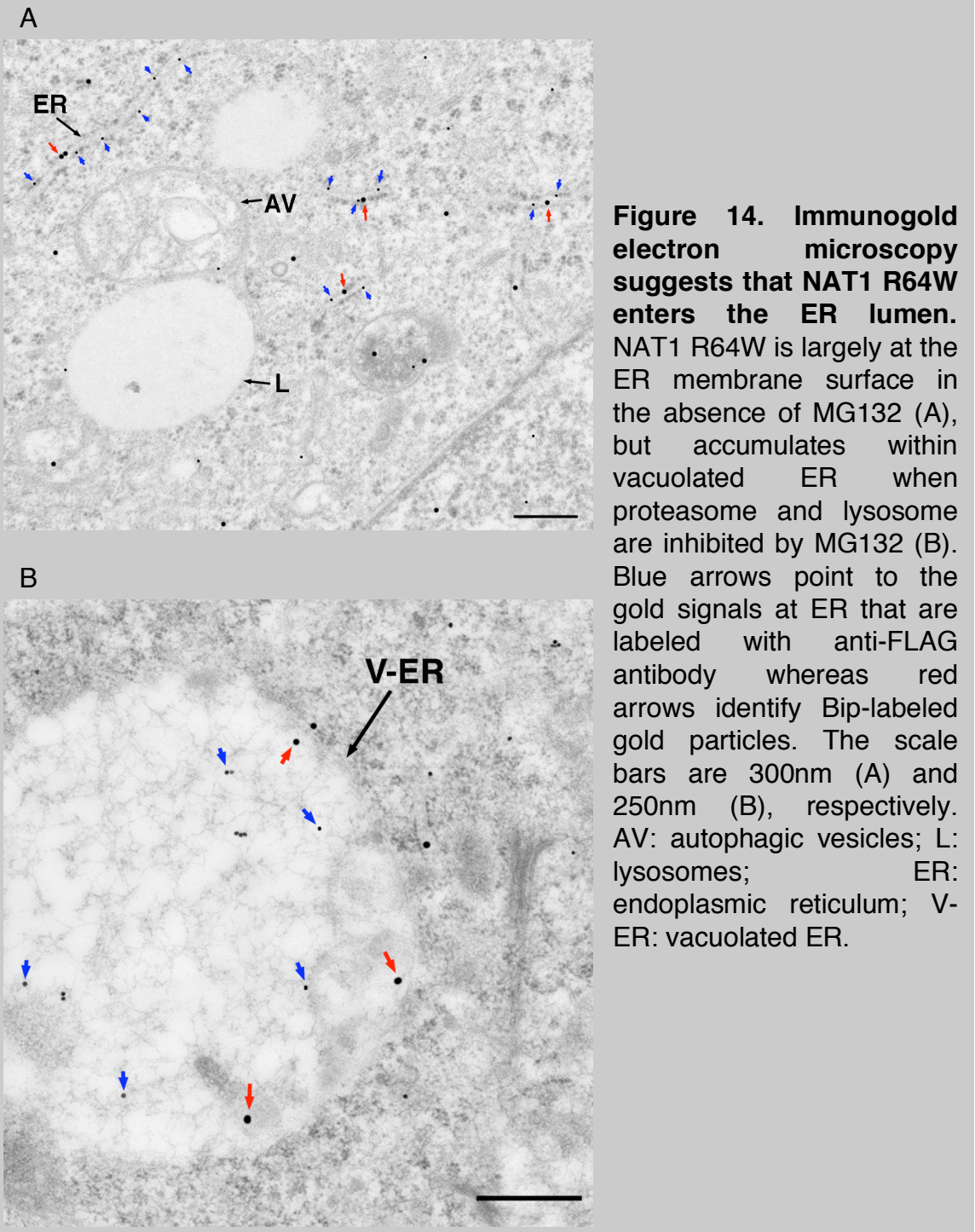

Figure 14. Immunogold electron microscopy suggests that NAT1 R64W enters the ER lumen. NAT1 R64W is largely at the ER membrane surface in the absence of MG132 (A), but accumulates within vacuolated ER when proteasome and lysosome are inhibited by MG132 (B). Blue arrows point to the gold signals at ER that are labeled with anti-FLAG antibody whereas red arrows identify Bip-labeled gold particles. The scale bars are 300nm (A) and 250nm (B), respectively. AV: autophagic vesicles; L: lysosomes; ER: endoplasmic reticulum; V-ER: vacuolated ER.

Although the image of cells under immunogold electron microscope can provide a visualized qualitative description for the subcellular distribution of a particular antigen, quantitative morphometry can provide quantitative information and comparison of the distribution of gold signals in different cellular compartments. Therefore, to further validate the ER localization of NAT1 R64W, quantitative morphometric analysis was done with HeLa cells transfected with NAT1 R64W with or without MG132 treatment (Figure 15 and Table 2). NAT1 R64W is present in the ER, cytosol and nucleoplasm in both DMSO- and MG132-treated cells. Mitochondria was used to estimate the background staining and its abundance is <1%. About 50% of total NAT1 R64W signals is ER-associated in both treatments; however, only ~4.8% was in the ER lumen under DMSO treatment, which increased to ~32% under MG132 treatment. It is worth noting that gold labeling at membranes is intrinsically under-represented and a correction factor of 9.3 times the observed gold particles is used for membrane abundance estimates[128]. The trend of increased abundance in the ER lumen upon MG132 treatment is not biased by this correction, however, and is consistent with what was observed in the trypsin digest assay (Figure 13A and 13B).

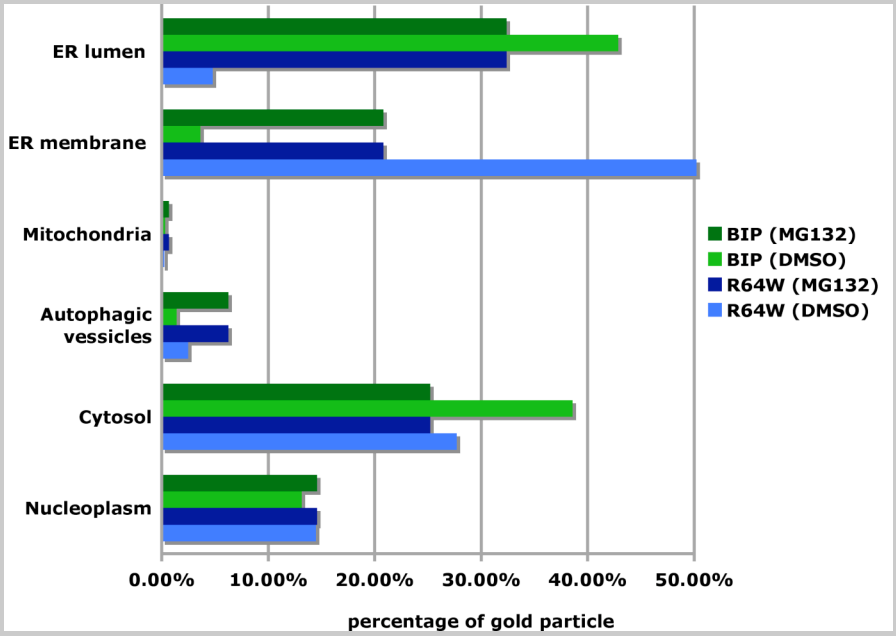

Figure 15. Quantitative morphometric analysis of HeLa cells transfected with NAT1 R64W demonstrated that this protein enters the ER lumen. Gold signals at different cellular compartments were counted for NAT1 R64W and Bip under either DMSO or MG132 treatment. This plot is an illustrative presentation of data in Table 2. It reveals that a large portion of this protein is localized at the ER membrane, but accumulates in the ER lumen while protein degradation is inhibited.

Table 2. Summary of quantitative morphometric analysis of immunogold labeled NAT1 R64W and Bip in HeLa cells transfected with FLAG-NAT1.

NAT1 R464W (DMSO)		
Cellular compartments	**Observed Gold Particles**	**(%)**
Nucleoplasm	169	14.50%
Cytosol	323	27.72%
Autophagic vessicles	29	2.49%
Mitochondria	3	0.26%
ER membrane	(63) 585.3 *	50.22%
ER lumen	56	4.81%
Total	1165.3	100.00%
BIP (DMSO)		
Cellular compartments	**Observed Gold Particles**	**(%)**
Nucleoplasm	168	13.15%
Cytosol	493	38.59%
Autophagic vessicles	18	1.41%
Mitochondria	4	0.31%
ER membrane	(5) 46.5 *	3.64%
ER lumen	548	42.90%
Total	1277.5	100.00%
NAT1 R64W (MG132)		
Cellular compartments	**Observed Gold Particles**	**(%)**
Nucleoplasm	189	14.60%
Cytosol	328	25.23%
Autophagic vessicles	81	6.26%
Mitochondria	9	0.70%
ER membrane	(26) 269.7 *	20.83%
ER lumen	418	32.38%
Total	1294.7	100.00%
BIP (MG132)		
Cellular compartments	**Observed Gold Particles**	**(%)**
Nucleoplasm	148	10.89%
Cytosol	449	33.05%
Autophagic vessicles	22	1.62%
Mitochondria	5	0.30%
ER membrane	(16) 176.7 *	13.00%
ER lumen	558	41.14%
Total	1358.7	100.00%

* A correction factor of 9.3 times the observed gold particles (the number in the parenthesis) was used to yield the estimated total number of gold particles at the membrane. This number is in accordance with[128], as described in the text.

Next, I tested whether NAT1 R64W interacts with the ER luminal Hsp70 protein Bip. Experiments performed on the $CaCl_2$ ER-enriched fraction revealed Bip to co-immunoprecipitate with NAT1 R64W with an enhanced interaction in LLNL-treated cells (Figure 16A), consistent with the greater abundance of NAT1 R64W in the ER lumen of LLNL-treated cells (Figure 13A and 14B). Immunoprecipitations performed in parallel with untransfected HeLa cells and cells expressing FLAG-tagged human NAT1 "wild-type" or R64W protein revealed a barely detectable interaction between Bip and "wild-type" NAT1 (Figure 16B, lane 4) and strong co-immunoprecipitation with NAT1 R64W (Figure 16B, lane 6). Hence, only the aberrant R64W protein interacts significantly with Bip. The interaction with Bip provides the third piece of evidence for the ER luminal translocation of NAT1 R64W.

However, the immunoprecipitation experiments described above use buffers containing 1% Triton X-100 and 0.1% SDS, which disrupt membranes and therefore could be interfered with by protein interactions formed after the membrane is broken. To bypass this problem, membranes were lysed under strong denaturing condition after cross-linking. In brief, cells were gently lysed by Dounce homogenization and protein complexes in the supernatant following 12,000g centrifugation stabilized by crosslinking with dithiobis[succinimidyl propionate] (DSP). Microsomes were enriched then by ultracentrifugation at 100,000g that were next dissolved in denaturing buffer containing 1% SDS, which lyses the ER membrane and breaks interactions formed after that. The sample was then diluted to 0.1% SDS to immunoprecipitate with anti-FLAG antibody. As shown in Figure 16C, Bip was crosslinked within large protein complexes that co-immunoprecipitated with NAT1 R64W. The crosslinking was reversed by DTT addition in the loading buffer before SDS-PAGE to reveal Bip at its expected molecular weight. Consistent with its increased abundance in the ER lumen upon MG132 treatment, I observed increased Bip co-immunoprecipitation with NAT1 R64W upon MG132 exposure.

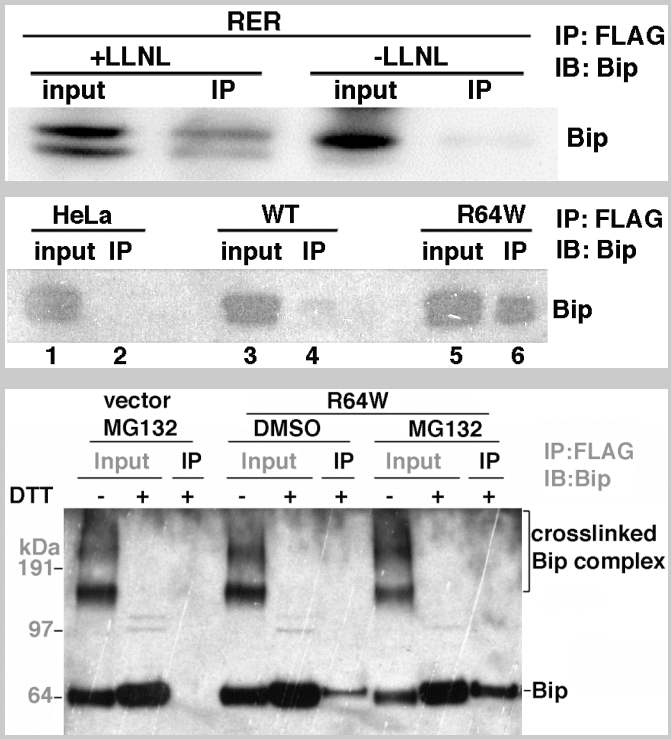

Figure 16. NAT1 R64W interacts with the ER luminal Hsp70 protein Bip. A. NAT1 R64W co-immunoprecipitated with Bip in the ER fraction. ER-enriched fractions from HeLa cells expressing FLAG-tagged NAT1 R64W and treated with or without 50 μM LLNL for 8 hours were prepared by $CaCl_2$ precipitation, dissolved in TBS buffer containing 0.1% SDS and 1% Triton-X100, immunoprecipitated with anti-FLAG antibody, and subjected to Western blot analysis with anti-Bip antibody. An increased amount of Bip was co-immunoprecipitated with NAT1 R64W after LLNL treatment. **B.** Bip specifically co-immunoprecipitates with NAT1 R64W, but not the "wild-type" protein (WT). HeLa cells expressing FLAG-tagged NAT1 R64W or the "wild-type" proteins were lysed with 1% Triton-X100 buffer and total cell lysates were used for immunoprecipitation with anti-FLAG antibody and the bound Bip protein detected by Western blot with anti-Bip antibody. Non-transfected HeLa cells (HeLa) were used as a control. **C**. Bip crosslinks to NAT1 R64W prior to the disruption of ER membrane. HeLa cells expressing FLAG-NAT1 R64W treated or not with MG132 were lysed by homogenization and the post mitochondria fractions were exposed to the cross-linking reagent DSP. ER was isolated by ultracentrifugation at 100,000g and dissolved in 1% SDS buffer. Bip Co-immunoprecipitated with anti-FLAG antibody in the ER fractions was visualized with anti-Bip antibody. HeLa cells transfected with vector were used as a control to show that no background level of Bip was immunoprecipitated under this condition. DTT was added before SDS-PAGE to reverse the crosslinking.

Finally, to further confirm that the cytosolic NAT1 R64W variant enters the ER lumen, I tested whether N-glycosylation can happen if glycosylation consensus sequences were incorporated into NAT1 R64W. The protease protection assay described in Figure 13 was used to selectively display the portion of NAT1 R64W that goes into the ER lumen, and endoglycosidase H (EndoH) treatment was used to detect the glycosylation. EndoH is a glycosidase that cleaves N-linked glycoproteins within the chitobiose core of high mannose and some hybrid oligosaccharides. As illustrated in Figure 17A, two glycosylation sequences were incorporated at both the C- and N-terminus according to previously published reports[129,130]. When the glycosylation site incorporated NAT1 R64W (Glc-R64W) plasmid was transfected into HeLa cells and cell lysate treated with EndoH, the band corresponding to N-glycosylated Glc-R64W was shifted down to a lower molecular weight in the ER luminal fraction generated by trypsin digestion (Figure 17B[*]). This is consistent with the specific cleavage of N-glycans from Glc-R64W by EndoH, which demonstrated that R64W mutation cause NAT1 to enter the ER lumen.

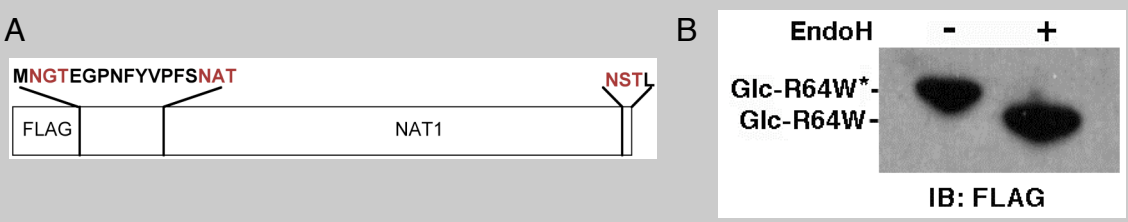

Figure 17. Human NAT1 R64W is glycosylated in the ER when glycosylation sites are incorporated into its sequence. A. Schematic representation of the NAT1 R64W with N-glycosylation sites incorporated at both the N- and C-terminal ends (Glc-R64W). The consensus sequence for N-glycosylation (N-X-S/T) is highlighted in red. **B.** Glc-R64W is glycosylated. HeLa cells were transfected with Glc-R64W and treated with 20 μM MG132 for 8 hours before harvesting. Cells were lysed by homogenization and supernatant of 12,000g was treated with 50 μg/ml trypsin for 2 hours on ice, and then denatured and incubated with EndoH for 1 hour at 37 °C. Reaction products were separated by SDS-PAGE and visualized by Western blot with anti-FLAG. Glc-R64W* is denoted to glycosylated Glc-R64W.

[*] Glycosylation assay was performed by Dr. Bala Medicherla and Dr. Yang Kang.

To test whether the autophagic pathway is required for NAT1 R64W trafficking through the ER lumen, I monitored this variant's localization by immunofluorescence in 3-methyladenine (3-MA) treated cells. 3-MA is an established inhibitor of autophagy. Although 3-MA treatment led to vacuolization in HeLa cells, NAT1 R64W is largely cytoplasmic with punctuated aggregates (Figure 18, upper panel). Treatment with both 3-MA and MG132 led to perinuclear accumulation of NAT1 R64W, which colocalized with calnexin (Figure 18, lower panel), as was observed with only MG132 present (Figure 11A). Co-localization analysis with ImagePro Plus on the entire 3D stack of multiple cells in the confocal images, yielded similar Pearson's Correlation Coefficients (Rr) for calnexin and NAT1 R64W in cells treated with 3-MA and MG132 (Rr=0.77±0.09) compared to MG132-treated cells (Rr=0.69±0.14). Therefore, our data do not support a model in which NAT1 R64W is trafficked to the ER via the autophagy pathway.

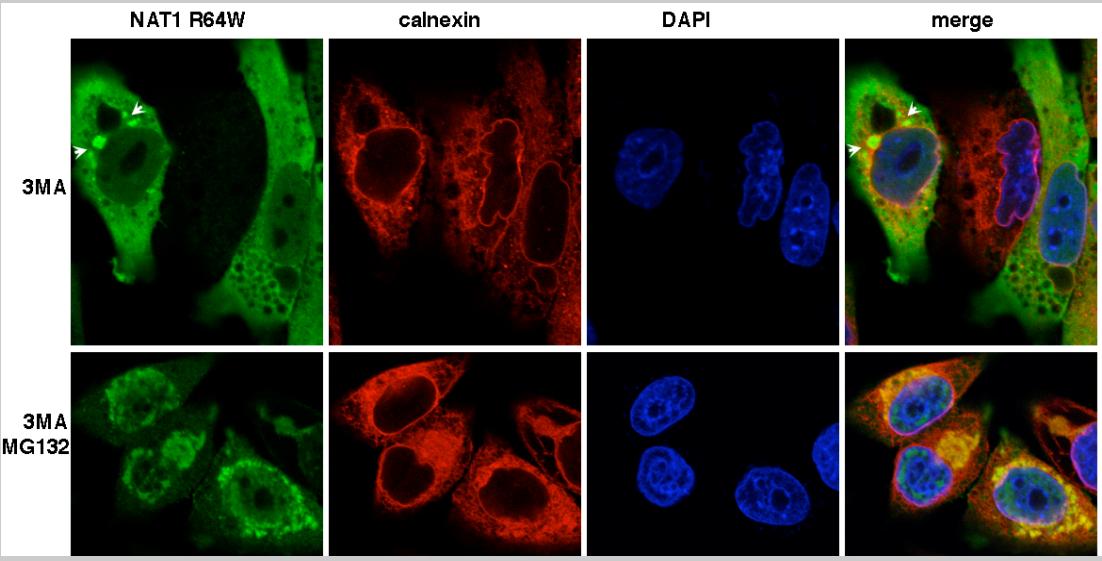

Figure 18. NAT1 R64W is not shuttled to the ER through the autophagy pathway. HeLa cells expressing NAT1 R64W were treated with 10 mM 3-MA to inhibit the autophagy pathway, and 20 μM MG132 to inhibit degradation (lower panel) or DMSO as a control (upper panel). Cells were then subjected to indirect immunofluorescence to detect the co-localization of NAT1 R64W and calnexin. White arrows highlight R64W aggregates.

NAT1 R64W is retrotranslocated back to the cytosolic surface of the ER where it is ubiquitinated

The previous data showed that R64 to W mutation causes human NAT1 to translocate into the ER lumen. It is not clear whether the NAT1 R64W transported into ER lumen is then retro-translocated back to the cytosolic surface of the ER for ubiquitination as what happen for ERAD substrates. To test this hypothesis, I monitored the flux of human NAT1 R64W through the ER by using a pulse-chase experiment. NAT1 R64W was expressed under the control of a tetracyline-based inducible promoter. After inducing NAT1 R64W expression by the removal of tetracycline in the medium, the protease protection assay described in Figure 13 was used to assay its presence in the ER lumen. Protein protected from proteolysis was apparent within 60 minutes of induction with increased abundance up to two hours (Figure 19A*, middle panel), suggesting a constant import of NAT1 R64W into the lumen. Total NAT1 R64W similarly exhibited increased abundance of the free and ubiquitinated species as the degradation was inhibited by MG132 (Figure 19A, top panel). In contrast, treatment with cycloheximide and MG132 after two hours of induction stabilized the total protein abundance (Figure 19B*, top panel), but resulted in a continuous loss of protected NAT1 R64W (Figure 19B, middle panel). Hence, NAT1 R64W within the ER lumen was exported. This result also suggests that the import of R64W from the cytosolic pool is not efficient under these conditions even though a significant amount of NAT1 R64W was present. It is not known whether the translocation into ER lumen is impaired by cycloheximide treatment, or only newly synthesized protein is competent for translocation into the ER lumen. In both experiments, Bip was probed as a loading control and its levels were stable (Figure 19A and B, bottom panels).

* This assay was performed by Dr. Bala Medicherla and Dr. Yang Kang.

Although it is very unlikely, the disappearance of protected NAT1 R64W observed in Figure 18B could be a consequence of this protein being secreted outside of the cell rather than into the cytosol. Therefore, cell culture medium was collected and Western blot was used to demonstrate that no NAT1 R64W was present in the medium, even though the α subunit of glycoprotein tropic hormones was detected, which HeLa cells are known to secrete[131]. This is consistent with our earlier observation that NAT1 R64W was not co-localized with Golgi apparatus marker. Therefore, NAT1 R64W is retro-translocated back into the cytosol after it enters the ER lumen.

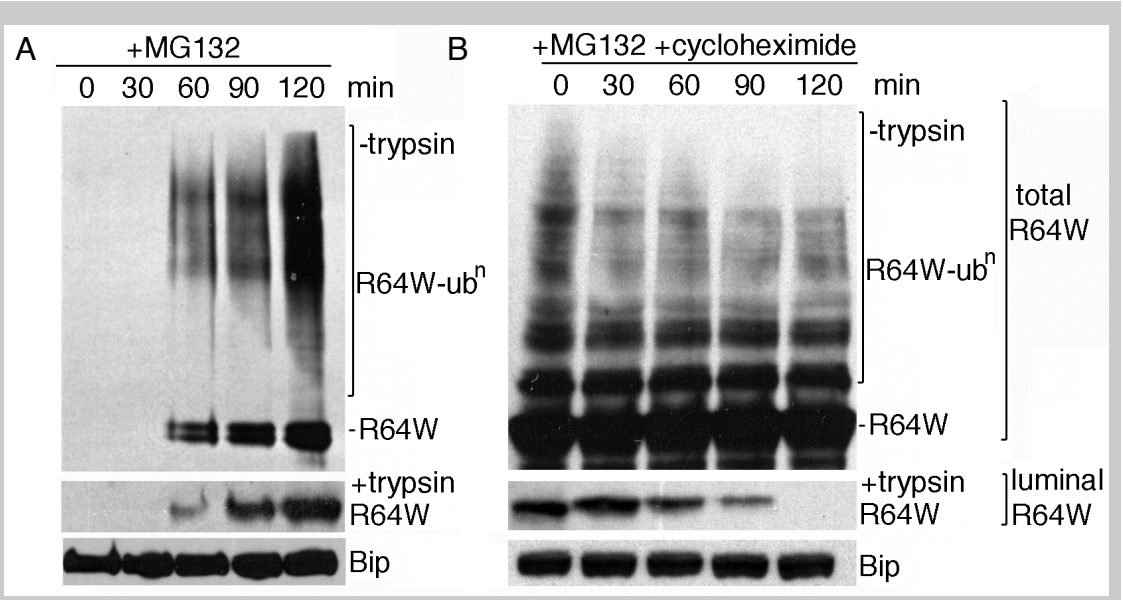

Figure 19. NAT1 R64W is trafficked into (A) and out of (B) the ER lumen. NAT1 R64W was expressed with a "tet-off" system. In (A), cells were harvested at specific time points as indicated after inducing NAT1 R64W expression by removing tetracycline and treating with MG132. In (B), cells were first induced NAT1 R64W expression for 2 hours and then treated with both MG132 and cycloheximide and harvested at 0, 30, 60, 90 and 120 minutes. In both cases, protease protection assays were used to detect the NAT1 R64W protein in the ER lumen (middle panels). Total NAT1 R64W without trypsin digestion was shown in the upper panels and Bip was used as a loading control in the bottom panels.

In the classic ERAD pathway, misfolded ERAD substrates are retrotranslocated from lumen into the cytosol and during this process the protein is ubiquitinated by the E2 and E3 enzymes associated to the ER membrane. In this study, I observed that the ubiquitinated species of NAT1 R64W is almost exclusively in the ER fraction prepared by either ultra-centrifugation or $CaCl_2$ precipitation (Figure 11B and E), which indicates that the ubiquitination happens at the ER membrane. Furthermore, the pulse-chase experiment described above (Figure 19) demonstrated that NAT1 R64W that constantly imports into the ER lumen is exporting out into the cytosol. Taken together, these data suggest that NAT1 R64W is retro-translocated back for ubiquitination at the cytosolic surface of ER membrane after it enters the ER lumen.

However, it is not clear whether translocation into the ER lumen is prerequisite for the ubiquitination of NAT1 R64W from current data. It is possible that a portion of the protein is ubiquitinated at the cytosolic surface of ER membrane without entering the ER lumen.

In summery, our findings show that at least a portion of NAT1 R64W enters the ER lumen and interacts with Bip, and then retro-translocates back to the cytosolic surface of the ER membrane, where it is ubiquitinated. NAT1 R64W is most likely in the ER lumen only transiently, as the majority of the NAT1 R64W is localized at the membrane surface without the proteasome inhibitor as visualized by electron microscopy (Figure 14A and Table 2).

Knock-down of p97, a key component of ERAD, interferes with the degradation of ubiquitinated NAT1 R64W.

I reasoned that if NAT1 R64W is processed through the ER, then established ERAD components may play a role in its degradation. The ATPase p97 plays an overlapping role with a proteasome ATPase in the dislocation of ERAD substrates and RNAi knockdown of p97 protein levels stabilizes some ERAD substrates[132]. I determined that NAT1 R64W co-immunoprecipitates with p97 in the $CaCl_2$ precipitated ER fraction of LLNL-treated cells (Figure 20A). To test whether p97 participates in NAT1 R64W degradation, I reduced its protein levels by RNAi (Figure 20B, top panel). Knock-down of p97 resulted in an inefficient degradation of ubiquitinated NAT1 R64W under normal proteasome activity (Figure 20B, bottom panel, compare lanes 1 and 3), suggesting that p97 is required for robust degradation of ubiquitinated NAT1 R64W.

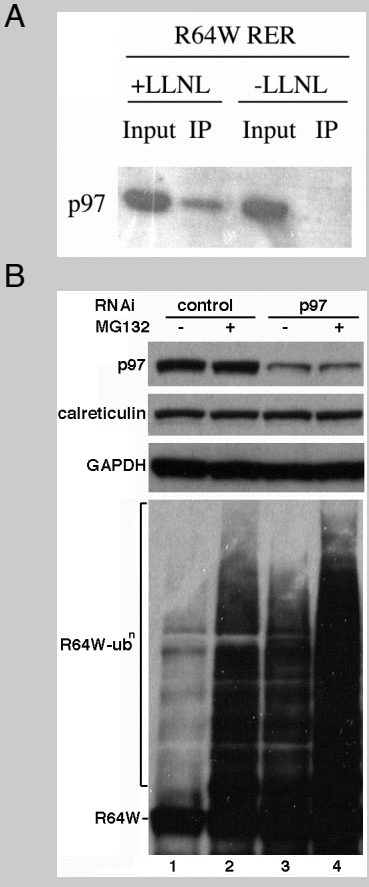

Figure 20. Knockdown of p97 compromises the degradation of ubiquitinated NAT1 R64W. A. p97 co-immunoprecipitates with NAT1 R64W at the ER when proteasome and lysosome is inhibited by LLNL treatment. The ER fraction from HeLa cells transfected with FLAG-NAT1 R64W was enriched by $CaCl_2$ precipitation and used for immunoprecipitation with anti-FLAG antibody. p97 was detected by Western blot with anti-p97 antibody. **B.** p97-RNAi interferes with the efficient degradation of NAT1 R64W ubiquitin conjugates. HeLa cells were transfected with p97-RNAi and 24 hours later with FLAG-NAT1 R64W. Cells were harvested 8 hours after MG132 or DMSO treatment and the lysates prepared with 1% Triton-X100 TBS buffer. Western blot analysis was performed to detect the p97 (upper panel) and NAT1 R64W (lower panel). Calreticulin and GAPDH were used as loading control for ER luminal protein and total protein, respectively.

As p97 functions to dislocate the retro-translocated ERAD substrate from ER membrane into cytosol, I speculated that knockdown of it will result in the accumulation of NAT1 R64W at the ER membrane. However, to our surprise, immunofluorescence experiments did not reveal the perinuclear ER accumulation of NAT1 R64W in p97 knock-down cells (Figure 21). Rather, distributed NAT1 R64W puncta that co-localize with ubiquitin (Figure 21, top panel) but not with the ER membrane protein calnexin (Figure 21, bottom panel) increase in both abundance and size upon p97 knock-down.

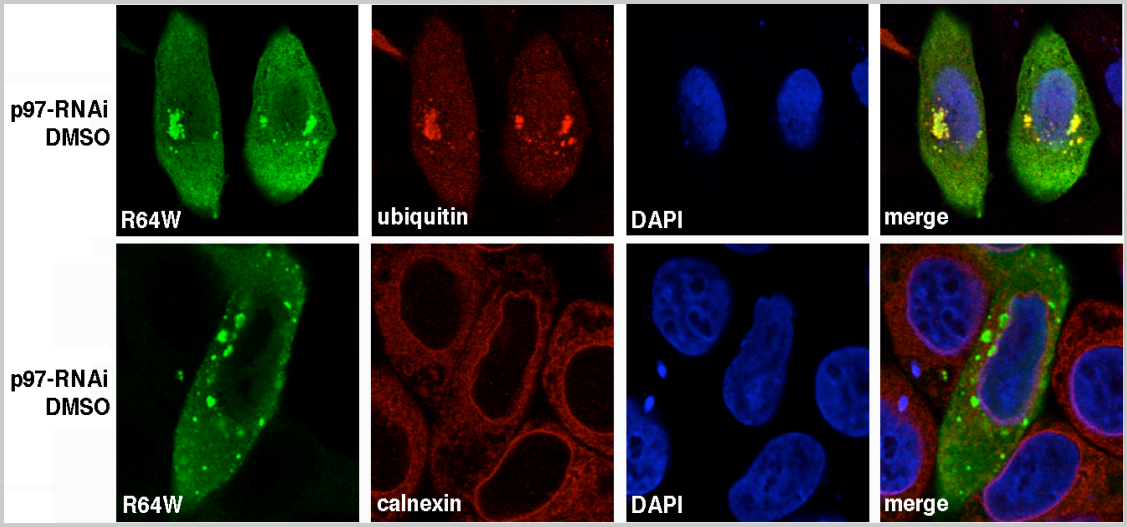

Figure 21. p97 knockdown causes NAT1 R64W to accumulate in puncta that colocalizes with ubiquitin (upper panel), but not calnexin (lower panel). Indirect immunofluorescence was used to detect the localization of NAT1 R64W in HeLa cells co-transfected with p97-siRNA and FLAG-NAT1 R64W. To detect the ubiquitin, HA-ubiquitin was co-transfected with FLAG-NAT1 R64W. Confocal optical section stacks with a Z-depth of 1 mm were collected and only one optical section is displayed for each sample.

Although these punctuated structures do not colocalize significantly with calnexin (Figure 21, bottom panel), they exhibit strong colocalization with LC3B (also named as LC3II), an autophagy marker (Figure 22, first panel). Such co-localization was not observed in cells with endogenous levels of p97 (Figure 22, second panel). It has been shown that p97 inhibition leads to ER stress[132], which can stimulate autophagy[133,134]. Our data suggest that when p97 function is defective, autophagy may be used to destroy NAT1 R64W. In consistent with this model, treating the p97 suppressed cells with choroquine, which inhibits lysosomal degradation, resulted in partial co-localization between NAT1 R64W and the lysosomal marker LAMP1 (Figure 23, middle panel), whereas treatment with VELCADE which specifically inhibit proteasome but not lysosome activity did not (Figure 23, bottom panel).

In contrast, chloroquine treatment of cells expressing endogenous p97 does not change NAT1 R64W localization (Figure 24), indicating that the lysosome does not play a major role in clearing NAT1 R64W aggregates when ERAD function is normal. Moreover, when cells were treated with VELCADE, NAT1 R64W co-localized with LC3B and formed punctuated structures (Figure 22, bottom panel) similar to p97 knock down cells (Figure 22, top panel) but not like the perinuclear accumulation Iobserved for MG132 treated cells. I reasoned that for degradation of NAT1 R64W, the proteasome pathway plays the major role while the autophagy/lysosome pathway is a supplementary process. If the proteasome pathway is compromised, for example by knocking down p97 or by VELCADE treatment, the autophagy pathway takes over. MG132 inhibits both the proteasome and lysosome pathways and therefore, the NAT1 R64W protein accumulates at an earlier step, namely, in the ER. Together, these findings suggest that loss of p97 activity leads to the lysosomal clearance of NAT1 R64W variant via the autophagy pathway.

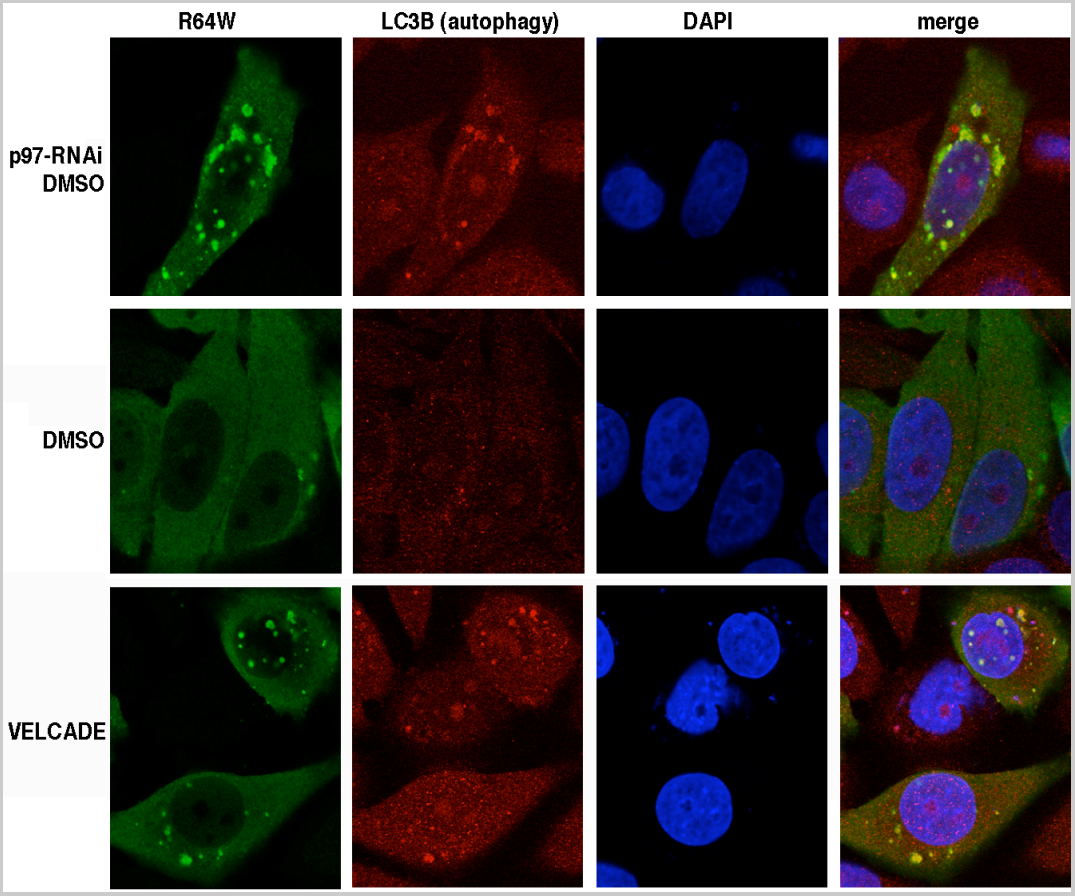

Figure 22. p97 knockdown causes NAT1 R64W to colocalize with autophagy marker LC3B. Indirect immunofluorescence was used to detect the co-localization of NAT1 R64W and autophagy marker LC3B in HeLa cells transfected with FLAG-NAT1 R64W alone (middle and bottom panel), or co-transfected with p97-siRNA and FLAG-NAT1 R64W (top panel). Cells were treated with 20 nM of VELCADE to specifically inhibit proteasome activity (bottom panel). Confocal optical section stacks with a Z-depth of 1 μm were collected and only one optical section is displayed for each sample.

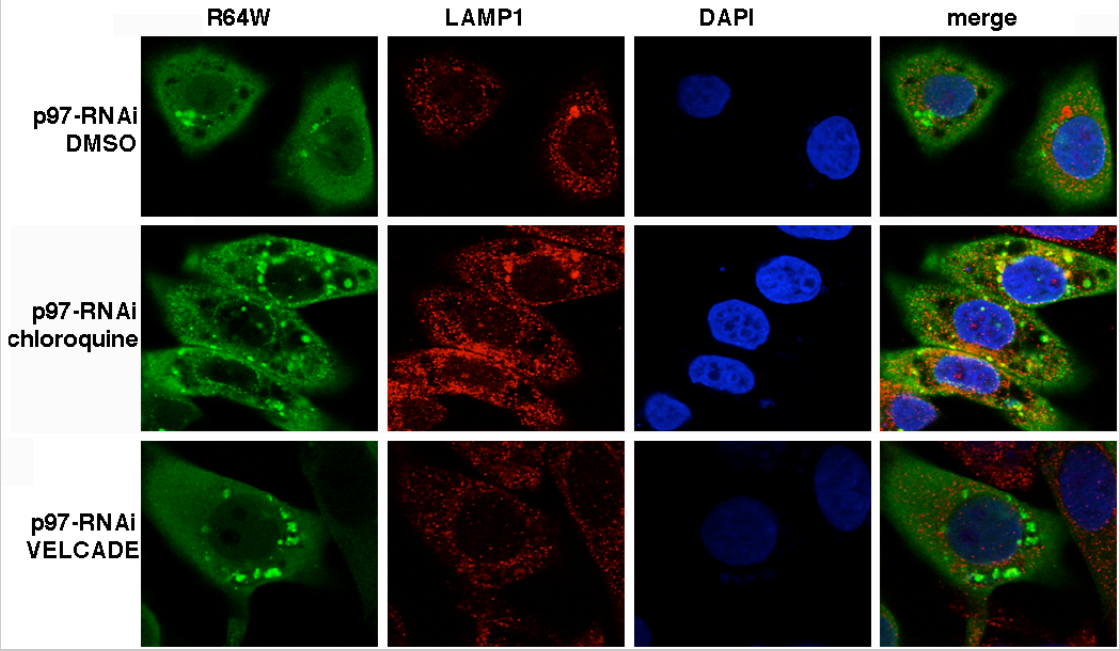

Figure 23. p97 knockdown causes NAT1 R64W to partially colocalize with lysosome marker LAMP1 when treated with lysosome specific inhibitor chloroquine. Indirect immunofluorescence was used to detect the co-localization of NAT1 R64W and lysosome marker LAMP1 in HeLa cells co-transfected with p97-siRNA and FLAG-NAT1 R64W. Cells were treated with 15 μM chloroquine to specifically inhibit lysosomal degradation (middle panel), or 20 nM of velcade to specifically inhibit proteasome (bottom panel). DMSO was used as a control (top panel). Confocal optical section stacks with a Z-depth of 1 μm were collected and only one optical section is displayed for each sample.

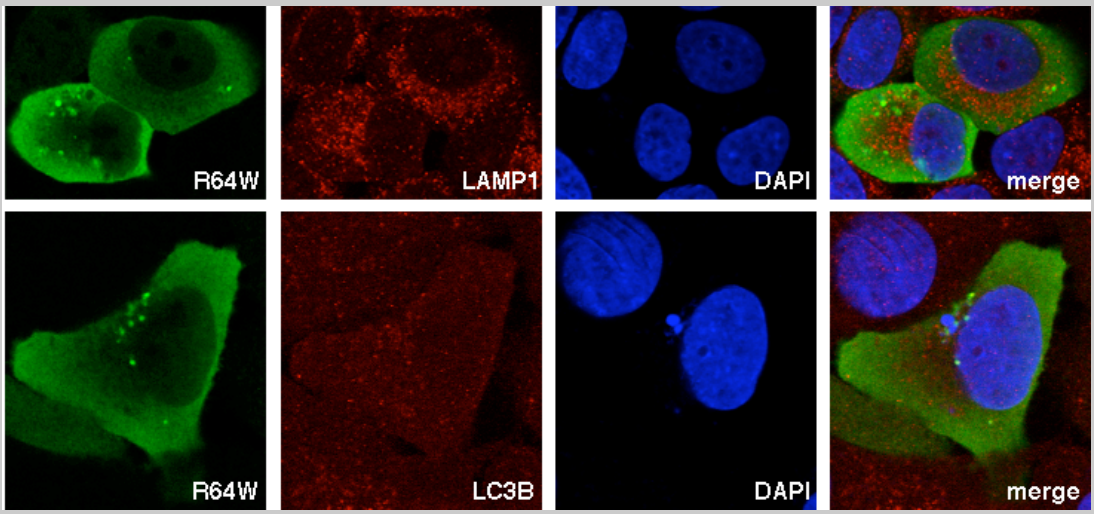

Figure 24. With normal p97 activity, NAT1 R64W puncta does not co-localize with the lysosomal marker LAMP1 or autophagy marker LC3B when lysosome activity is inhibited with chloroquine. HeLa cells transfected with FLAG-NAT1 R64W were treated with 15 μM chloroquine overnight and immunofuorescence was used to detect its colocalization with LAMP1 and LC3B. No significant colocalization was observed between R64W and LAMP1 or LC3B. Confocal optical section stacks with a Z-depth of 1 μm were collected and only one optical section is displayed for each sample.

Human NAT1 R64W is recognized by Hsc70.

To identify how human NAT1 R64W is identified in cells prior to its shuttling to the ER, a gel electrophoresis based proteomics analysis was performed to screen NAT1 R64W binding partners. Cell lysates from HeLa cells expressing FLAG-tagged human NAT1 R64W or "wild-type" protein were used for immunoprecipitation with anti-FLAG antibody. Proteins that co-immunoprecipitated were separated by SDS-PAGE, visualized by silver staining, and specificity established by comparing NAT1 R64W to the "wild-type" protein. In-gel digestion and mass spectrometry* was used to determine identity of putative binding partners, and the interaction verified by using immunoprecipation experiments and Western blot analysis. Hsc70 was identified as a strong binding partner of human NAT1 R64W and not of the "wild-type" protein (Figure 25A). Hsc70 is a multifunctional molecular chaperone abundant in cytosol, which can attach to the cytosolic surface of several organelles' membranes, including the endoplasmic reticulum[135]. I therefore tested whether the interaction occurs in the cytosol and/or the ER by using $CaCl_2$ to enrich for ER, as described previously.

Hsc70 interacted strongly with human NAT1 R64W in the cytosol in both the presence and absence of proteasome inhibitor (Figure 25B). In addition, the interaction was apparent in the ER-enriched fraction, especially after proteasome inhibition with LLNL (Figure 25B, lane 2). A large portion of NAT1 R64W present in the cytosolic fraction is not ubiquitinated (Figure 11E, lane 2). Together, it is suggested that Hsc70 can interact with non-ubiquitinated NAT1 R64W in the cytosol. To test this hypothesis, immunoprecipitation was done with anti-Hsc70 antibody to pull down the Hsc70-associated proteins. NAT1 R64W species were visualized with anti-FLAG antibody to demonstrate that ubiquitination is not required for NAT1 R64W's interactions with Hsc70 (Figure 25C).

* Mass spectrometry analysis was performed by Dr. Cheryl M. Ethen.

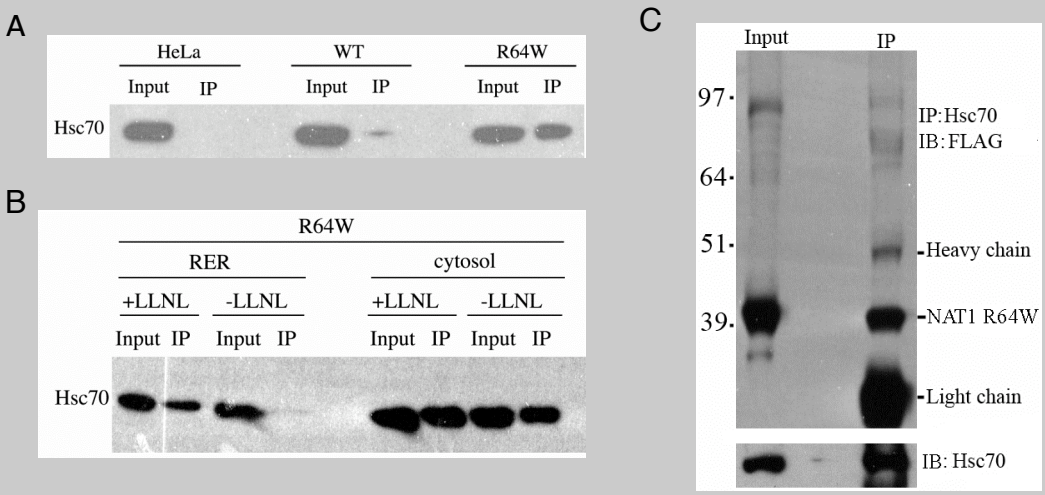

Figure 25. Hsc70 recognizes non-ubiquitinated NAT1 R64W in the cytosol. A. Hsc70 co-immunoprecipitates with NAT1 R64W protein. HeLa cells expressing FLAG-tagged NAT1 R64W were lysed with 1% Triton-X100 buffer, immunoprecipitated by anti-FLAG antibody, and subjected to Western blot analysis with anti-Hsc70 antibody. Input lanes were loaded with 10 μg aliquots of the samples used for immunoprecipitation and IP lanes were loaded with proteins eluted from the beads by SDS loading buffer. Non-transfected HeLa cells (HeLa) and NAT1 "wild-type" transfected cells (WT) were used as controls. **B.** NAT1 R64W interacts with Hsc70 in the cytosol and ER. Cytosolic and ER fractions of HeLa cells transfected with FLAG-tagged NAT1 R64W were separated by $CaCl_2$ precipitation as described in Materials and Methods. Immunoprecipitation was performed for both the ER and cytosol fractions with anti-FLAG antibody and Western blot analysis was performed with anti-Hsc70 antibody. **C.** Hsc70 interacts with non-ubiquitinated NAT1 R64W. HeLa cells transfected with FLAG-tagged NAT1 R64W were lysed by 1% Triton-X100 buffer and 500 μg of total protein immunoprecipitated with anti-Hsc70 antibody. Western blot analysis was achieved with anti-FLAG antibody (upper panel) or anti-Hsc70 antibody (lower panel).

Hsc70 is well known for its role in facilitating protein unfolding/folding, sorting and post-translational transport into different organelles, including the ER[135-137]. It binds to hydrophobic patches of newly synthesized polypeptides to prevent their aggregation and maintain them in a translocation-competent state[138,139]. However, other molecular chaperones may also be involved in recognizing aberrant NAT1 R64W, as Hsp70 and TCP1 were also identified as being immunoprecipitated by NAT1 R64W but not "wild-type" NAT1 by mass spectrometry (Figure 26A, and Table 3). To determine whether Hsc70 plays a non-redundant role in NAT1 R64W protein processing, I suppressed its translation by RNAi to a level that is almost undetectable by Western blot analysis (Figure 26B, upper and second panel). NAT1 R64W protein ubiquitination was unaffected by Hsc70 knockdown (Figure 26B, third panel); however, a significant increase in the Hsp70 protein abundance was observed under this condition (Figure 26B, bottom panel). It is reasonable to speculate that Hsp70 plays a more dominant role in recognizing misfolded NAT1 R64W in the absence of Hsc70.

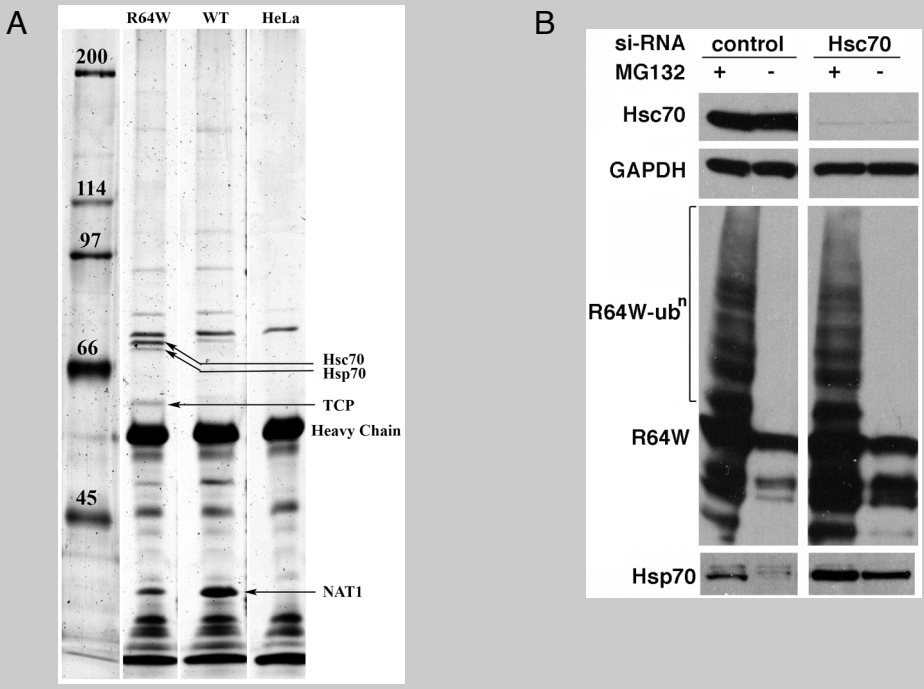

Figure 26. Other molecular chaperons may play redundant role as Hsc70. A. Co-immunoprecipitation and mass spectrometry-based screen identifies Hsc70, Hsp70 and TCP as binding to NAT1 R64W. HeLa cells transfected with FLAG-tagged human NAT1 WT or R64W plasmids were lysed by 1% Triton-X100 TBS buffer and immunoprecipitated by using anti-FLAG antibody. Proteins were eluted by SDS loading buffer and subjected to SDS-PAGE and silver staining. Band labeled as TCP is a mixture of the α and θ subunits of the TCP-1 complex. **B.** Knockdown of Hsc70 by RNAi did not affect the ubiquitination of NAT1 R64W. HeLa cells were transfected with siRNA specific to Hsc70, and FLAG-NAT1 R64W was transfected 48 hours after siRNA transfection. Cells were treated with 20 μm MG132 or DMSO for 8 hours before harvesting. Western blot was used to show the effective knockdown of Hsc70 (top panel). GAPDH is a control for loading and specificity (middle panel). NAT1 R64W is ubiquitinated even in the Hsc70 knockdown cells (third panel). However, Hsp70 is greatly induced when Hsc70 is knocked down (bottom panel).

Table 3. Summary of mass spectrometry identification of proteins.

			MALDI-TOF MS			MS/MS	
Protein	**Accession No.[1]**	**Theoretical MW (Da)**	**Peptides (No.) [2]**	**Cov (%) [3]**	**Score [4] (ppm)**	**Peptide (res) [5]**	**Score [6]**
HSC 70	P11142	71,082	12	27	107 (31)	57-71	71*(26)
						329-342	71*(26)
HSP 70	P08107	70,280	9	20	103 (29)	57-71	81*(23)
						302-311	81*(23)
						329-342	81*(23)
TCP 1α	P17987	60,819	12	26	94 (24)	131-145	27*(23)
						516-526	27*(23)
TCP 1θ	P50990	60,153	9	20	62 (26)	63-74	26*(23)
						441-450	26*(23)

[1] Primary accession number from the Swiss Prot database. [2] Number of peptides whose mass matched the protein. [3] Percent of protein sequence covered by matching peptides. [4] MOWSE score from Mascot analysis; significant scores are >55. Error (ppm) is in parenthesis. [5] Peptide sequenced for the indicated residues. [6] MOWSE score for peptide sequencing. Significant scores are greater than the number in parenthesis, * reflects collective score for sequenced peptides.
Cov, coverage; HSC, heat shock cognate; HSP, heat shock protein; MOWSE, molecular weight search; MW, molecular weight; No., number; ppm, parts per million; res, amino acid residues; TCP, T complex protein.

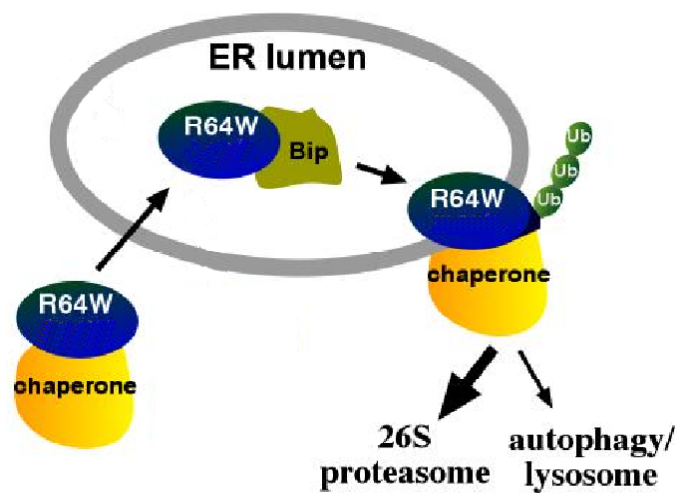

Figure 27. A schematic model of how human NAT1 R64W is removed from cells. NAT1 R64W is recognized in the cytosol by molecular chaperones, and then translocated into the ER lumen, where it interacts with Bip. NAT1 R64W is retro-translocated back to the cytosolic surface of the ER, where it gets ubiquitinated.

Summary

Altogether, our data suggest a broader than anticipated role for the ER in protein quality control. In particular, our data indicate that the gene variation in human NAT1 R64W results in the protein being identified by molecular chaperones including Hsc70 in cytosol, which in turn leads to NAT1 R64W being transported to ER and ultimately into its lumen. The variant protein is ultimately retro-translocated back to the cytosolic surface for ubiquitination and in turn degradation. Our data do not preclude the possibility that some NAT1 R64W is able ubiquitinated at the ER without having entered its lumen. Future experiments are needed to test whether passage through the ER lumen is required for NAT1 R64W ubiquitination and degradation.

Ubiquitinated NAT1 R64W is predominately degraded by the proteasome; however, when this degradation mechanism is compromised, the autophagy / lysosomal pathway is used to remove the aberrant protein (see the model, Figure 27). The endoplasmic reticulum is enriched with chaperones and ubiquitination machinery and is distributed throughout the cytosol. Therefore, the use of the ER as a platform for protein quality control is compelling. In the next chapter, I test whether this pathway is used to dispose of other cytosolic aberrant proteins.

CHAPTER 3

Like NAT1 R64W, parkin R42P is trafficked through ER for its degradation

Introduction

In the previous chapter, I demonstrated that the R64W variant of cytosolic human NAT1 is ubiquitinated and degraded *in vivo* through a novel pathway that unexpectedly, involves the trafficking of this protein through the ER. To investigate whether this pathway is specific to human NAT1 R64W, I studied the proteolysis of another cytosolic protein variant, parkin R42P, which is associated with Parkinson's disease[80].

Parkinson's disease (PD) is the most common neurodegenerative movement disorder and it is characterized by the progressive loss of dopamine neurons. It occurs sporadically with a trend towards aged people and in most cases, without positive family history. Autosomal recessive juvenile parkinsonism (AR-JP) is a rare monogenetic familial form of PD that has an early onset. Mutation of the PARK2 gene is linked with most AR-JP[81]. This gene encodes the E3 ubiquitin ligase parkin, whose function is impaired in familial associated mutations that result in AR-JP[81].

Parkin is a 465 amino acid protein with an N-terminal ubiquitin-like domain (UBL) and an IBR (in-between RING fingers) domain flanking with two RING finger motifs at the C-terminus (Figure 28). Parkin is an E2 dependent RING finger-type E3 ubiquitin ligase[140] that in the presence of E2s, can ubiquitinate a variety of protein substrates, including α-synuclein, Pael-R, synaptotagmin XI, G1/S-specific cyclin E1, and α-synuclein interacting protein synphilin-1. Many of parkin's substrates are involved in the development of neuron degenerative diseases.

The recessive property of parkin mutations in AR-JP patients indicates a loss-of-function pathogenesis. However, the accumulation of parkin substrates such as Pael-R because of the inactivation of parkin activity might cause a toxic gain-of-function effect leading to the final damage of neuron cells[141]. Depending on where the mutations are localized in parkin, the mutated protein will either be rapidly degraded by the proteasome or form protein aggregates[142]. The naturally occurring R42P mutation leads to a misfolded UBL domain[143] and its constitutive degradation by the proteasome[142]. To investigate whether parkin R42P is processed through the same pathway as human NAT1 R64W, I studied the mechanism of its ubiquitination. Although parkin associates with some membrane structures *in vivo*[144], it is not an ERAD substrate. My data indicate that parkin R42P is disposed of in a similar fashion compared to human NAT1 R64W; namely, it is also trafficked into the ER lumen.

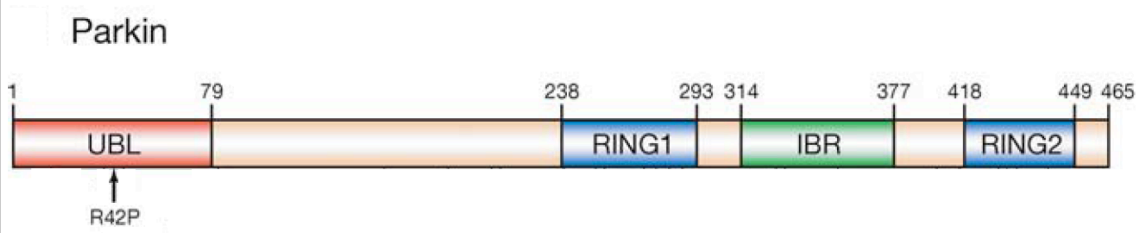

Figure 28. The schematic representation of the domains in protein parkin. The mutation R42P is located in the UBL domain and causes the UBL domain unfolded.

Parkin R42P is routed to the ER

To assess whether other proteins are trafficked from the cytoplasm to the ER for ubiquitination, I studied parkin R42P, which is associated with juvenile Parkinson's disease[80], contains an unfolded N-terminal UBL domain[143] and is constitutively ubiquitinated and degraded[142]. Parkin R42P stably expressed in a neuroblastoma SH-SY5Y cell line[145] accumulates in a perinuclear region that partially colocalizes with calnexin in MG132-treated cells (Figure 29, bottom

panels). The white arrow points to a vesicular structure that is the vacuolated ER where parkin and calnexin are highly co-localized. Parkin was also observed to co-fractionate with ER in LLNL-treated cells (Figure 30A). Compared to NAT1 R64W (Figure 11E, lane 3), less ubiquitinated parkin R42P was observed; however, immunoprecipitation with anti-parkin antibody revealed that a higher molecular weight smear was greatly enhanced in the ER-enriched fraction of LLNL-treated cells compared to the cytosol fraction (Figure 30B) that was confirmed to be ubiquitinated protein by anti-ubiquitin antibody (Figure 30C). Hence, this structurally compromised protein is also trafficked to the ER for ubiquitination.

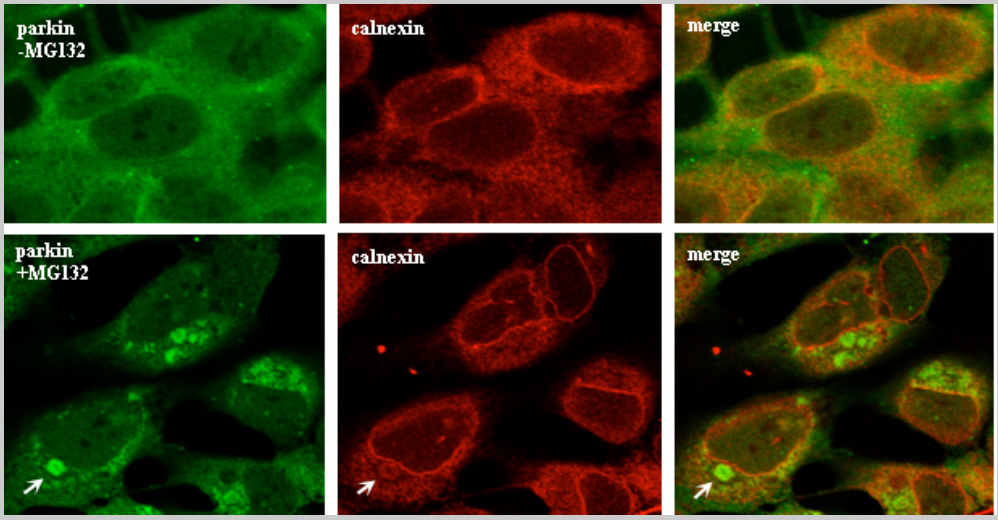

Figure 29. parkin R42P is partially co-localized with ER marker calnexin. Immunofluorescence of SH-SY5Y cells that stably express human parkin R42P (displayed by anti-parkin antibody in green) reveals co-localization of parkin R42P and calnexin (displayed by anti-calnexin antibody in red) after proteasome inhibition. Cells were treated with 20 μM MG132 (bottom panel) or DMSO control (upper panel) for 16 hours and then prepared for immunofluorescence as described in the Materials and Methods. White arrow hightlights one region of clear co-localization between parkin R42P and calnexin. Confocal optical section stacks with a Z-depth of 1μm were collected by using Olympus FluoView FV1000 confocal microscope. One optical section is displayed for each sample.

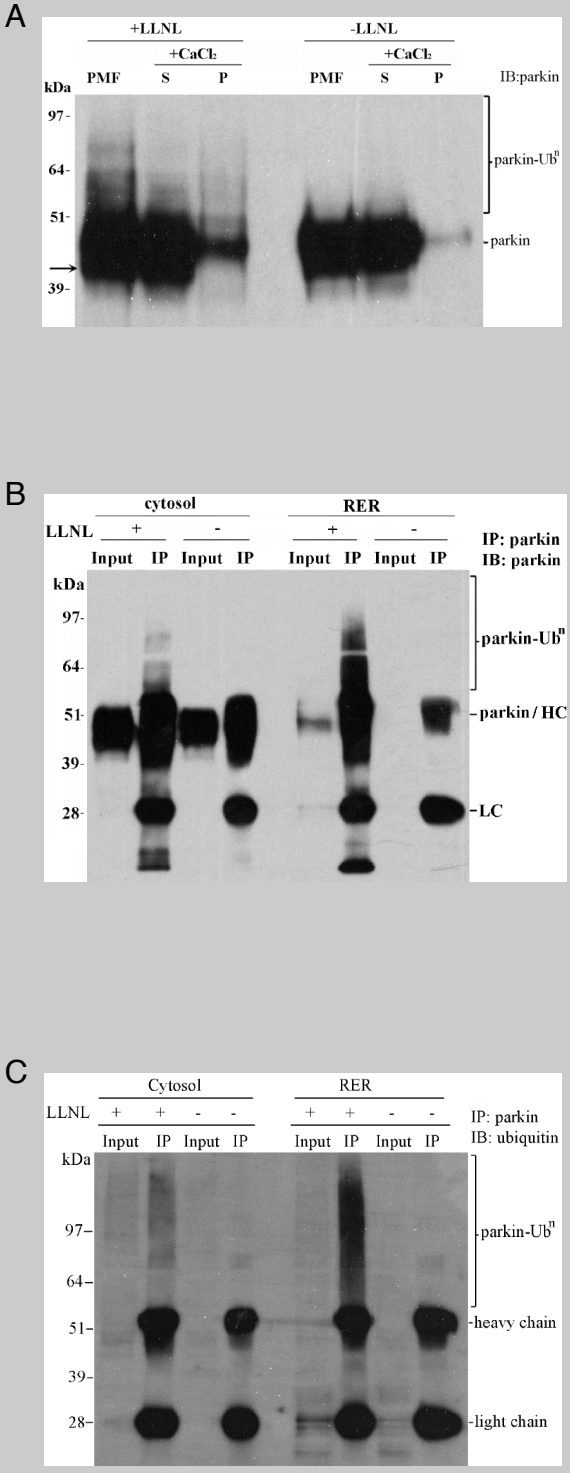

Figure 30. Parkin R42P is ubiquitinated at the endoplasmic reticulum. A. Parkin R42P is present at the ER. The rough ER was enriched by $CaCl_2$ precipitation of the post mitochondrial fraction (PMF) of cell lysate from SH-SY5Y cells that stably express parkin R42P. Western blot analysis using anti-parkin antibody was performed on an ER-enriched pellet (P) and supernatant (S) of cells exposed or not exposed to 50 μM proteasome inhibitor LLNL for 8 hours. The lower band labeled with an arrow is the N-terminally truncated form of parkin. The molecular markers are included on the left and polyubiquitinated parkin species labeled as parkin-Ub^n. **B.** Ubiquitinated parkin R42P is enriched in an ER-enriched fraction. Cytosolic and ER fractions of SH-SY5Y cells expressing parkin R42P were separated by $CaCl_2$ precipitation. Immunoprecipitations were performed with anti-parkin antibody from 700 μg total protein and detected with anti-parkin antibody using Western blotting. 8 μg of total protein was loaded into the input lanes. LC: light chain. HC: heavy chain. N. B. Non-ubiquitinated parkin overlaps with heavy chain. **C**. The higher molecular weight smear is ubiquitinated parkin. Samples were prepared as in Figure 30B, but the Western blot was performed with anti-ubiquitin antibody to detect ubiquitinated parkin R42P protein.

Parkin R42P enters the ER lumen

To test whether parkin R42P similarly enters the ER lumen, immunogold electron microscopy* was performed on SH-SY5Y cells that stably express parkin R42P. Parkin R42P and Bip were labeled with 10 and 20 nm gold particles, respectively. In MG132-treated cells, parkin R42P is abundant in single-membrane bounded vesicles that also contain Bip (Figure 31B). Without such treatment, parkin is largely at the surface of the membrane (Figure 31A), as was also observed for NAT1 R64W (Figure 14).

Quantitative morphometric analysis on the images (Table 4, Figure 31C) revealed parkin R42P's presence in the ER, cytosol and nucleoplasm in DMSO- and MG132-treated cells. Mitochondria was used to estimate background staining with <1% abundance. In the sections analysed, the overall abundance of ER-associated parkin is not significantly affected by MG132 treatment; however, a shift is observed from ~39% at the membrane and ~7% in the lumen under DMSO conditions to ~12% at the membrane and ~31% in the lumen in MG132-treated cells. A correction factor of 9.3 times the observed gold signals was used to estimate the membrane abundance since gold labeling at membranes is intrinsically under-represented[128]. The trend of increased abundance in the ER lumen upon MG132 treatment is not biased by this correction, and is consistent with what was observed in NAT1 R64W (Figure 15).

Furthermore, like NAT1 R64W, parkin R42P also co-immunoprecipitated with Bip in an ER-enriched fraction upon MG132 treatment (Figure 32). Altogether, the unexpected localization to the ER lumen of two unrelated aberrant cytosolic proteins, namely NAT1 R64W and parkin R42P, strongly indicates the existence of a general pathway for misfolded cytosolic proteins that uses ER components in their ubiquitination and degradation.

* Immunogold electron microscopy and quantitative morphometric analysis were performed by Dr. Mark A. Sanders.

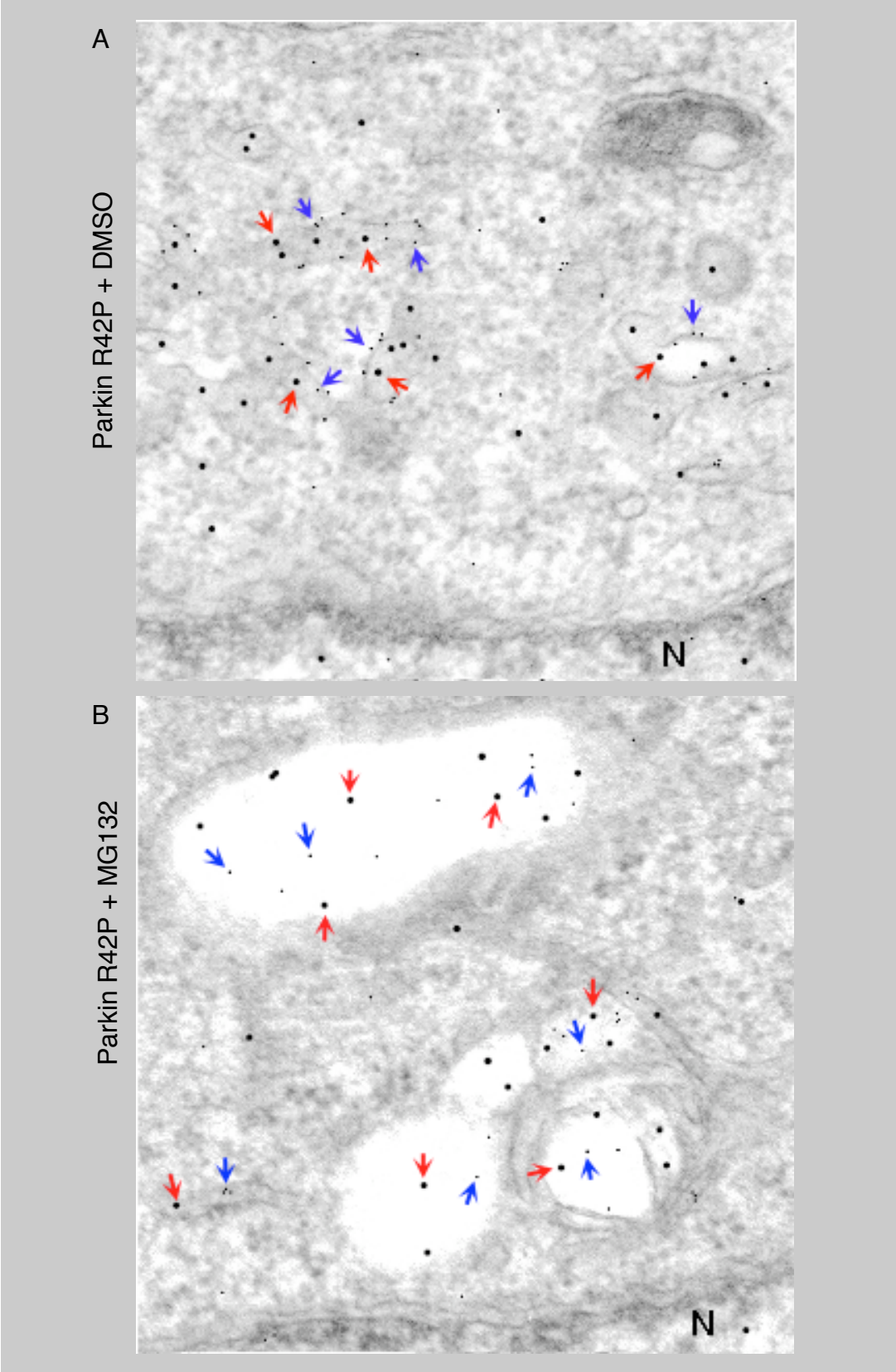
A
Parkin R42P + DMSO
N
B
Parkin R42P + MG132
N

C

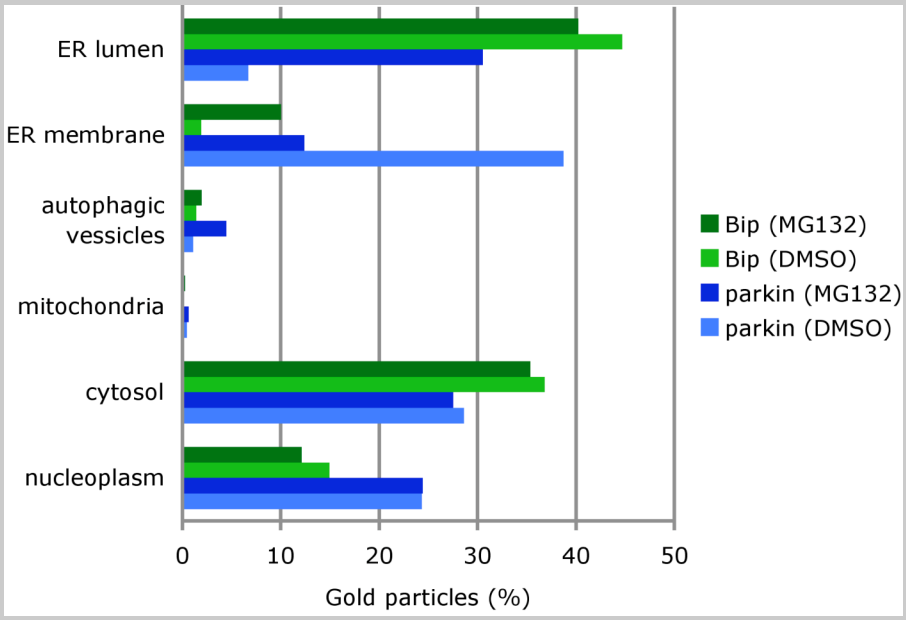

Figure 31. Parkin R42P is transported into the lumen of the endoplasmic reticulum. A, B. Immunogold electron microscopy reveals that parkin R42P and the ER luminal protein Bip colocalize in the lumen of vesicles after the proteasome is inhibited by MG132 (B). In cells treated with DMSO as a control, parkin R42P is largely at the surface of vesicles containing Bip (A). Parkin R42P and Bip labels are indicated by blue and red arrows, respectively. "N" indicates the nucleus. **C.** Quantitative morphometric analysis of SH-SY5Y cells stably expressing parkin R42P reveals that a large portion of this protein is localized at the ER membrane, but accumulates in the ER lumen while protein degradation is inhibited. Gold signals at different cellular compartments were counted for parkin and Bip under either DMSO or MG132 treatment. This plot is an illustrative presentation of data in Table 4.

Table 4. Summary of quantitative morphometric analysis of immunogold labeled parkin R42P and Bip in SH-SY5Y cells.

Parkin R42P (DMSO)		
Cellular compartments	**Observed Gold Particles**	**(%)**
Nucleoplasm	310	24.36%
Cytosol	360	28.61%
Autophagic vessicles	14	1.10%
Mitochondria	6	0.47%
ER membrane	(53) 493*	38.75%
ER lumen	83	6.71%
Total	1272	100.00%
BIP (DMSO)		
Cellular compartments	**Observed Gold Particles**	**(%)**
Nucleoplasm	221	14.93%
Cytosol	570	36.85%
Autophagic vessicles	21	1.42%
Mitochondria	4	0.20%
ER membrane	(3) 27.9*	1.90%
ER lumen	660	44.70%
Total	1476	100.00%
Parkin R42P (MG132)		
Cellular compartments	**Observed Gold Particles**	**(%)**
Nucleoplasm	349	24.44%
Cytosol	393	27.52%
Autophagic vessicles	64	4.48%
Mitochondria	9	0.64%
ER membrane	(19) 176.7*	12.39%
ER lumen	436	30.53%
Total	1251	100.00%
BIP (MG132)		
Cellular compartments	**Observed Gold Particles**	**(%)**
Nucleoplasm	161	12.12%
Cytosol	537	35.37%
Autophagic vessicles	29	1.97%
Mitochondria	4	0.27%
ER membrane	(16) 148.8*	10.04%
ER lumen	594	40.23%
Total	1325	100%

* A correction factor of 9.3 times the observed gold particles (the number in the parenthesis) was used to yield the estimated total number of gold particles at the membrane. This number is in accordance with[128], as described in the text.

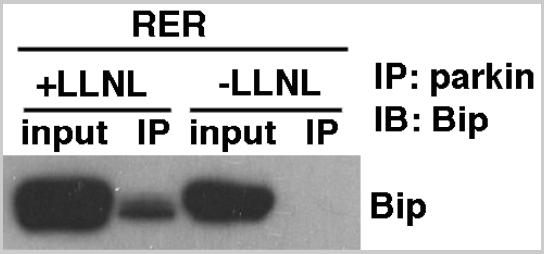

Figure 32. Parkin R42P interacts with the ER luminal Hsp70 protein Bip in the ER. ER-enriched fractions from SH-SY5Y cells stably expressing parkin R42P were dissolved in TBS buffer containing 0.1% SDS and 1% Triton-X100, immunoprecipitated with anti-parkin antibody, and subjected to Western blot analysis with anti-Bip antibody.

Hsc70 recognizes aberrant parkin R42P protein, but not its truncated form.

I tested whether parkin R42P, like NAT1 R64W, is recognized by Hsc70 by performing an immunoprecipitation experiment similar to that of Figure 25B, but using anti-parkin antibody for immunoprecipitation. Similar to our observations with NAT1 R64W, Hsc70 interacts with parkin R42P in the cytosol in both the presence and absence of proteasomal inhibition (Figure 33A). In addition, the parkin R42P:Hsc70 interaction is readily detectable in an ER-enriched sample upon proteasomal inhibition (Figure 33A).

Interestingly, I observed two molecular weight forms of parkin R42P in the post-mitochondrial and cytosolic fractions of Figure 33B. Indeed, parkin exists in human cells as a full-length protein and an N-terminally truncated form that lacks the N-terminal UBL domain[142]. Only full-length parkin R42P protein, whose UBL domain is misfolded[143], was detected in the ER-enriched fraction (Figure 33B, right lane). This finding suggests that misfolding is required for parkin to be shuttled to the ER for ubiquitination. I therefore tested, whether the truncated form of parkin is recognized by Hsc70. Indeed, only full length parkin R42P was co-immunoprecipitated with anti-Hsc70 antibody (Figure 33C).

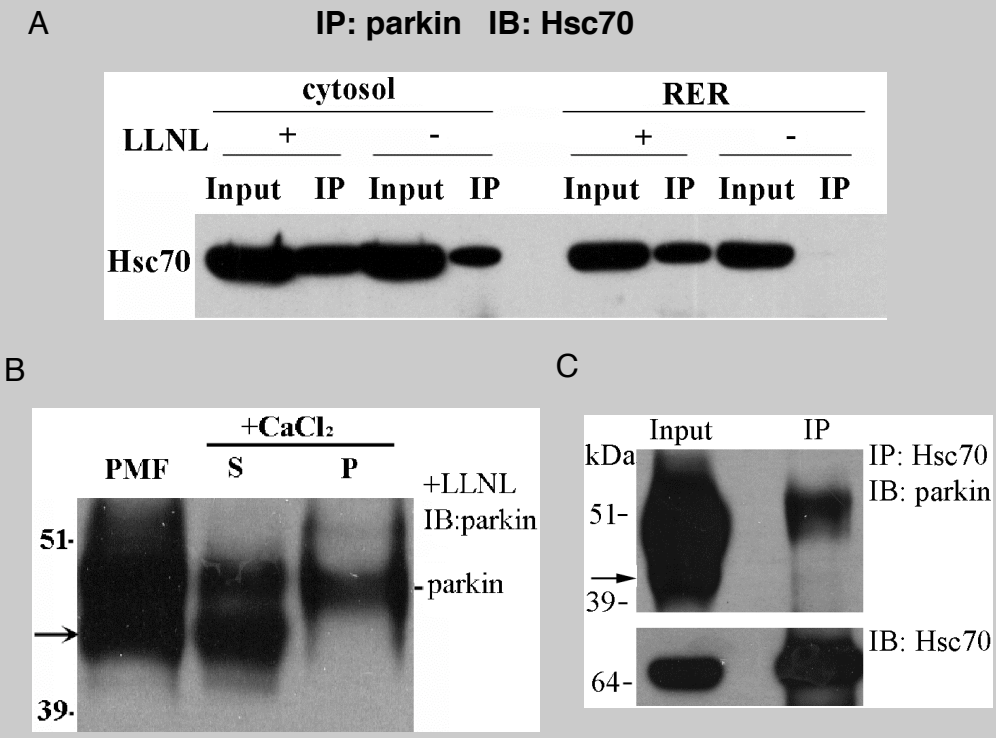

Figure 33. Hsc70 recognizes parkin R42P that has a misfolded N-terminal domain. A. Hsc70 co-immunoprecipitates with parkin R42P in the cytosol independent of proteasomal inhibition, whereas the interaction is greatly enhanced in the ER fraction when cells are treated with LLNL. Samples were prepared as in Figure 30B but the Western blot was probed with anti-Hsc70 antibody. **B.** Only full-length parkin R42P was precipitated into the ER fraction by $CaCl_2$. The experiment was done as described in Figure 30A but with less protein loaded for SDS-PAGE. The lower band labeled with an arrow is the N-terminally truncated form of parkin. **C.** Only full-length parkin is recognized by Hsc70. SH-SY5Y cells expressing parkin R42P were lysed by 1% Triton X-100 and the cell lysates subjected to immunoprecipitation with anti-Hsc70 antibody. Detection was achieved using anti-parkin antibody by Western blotting.

Summary

Iin this chapter, I demonstrate that parkin R42P, which has an unstructured UBL domain, is recruited to the ER for ubiquitination. Ubiquitinated parkin R42P is abundant in an ER-enriched fraction and immunogold labeling and quantitative morphometry revealed that this protein is trafficked into the ER lumen. Like human NAT1 R64W, parkin R42P interacts with Hsc70 in the cytosol, as demonstrated by immunoprecipitation. Interestingly, only full-length but not the truncated parkin R42P interacts with Hsc70 and is recruited to the ER. The correlation between Hsc70 association and ER recruitment is a strong indication that the recognition of aberrant proteins in the cytosol by molecular chaperones is prerequisite for the ER translocation.

Together with previous chapter, my thesis research suggests a common pathway exists to clear misfolded cytosolic proteins that involves recognition in the cytosol by molecular chaperones and in turn trafficking into the ER lumen (Figure 34). Parkin R42P and NAT1 R64W are unrelated cytosolic proteins that have distinct structural deficits; yet, they are processed in the same way.

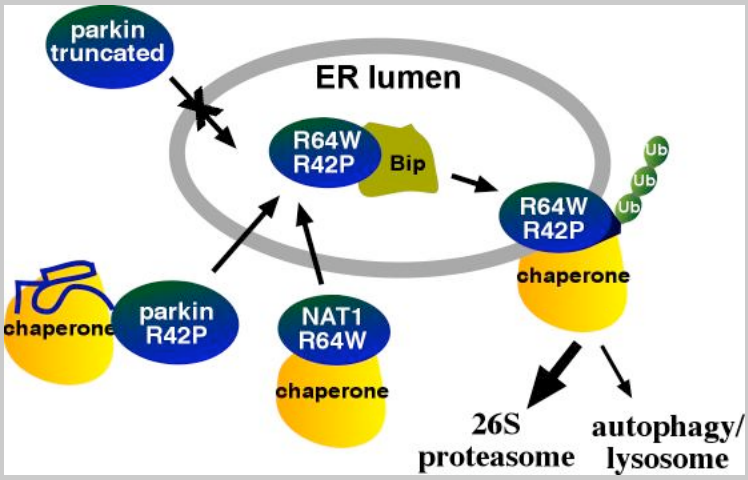

Figure 34. Schematic model of how NAT1 R64W and parkin R42P are removed from cells.

Summary and Discussion

The aggregation of human NAT1 R64W and its ubiquitination

Human arylamine N-acetyltransferases (NATs) can both detoxify and bioactivate arylamines, arylhydrazines and their N-hydroxylated metabolites through the N- or O-acetylation respectively[89,90]. Gene variations within NAT proteins result in a slow acetylator phenotype, which is associated with certain cancer types, the most well-established of which is urinary bladder cancer[79,91,92]. Such variants also exhibit reduced enzymatic activity in cells, which correlates with reduced protein levels but no change in the rate of gene transcription[98]. These early findings are consistent with the report of their constitutive ubiquitination and degradation by the 26S proteasome[82].

In chapter one, I provided a rationale for the constitutive ubiquitination of the protein product of NAT1*17 (R64W), which attributes the reduced cellular activity of this variant[98] to changes in its surface properties that favor protein aggregation. Since recombinant human NAT1 R64W forms inclusion bodies and cannot be solubilized with structural integrity from *E.coli*, I established a model system to study the consequences of the R64W mutation in the NAT1 ortholog, hamster NAT2. I determined that like its human counterpart, hamster NAT2 R64W is constitutively ubiquitinated *in vivo*, whereas the wild-type protein is not. By using different biophysical techniques, I found NAT1 R64W to maintain catalytic activity, overall protein fold and thermostability *in vitro*, but to aggregate both *in vitro* and *in vivo*. Likewise, I found over-expressed human NAT1 R64W to form protein aggregates *in vivo*. These data strongly suggest that the reduced level of cellular enzymatic activity of the R64W variant is not caused by an intrinsic loss of catalytic activity, but rather originates from surface property changes, which lead to its aggregation and recognition by cellular protein quality control systems as a ubiquitination target.

Protein aggregation is a well-established cause for activating protein quality control pathways. Failure to clear protein aggregates properly contributes to the pathogenesis of many neurodegenerative diseases. It is believed that molecular chaperones can disaggregate and refold polypeptides trapped in protein aggregates[5]. Although the mechanisms of protein disaggregation have not been fully unraveled yet, there is evidence for the highly specific cooperation of a Hsp70/Hsp100 bi-chaperone system for this process[5]. One model for the disaggregation process depicts Hsp70 chaperones disentangling polypeptides from aggregates and threading them into the core of the Hsp100 complex for unfolding and refolding[5]. Hsp70 chaperones can transiently associate with hydrophobic segments within substrates, thereby shielding them from aggregation and thereby facilitating proper refolding[146]. In agreement with the Hsp70 chaperone system's role in disaggregation and the prevention of protein aggregation, aggregation-prone human NAT1 R64W strongly associates with the cognate form of Hsp70, namely Hsc70, *in vivo*.

The novel pathway of cytosolic protein quality control involves the trafficking through the ER lumen

The mechanistic pathway for the proteasomal degradation of misfolded cytosolic protein is poorly defined. In the effort to identify cellular components involved in the *in vivo* ubiquitination and degradation of human NAT1 R64W, this research revealed a cytosolic protein quality control pathway that unexpectedly involves trafficking of substrates into the ER lumen. The first implication of the involvement of ER in the ubiquitination of NAT1 R64W comes from the confocal immunofluorescence and cell fractionation experiments, both of which consistently indicate that ubiquitinated NAT1 R64W accumulates at the ER after proteasome and lysosome inhibition. A protease protection assay revealed that a population of NAT1 R64W remains intact when cell lysate is subjected to trypsin digestion, indicating its presence within a membrane compartment. By using

immunogold electron microscopy, NAT1 R64W was visualized to be in the lumen of a single membrane-bound vesicular structures that resemble dilated ER when proteasome and lysosome are inhibited. Immunoprecipitation experiments demonstrated that NAT1 R64W interacts with the ER luminal Hsp70 protein Bip within the ER. Altogether these data indicate that cytosolic NAT1 R64W is recruited into the ER lumen. To verify that misfolded cytosolic proteins enter the ER lumen, N-glycosylation consensus sequences were incorporated in frame, both between the FLAG tag and the NAT1 start codon, and at the very C-terminus. In agreement with the model, NAT1 R64W modified in this manner is N-glycosylated. The generality of this pathway is demonstrated by another aberrant cytosolic protein variant, namely parkin R42P, also being translocated into ER lumen, as illustrated by using immunogold electron microscopy. The ubiquitinated species of parkin R42P accumulates in the ER fraction upon proteasome and lysosomal inhibition as demonstrated by immunoprecipitation after cell fractionation.

Collectively, these data indicate that two functionally unrelated human cytosolic protein variants are trafficked to the ER where they enter its lumen. Since the ubiquitinated species of both NAT1 R64W and parkin R42P accumulate at the ER upon proteasome and lysosome inhibition, I propose that after trafficking into the ER lumen, these proteins are sorted to undergo ubiquitination through a pathway that uses ERAD components. This decision was most likely triggered by their inability to obtain proper folding status. Ultimately, they are retro-translocated from the ER lumen and ubiquitinated at the cytosolic surface of the ER membrane. Whereas the mutation in NAT1 results in an aggregation-prone protein, that in parkin R42P yields an unstructured domain. Nevertheless, they are processed in a similar fashion, which suggests that this novel pathway may be commonly used to dispose of misfolded cytosolic proteins. Altogether, this research provides strong evidence for a broader than anticipated role for the ER in protein quality control.

The ER is competent to serve as a platform for protein quality control, since it is distributed throughout the cytosol and is enriched with chaperones and ubiquitination machinery. Studies in yeast have demonstrated that ER-localized ubiquitination machinery including Ubc6p, Ubc7p-Cue1p and Doa10p that are used by ERAD substrates participate in the degradation of synthetic degron-protein fusions that are cytosolic[52,53]. The current model is that these proteins are directed to the cytoplasmic surface of the ER membrane for ubiquitination prior to their degradation by the proteasome. My data suggest however that misfolded cytosolic protein substrates actually traffick into the ER lumen for degradation.

It is not clear how the trafficking of substrates into ER lumen for their destruction evolved. One possibility is that misfolded cytosolic proteins are forced into this route via strong interaction with Hsc70. The ubiquitous Hsc70 molecular chaperone is well known for its role in facilitating protein post-translational transport into different organelles, including the ER[135-137]. Abell et. al. showed that Hsc70 alone can stimulate the post-translational integration at the ER of a tail-anchored protein in an *in vitro* reconstitution system[137]. Therefore, given the important role of Hsc70 in ER post-translational translocation, human NAT1 R64W and parkin R42P may be forced to transport into ER lumen due to their strong interaction with Hsc70 (Figure 25, 33). Moreover, misfolded ER proteins are refolded to their native conformation in the ER, and if the refolding fails, mechanisms are in place for their ubiquitination and shuttling to the proteasome for degradation. The ER provides a highly specialized compartment for protein quality control, as it is equipped with molecular chaperones, E2s and E3s to perform these functions. By hijacking the route to the ER, cytosolic proteins may possibly use its components for more efficient ubiquitination, or even be rescued from aberrant conformations. Alternatively, taking the ER route for degradation may be a desperate attempt to rid cells of misfolded and aggregation prone cytotoxic proteins despite potentially high energy requirements for import and export. Finally, the translocation of misfolded cytosolic protein into the ER lumen

may facilitate its final destruction by the autophagy/lysosome pathway when the aberrant proteins overwhelm the proteasome pathway. Increasing evidence indicates that the ER can serve as a hub for either proteasomal or lysosome degradation. Consistent with this hypothesis, my data suggest that impairment of ERAD machinery, either by knocking down p97 protein levels or by treating cells with the proteasome specific inhibitor Velcade, triggers the activation of autophagy/lysosome pathway (Figure 22, 23). When both proteasome and lysosome are inhibited by MG132, NAT1 R64W accumulates at an earlier step, the ER (Figure 11, 13, 14).

ER, the hub coordinating autophagy and the ubiquitin-proteasome system?

As noted in Introduction, misfolded ER proteins are degraded by the ubiquitin-proteasome system through the ERAD pathway, in which proteins are retrotranslocated to the cytosolic surface of the ER, ubiquitinated by ER-associated ubiquitination enzymes and in turn degraded by the proteasome either at the ER membrane or after being dislocated into the cytosol. On the other hand, a strong interplay exists between the ER and autophagy. Firstly, the ER is a putative source of autophagic membranes[73]. Secondly, the digestive enzymes functioning in autophagic/lysosomal degradation are synthesized in the ER and matured in the Golgi apparatus. Thirdly, autophagy/lysosomal degradation contributes to the turnover of the ER itself[117]. Most importantly, increasing evidence has recently emerged to indicate that autophagy is activated by ER stress[133,134]and could be used to restore ER homeostasis when the unfolded protein response (UPR) and/or ERAD are overwhelmed. Under certain conditions, some ERAD substrates can be targeted for degradation via autophagy[114-116]. For example, mutated dysferlin that aggregates in the ER impair the retrotranslocon and are degraded via the autophagy/lysosome pathway instead of by ERAD, which is used to degrade the wild-type protein[116]. Together, these observations suggest that the autophagy/lysosome pathway can be used

to remove misfolded ERAD substrates that are normally degraded by the ubiquitin-proteasome system when degradation by the proteasome becomes impaired or overwhelmed.

Canonically, ER turnover or the elimination of misfolded proteins accumulated in the ER by autophagy is believed to occur by engulfment of the whole ER and consequently its associated proteins[147] during the formation of autophagosomes. However, autophagy-independent pathways to direct ER secretory proteins to lysosomes have also been reported[148]. Accumulation of misfolded ER proteins leads to the formation of dilated ER in both yeast and mammalian cells[126,127,149]. Dilated ER can evolve into discrete vacuoles in which aggregated proteins accumulate[150]. By using electron microscopy, Toru et. al. showed that ER subdomains which contain intracisternal granules become dramatically dilated, lose their ribosomes, and sequentially acquire lysosome-type membrane properties and lysosomal enzymes[148]. This work suggests that ER proteins can be degraded by direct conversion of ER cisternae into lysosomes.

It is not clear how the lysosome pathway degrades misfolded cytosolic proteins accumulated in the ER lumen. However, given the great ER vacuolation observed for both parkin R42P and NAT1 R64W under MG132 treatment (Figure 14, 31), it is possible that the misfolded cytosolic proteins are degraded by lysosomes that are directly matured from the ER. If this hypothesis is true, then the transport of cytosolic proteins into ER lumen can greatly facilitate its elimilation by the lysosome pathway when the proteasome is inhibited or overloaded. Altogether, my data indicate that the ER can serve as a platform for degradation of a much wider spectrum of proteins than has been previously anticipated. My findings suggest that the ER is a critical organelle for coordinating different protein quality control pathways not only for ER proteins, but also for cytosolic proteins. Consistent with my observations, ER stress was induced by the cytosolic polyglutamine protein (polyQ72) and autophagy formation activated

as a defense mechanism against cell death, which can result from ER stress induced by polyQ72 aggregation[134,151,152].

Protein misfolding is required for ER translocation and recognition by cytosolic molecular chaperones

NAT1 R64W and parkin R42P require distortions to their protein structure for trafficking to the ER. NAT1 "wild-type" protein is cytosolic, as it is not detected in the $CaCl_2$ pelleted ER fraction (Figure 11C, bottom panel) and it does not co-immunoprecipitate with Bip (Figure 16B). Similarly, the truncated form of parkin R42P, which lacks the N-terminal misfolded UBL domain, is not present in the ER-enriched fraction (Figure 33B); nor is this protein recognized by Hsc70 (Figure 33C). Therefore, a distinct pathway consisting of molecular chaperones may exist to specifically direct structurally compromised and aggregation prone cytosolic proteins to the ER for their ubiquitination and elimination.

For most ubiquitination events, the E3, sometimes with the assistance from E2, recognizes the substrate and determines whether a protein will be ubiquitinated or not. However, it remains elusive whether E2 or E3 enzymes can differentiate misfolded from properly folded proteins. Molecular chaperones may make this distinction prior to association with E2s or E3s. Given the fact that most misfolding involves the inappropriate exposure of hydrophobic segments, it is reasonable to propose that molecular chaperones, instead of E3s, recognize misfolded substrates by their ability to bind hydrophobic fragments.

Indeed, by using immunoprecipitation, both NAT1 R64W and parkin R42P were revealed to interact strongly with molecular chaperone Hsc70 in the cytosolic fraction regardless of proteasome activity (Figure 25B, 31A). Hsc70 interacts with the non-ubiquitinated species of both protein variants (Figure 25C, 33C). These observations suggest that Hsc70 recognizes both proteins in the cytosol and before their ubiquitination. Moreover, only full-length parkin R42P is capable of both Hsc70 association and ER localization whereas the truncated

form can do neither. This strong correlation between Hsc70 association and ER localization observed in the two different forms of parkin R42P strongly indicates that recognition by Hsc70 in the cytosol is required for ER localization; but how or whether association with Hsc70 facilitates the ER luminal translocation is not clear from our current data.

Other molecular chaperones may play a similar role to Hsc70. Hsp70 and subunits of chaperonin TRiC (CCT complex) were identified as strong binding partners for NAT1 R64W by immunoprecitation and mass spectrometry (Figure 27A). When Hsc70 protein levels are suppressed, the expression of Hsp70 is greatly induced and the ubiquitination of NAT1 R64W is not compromised (Figure 27B).

How are misfolded cytosolic proteins transported into the ER lumen?

Our current understanding of ER translocation is based on a model in which a signaling peptide on a protein directs it to the ER. Proteins targeted to the ER have an N-terminal leader peptide, which when synthesized in the cytoplasm, is recognized by the signal-recognition particle (SRP). SRP also wraps around the large ribosome subunit and blocks protein synthesis until it reaches the ER. An SRP receptor in the ER membrane grabs the SRP-ribosome complex and brings it to the translocon, where the newly synthesized polypeptide chain is transferred across the membrane after the SRP and SRP receptor are released. The signaling peptide is cleaved off the growing polypeptide by a peptidase in the ER lumen. However, neither NAT1 nor parkin contains a classic ER signaling sequence, and the wild-type proteins do not enter the ER lumen. This leads to the hypothesis that the variants are probably transported into the ER lumen in an SRP-independent manner, which is most likely post-translational.

Human NAT1 R64W was found to actively flux in and out of ER lumen in pulse-chase experiments (Figure 19), which indicates that a significant population of the protein is transported into the ER lumen and ultimately retrotranslocated

back to the cytosol. When NAT1 R64W's expression was stopped with cycloheximide and degradation inhibited by MG132, there was no evidence of continued NAT1 R64W import into the ER lumen even though a significant pool of this protein is present in the cytoplasm (Figure 19B). This observation suggests that only newly synthesized NAT1 R64W can be imported into the ER lumen, or alternatively, that the cycloheximide treatment interferes with the protein import process.

Whereas both co-translational and post-translational translocation is common in yeast, very few ER proteins in mammalian cells are reported to perform post-translational translocation and the mechanism of transport is not well understood[153]. However, our data indicate that post-translational translocation into the ER lumen may be commonly used by misfolded and aggregation prone cytosolic proteins for quality control purposes in mammalian cells.

Proteins targeted to mitochondria and substrates of chaperone-mediated autophagy are post-translationally transported to their destinations through the molecular chaperone complexes including Hsc70[61]. Hsc70 binds to hydrophobic patches of newly synthesized polypeptides to prevent their aggregation and maintain them in a translocation-competent state[138,139]. In chaperone-mediated autophagy, Hsc70 and its co-chaperones recognize the substrate and target it to LAMP-2A, which forms the translocon on lysosomes[62]. By hydrolysis of ATP, Hsc70 unfolds the substrate and threads it into the translocon. My data demonstrated that human NAT1 R64W and parkin R42P interact with Hsc70 in the cytoplasm and the ER, and it is possible that this interaction is required for translocation. The resulting model then suggests that aberrant cytosolic proteins might be translocated into the ER lumen by using in a similar scenario to that used in chaperone-mediated autophagy.

Some toxins enter the cytosol of host cells by retrograde movement through the secretory pathway after endocytosis via endosomes. Although less

likely, it is also possible that cytosolic proteins are delivered to the ER lumen through retrograde trafficking or compartmental fusion of the autophagic vesicles. My data exclude this model however as no change in the ER accumulation of NAT1 R64W was observed upon inhibition of the formation of autophagosomes with 3-MA treatment (Figure 18).

Conclusions

My data demonstrate that two functionally unrelated human cytosolic protein variants, NAT1 R64W and parkin R42P are ubiquitinated at the ER. They are recognized by Hsc70 in the cytoplasm and trafficked to the ER where they enter its lumen. The data presented here provide new insights into how structurally compromised cytosolic proteins are destroyed. The pathway I have identified differs from ERAD-C, which degrades aberrant ER membrane proteins with misfolded cytosolic domains. Rather, our findings on the ER-mediated ubiquitination of cytosolic NAT1 R64W and parkin R42P share some common features with proteins processed through the ER quality control compartment (ERQC). The ERQC is derived from the ER, exhibits juxtanuclear positioning after proteasome inhibition, and is proposed to be a site for retrotranslocation of ERAD substrates, as the human asialoglycoprotein receptor H2a precursor retrotranslocates from the ERQC in a proteasome-dependent manner[154]. These attributes mirror our results and therefore it may be that ERQC components also contribute to the degradation of aberrant cytosolic proteins. Altogether, our data provide strong evidence for a novel perspective on the ER's role in protein quality control.

Materials and Methods

Preparation of recombinant human and hamster NAT variant proteins from *E. coli*

Prokaryotic expression vector pPH70-hamster-NAT2 and pPH70-human-NAT1 are gifts from Dr. Wagner and Dr. Patrick. Both proteins are expressed as a DHFR fusion protein. NAT variants were generated by site-directed mutagenesis (QuikChange, Strategene) and confirmed by DNA sequencing. Recombinant hamster NAT2 wild-type and R64W protein were expressed and purified from *E. coli* as described previously[101]. All tags are removed during purification, leaving only four additional residues at the N-terminus. ^{15}N labeled protein samples were produced in *E. coli* by growing in M9 minimal media with ^{15}N-labeled ammonium chloride as the only nitrogen source.

Spectroscopy

NMR samples were dissolved in 75 mM $NaPO_4$ pH 6.5, 100 mM NaCl, 0.1% NaN_3 and 10% D_2O. Spectra were acquired at 10°C on a Varian 800 MHz NMR spectrometer. CD spectra were recorded on a Jasco J-710 spectropolarimeter on samples dissolved in 10 mM sodium phosphate buffer at pH 7.0 by using quartz cells with a path-length of 1 mm. For the thermostability measurements, a water circulation temperature control was used and spectra in the far-UV region recorded after five minutes of incubation at temperatures ranging from 20 to 80 ºC.

Dynamic light scattering analysis

The hydrodynamic radius (Rh) of purified recombinant NAT protein was estimated by using a fixed scattering angle of 90° on a DynaPro MSTC Dynamic Light Scattering Instrument (Protein Solution Inc.). Samples were filtered, spun at 13,000 rpm on a bench-top centrifuge for 10 minutes, and subsequently injected

into a quartz cuvette. The data was collected at 10°C, analyzed with DYNAMICS 6.3 and size distributions displayed as regularization graphs.

Sedimentation velocity analysis

Hamster NAT2 R64W protein was prepared at concentrations of 1.67, 0.58 and 0.25 mg/ml in phosphate buffer (75 mM $NaPO_4$, 100 mM NaCl, 1 mM EDTA, and 3-4 mM DTT, pH 6.8) to be used for sedimentation velocity analysis at the National Analytical Ultracentrifugation Facility (NAUF) at the University of Connecticut. Synthetic boundary cells were loaded with 425 μl of buffer and 415 μl of sample. The cells were then accelerated to 15,000 rpm while monitoring the transfer of the excess buffer in each cell. Subsequently, the run was stopped and the rotor inverted gently to thoroughly mix the contents of the cells. After equilibration under vacuum at 10 °C for ~1 hour, the rotor was accelerated to 50,000 rpm. The data at each concentration was analyzed by using a continuous distribution of sedimenting species (c(s)) model in the program Sedfit (version 8.9).

Steady state kinetics analysis

Kinetic assays were conducted with 8, 6, 4, and 2 mM PNPA as the acetyl donor in the presence of a series of fixed concentrations of PABA at 1.2, 0.8, 0.4 and 0.2 mM, respectively. A fixed NAT protein concentration of 8.76 nM was incubated with PABA and PNPA in MOPS buffer (100 mM, pH 7.0, 150 mM NaCl, 0.1 mM DTT). Reactions were initiated by adding PNPA and initial velocities determined by monitoring the linear increase in absorbance at 400 nm due to the formation of p-nitrophenol (ε_{400nm}= 9,400 M^{-1} cm^{-1}). Each concentration combination was measured at 25°C in triplicate. The three known variables: V, [PNPA] and [PABA] were fit to Equation (1) by using the JMP IN software suite as described previously[102], which yielded values for K_{PNPA}, K_{PABA} and V_{max}. The k_{cat} was determined using Equation (2).

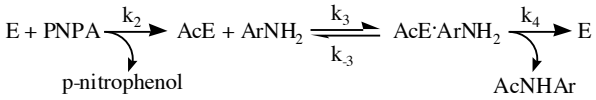

$$V = \frac{V_{\max}[PNPA][PABA]}{K_{PNPA}[PABA] + K_{PABA}[PNPA] + [PNPA][PABA]} \quad (1)$$

$$where K_{PNPA} = \frac{k_4}{k_2}, K_{PABA} = \frac{k_{-3} + k_4}{k_3}$$

$$k_{cat} = \frac{V_{\max}}{[E_t]} = k_4 \quad (2)$$

The rate at which acetyl-NAT hydrolyzes was determined in the absence of an acetyl acceptor with 8 μM NAT and a fixed PNPA concentration of 320 μM. The reactions were conducted in MOPS buffer (100 mM, pH 7.0, 150 mM NaCl, 0.1 mM DTT) and initiated by adding PNPA to NAT. The rate of hydrolysis was determined by monitoring the linear increase at 400 nm due to the formation of p-nitrophenol (l_{400nm}= 9,400 M^{-1} cm^{-1}). The rate of enzyme acetylation (k_2[PNPA]) at 320 μM PNPA is much faster than that of acetyl-enzyme hydrolysis, rendering deacetylation as the rate-limiting step[102]. Therefore, the steady state initial velocity represents k_{H2O} (k_3, Equation 3) and the half-life of acetyl-NAT is calculated by Equation (4).

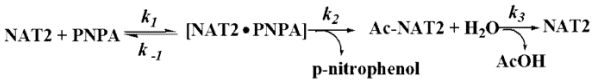

$$V \cong k_3 \times [E] = k_{H_2O} \times [E] \quad (3)$$

$$t_{1/2} = \frac{\ln 2}{k_{H_2O}} \quad (4)$$

Cell culture, drug treatment and plasmid transfection

293T cells and HeLa cells were grown at 37 °C in DMEM supplemented with 10% FBS in a humidified atmosphere of 5% CO_2. SH-SY5Y cells stably expressing parkin R42P were obtained from Dr. Jensen and grown similarly in DMEM supplemented with 10% FBS and containing 25 μg/ml Zeocin (invitrogen) to maintain selectivity. To harvest cells, 0.25% Trypsin-EDTA (Gibco) is used and after washing in PBS, cell pellets stored in -80 °C.

When desired, 20 μM MG132 or 50 μM LLNL (Sigma) were added to inhibit proteasome and lysosome activity; 20 nM VELCADE (LC laboratories) was added to specifically inhibit the proteasome; 15 μM chloroquine (Sigma) was added to inhibit lysosome activity; or 10 mM 3-Methyladenine (Sigma) was added to inhibit autophagy activation; 10 μg/ml cycloheximide (Sigma) was added to inhibit protein synthesis.

The genes encoding NAT wild-type and variant proteins were amplified by PCR from the prokaryotic vectors and cloned into the mammalian expression vector p3FLAG-CMV-7.1 (Sigma) as described previously[82]. Plasmid for HA-ubiquitin is a gift from Dr. Koepp. 293T cells and HeLa cells were transfected with plasmids using LipofectAMINE 2000 transfection reagent (Invitrogen) acording to the manufacturer's instruction.

Western blot and immunoprecipitation assays

In most cases, cells were harvested and lysed with TBS-T buffer (50 mM Tris, pH 7.4, 150 mM NaCl, 1 mM EDTA, 1% Triton X-100) supplemented with protease inhibitor cocktail (Roche) at 4°C for 30 minutes. After centrifugation at 12,000g for 10 minutes, the protein concentration of the supernatant was measured and 5~20 μg of total protein was separated by SDS-PAGE and Western blotted with different antibodies. The protein concentration was measured by the Bradford method (Pierce).

The supernatant of TBS-T lysate was also used for immunoprecipitation. In other cases, the $CaCl_2$ precipitated ER fraction was dissolved in TBS-T buffer containing 0.1% SDS for immunoprecipitation, whereas the supernatant fraction after $CaCl_2$ precipitation was concentrated to ~1 mg/ml by using Amicon Ultra Centrifugal Filter Devices (mass cutoff 5,000 Da, Millipore) before doing the immunoprecipitation.

To detect the ubiquitinated spieces of FLAG-tagged hamster-NAT2 variants, immunoprecipitation was done with 500 μg of total protein by incubating

with EZview Red ANTI-FLAG M2 affinity gel (Sigma) for 2 hours at 4°C. For all other immunoprecipitation experiments, the samples were precleared with protein G sepharose 4B beads (Sigma) at 4 °C for 3 hours or overnight and the beads removed after 12,000g spinning for 30 seconds. Primary antibodies were added to the samples and incubated at 4 °C for 1 hour. 30 μl protein G beads were then added to the samples and incubated for at least 2 hours. After washing the beads with TBS-T buffer 4 times, the proteins were eluted by the addition of SDS loading buffer and boiling for 5 minutes. Samples were subjected to SDS-PAGE and proteins transferred to PVDF membranes for detection using Western blot with different antibodies. The antibodies used in immunoprecipitation and Western blot were listed in Table 5. Films were developed after incubation of the PVDF membranes with ECL Western blotting detection reagents (Amersham).

Indirect immunofluorescence microscopy

HeLa cells were grown in 12-well dishes containing glass cover-slips (Fisher) and treated with different drugs overnight as needed. After rinsing in PBS buffer twice, cells were fixed with 3% paraformaldehyde for 10 minutes at room temperature. Then cells were washed with PBS four times and permeabilized with 0.5% Triton X-100 on ice. After blocking in PBS containing 5% BSA for 30 minutes at 37 °C, cells are incubated with primary antibody cocktail and subsequently secondary antibody cocktail for 60 minutes each at 37 °C with PBS wash in between. The nuclei were stained with 1 μg/ml DAPI (Pierce) for 3 minutes at room temperature. After washing with PBS, cover-slips were mounted with anti-fade reagent and sealed with nail polish painting around the edge. Images were acquired using Olympus FluoView FV1000 confocal microscope. Confocal optical section stacks with a Z-depth of 1 μm were collected and images were processed using Photoshop (Adobe).

Table 5. Antibody dilutions used in the experiments (IB: Wester blot, IP: Immunoprecipitation, IF: immunofluorescence)

Antibody against	Host	Source	Dilution	Comments
FLAG	mouse	Stratagene (200472)	IB 1:1000 IP 1:350 IF 1:1000	Detect FLAG-NAT1
FLAG	rabbit	Sigma F7425	IF 1:250	Detect FLAG-NAT1
HA	rabbit	Sigma H6908	IF 1:100 IB 1:1000	Detect HA-ubiquitin
Hsc70	rat	Abcam ab19136	IB 1:4000 IP 1:100	
Hsp70	mouse	Sigma H5147	IB 1:2000	
NAT1	rabbit	Dr. Edy Sim	IB 1:2000	Detect endogeous NAT1
CHIP	rabbit	Cell signaling 2080	IB 1:1000	
VCP/p97	mouse	Abcam ab11433	IB 1:2000	
VCP/p97	rabbit	Cell signaling 2648	IB 1:1000	
ubiquitin	rabbit	BostonBiochem A-100	IB 1:1000	
parkin	mouse	Sigma P6248	IB 1:5000 IF 1:350	
c-myc	mouse	Sigma M4439	IB 1:2000	
γ-tubulin	mouse	Sigma T6557	IF 1:500	Aggresome marker
dynein	mouse	Sigma D5167	IF 1:500	Aggresome marker
vimentin	mouse	Sigma V6630	IF 1:50	Aggresome marker
LAMP1	rabbit	Abcam ab24170	IF 1:100	Lysosome marker
LC3B	rabbit	Cell signaling 2775	IB 1:1000 IF 1:100	Autophagy marker
calreticulin	Rabbit	Cell signaling 2891	IB 1:1000	ER lumen marker
calreticulin	chicken	Abcam ab14234	IF 1:500	ER lumen marker
GRP78/Bip	rabbit	Sigma G9043	IB 1:3000	ER lumen marker
calnexin	rabbit	Sigma C4731	IB 1:3000 IF 1:250	ER membrane marker
β-actin	mouse	Sigma A5441	IB 1:3000	Loading control
GAPDH	mouse	Sigma G8795	IF 1:5000	Loading control
mouse IgG	goat	Sigma A9917	IB 1:4000	
Rat IgG	goat	Sigma A9037	IB 1:1000	
Rabbit IgG	goat	Sigma A4914	IB 1:5000	
Mouse IgG FITC	goat	Sigma F5262	IF 1:1000	
Rabbit IgG TxRed	Donkey	Pierce 31507	IF: 1:50	

ER enrichment by calcium chloride precipitation

$CaCl_2$ precipitation for ER-enrichment was performed according to the procedure described in the ER isolation kit (Sigma) and as previously described[123]. Briefly, cells were harvested and resuspended in isotonic extraction buffer containing 10 mM HEPES pH 7.8, 250 mM sucrose, 1 mM EGTA and 50 mM potassium chloride supplemented with protease inhibitor cocktail (Roche). Cells were then broken by 10 strokes of Dounce homogenizer and then subjected to differential centrifugation at 1,000g for 10 minutes and then 12,000g for 15 minutes. 7.5 volumes of $CaCl_2$ (8mM) was added dropwise to the supernatant or post mitochondrial fraction (PMF) under continuous stirring at 4 °C. After 15 minutes of additional stirring at 4 °C, the sample was centrifuged at 8,000g for 10 minutes to enrich for ER in the pelleted fraction (Figure 34). The pellet was resuspended in isotonic extraction buffer for Western blot analysis. For immunoprecipitations, the pelleted ER fraction was dissolved in 0.1% SDS, 1% Triton X-100, 50 mM Tris pH 7.4 and 150 mM sodium chloride. A complementary method for ER-enrichment was also performed by using ultracentrifugation, in which the PMF was spun at 100,000g for 60 minutes.

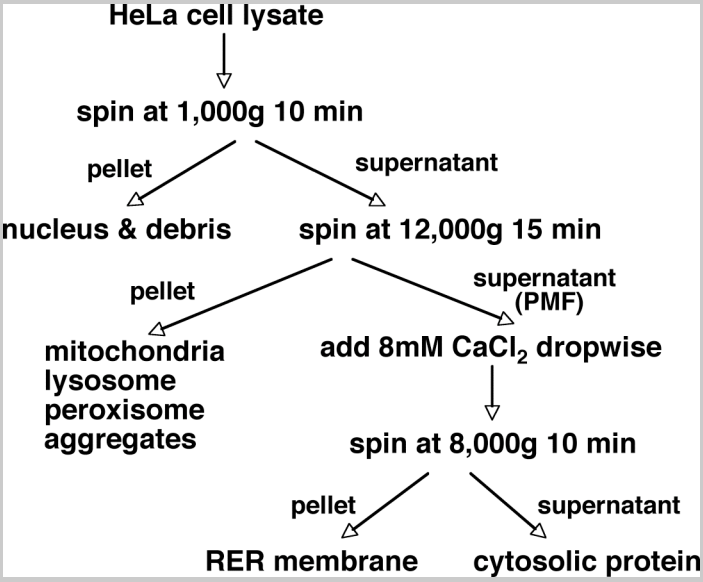

Figure 35. Flowchart of the ER enrichment by calcium precipitation. PMF: post mitochondrial fraction. RER: rough endoplasmic reticulum.

Protease protection assay

Cells were harvested and lysed as described above to obtain the post mitochondrial fraction (PMF). Trypsin (Promega) was added to a final concentration of 50 μg/ml into 20 ml of cell lysate. As a control to break the ER membrane, 10% NP-40 (Roche) was added to the sample to a final concentration of 0.5%. Samples were kept on ice for 2 hours and SDS loading buffer was added to end the reaction. Samples were subject to electrophoresis immediately and electro-blotted onto PVDF membrane for protein detection by Western blot analysis.

Glycosylation assay

A glycosylation tag from human rhodopsin (MNGTEGPNFYVPFSNAT) [130] was engineered between the N-terminal FLAG tag and human NAT1 R64W coding sequence. Another glycosylation tag (NSTL)[129] was then added at the very C-terminal end prior to the NAT1 stop codon. In both cases, underlined amino acids represent glycosylation consensus sequences. HeLa cells were transfected with the NAT1 R64W with the glycosylation sequences incorporated (Glc-NAT1 R64W) and treated with MG132 for 8 hours before harvesting. The cells were lysed by homogenization and the post mitochondrial fraction treated with trypsin as described in the protease protection assay to enrich the ER luminal proteins. The sample was then denatured and incubated with EndoH for 1 hour at 37 °C. Reaction products were separated by SDS-PAGE and visualized by Western blot analysis with anti-FLAG antibody.

RNA interfere assays

Commercially available RNAi molecules against p97 and Hsc70, as well as a negative control were obtained from Ambion, Inc. HeLa cells were transfected for RNAi by using LipofectaminRNAiMAX (Invitrogen) according to

the manufacturer's instruction. DNA was co-transfected 24 hours after RNAi transfection by using Lipofectamine2000 (Invitrogen).

Mass spectrometry

Preparation and analysis of peptides from in-gel trypsin digests of protein bands were as described[155]. Proteins were identified by matrix-assisted laser desorption ionization time-of-flight (MALDI-TOF) mass spectrometry (QSTAR XL quadrupole-TOF mass spectrometer, Applied Biosystems, Inc) using the Swiss Prot database for humans.

Immunogold electron microscopy

Cells were grown on 12 mm round, #1.5 thickness coverslips and fixed in 0.1% glutaraldehyde and 3% formaldehyde in 0.1 M phosphate buffer adjusted to pH 7.4. The samples were washed three times in 0.1 M phosphate buffer and then incubated in freshly prepared 0.1% aqueous sodium borohydride (Sigma Chemical) for 10 min at room temperature to reduce the free aldehyde groups that could contribute to the background signal. The samples were then rinsed in water and dehydrated in an ascending ethanol series up to 100% and embedded in LR White resin (Ted Pella Inc, CA) according to the manufacturer's protocol.

Ultrathin sections (90 nm) were mounted on nickel grids coated with Formvar. Sections were etched in 5% aqueous sodium metaperiodate (Sigma Chemical) for 5 min, rinsed three times with drops of distilled water for 5 min, incubated in freshly prepared 0.1% aqueous sodium borohydride (Sigma Chemical) for 10 min to reduce the free aldehyde groups that could contribute to the background signal, and then washed three times in distilled water for 5 min and labeled as described below.

Sections were double labeled for parkin and Bip, or FLAG and Bip using the indirect immunogold labeling technique. Grids with sections were floated on drops of blocking buffer consisting of PBS, pH 7.2, with 5% normal goat serum,

1% glycerol, 0.1% bovine serum albumin (Fraction V; Sigma), 1% fish skin gelatin, and 0.04% sodium azide (Sigma Chemical) for 15 minutes at room temperature. Specimens were sequentially reacted for 1-2 hours at 4°C with primary antibody consisting of anti-parkin monoclonal antibody at 1:250 dilution or anti-FLAG monoclonal antibody at 1:500 dilution, then washed seven times in droplets of PBS. The sections were incubated with 10 nm gold conjugated goat anti-mouse IgG (1:60 dilution: GE Healthcare, Chalfont Saint Giles, UK). After washing, the sections were exposed to anti-Bip antibody diluted 1:100 in blocking buffer for 1-2 hours. After washing seven times in droplets of PBS, the sections were incubated with 20 nm gold conjugated goat anti-rabbit IgG (1:60 dilution: GE Healthcare, Chalfont Saint Giles, UK), washed another seven times with droplets of PBS, fixed in 2% glutarardehyde, and rinsed eight times with a droplet of water. All sections were stained for 5 minutes with uranyl acetate and 5 minutes with lead citrate before observation on a Phillips CM 12 TEM.

Quantitation of probe density and analysis

The resultant gold probe density was quantified from random micrographs of cell sections as described[156]. To calculate the probe density, 10 (minimum) to 17 (maximum) individual cells were counted for each sample. At least 5 sections were used for analysis in each case. To compare the distributions of gold particles within compartments of different cells or under different conditions, labeling intensity was expressed as a labeling density (LD).

To control for LD changes at membranes influenced by sectioning conditions, I used a critical tilt angle loss calculation determined for epoxy resins by sterology and goniometry[157]. This membrane tilt in sections has been shown to increase LD, but does not decrease it.

The dimensions of the gold particle including the conjugate influences spacing and quantitation. I relied upon including an acceptance zone with a width sufficient to include all membrane-associated labels, but not large enough to

reduce LD occupying the volume of the organelle. For our double-labeling procedure using 10 nm and 20 nm gold, I counted the gold particles within two particle diameters and adopted a 20 nm acceptance zone on each side of a membrane trace of the 10 nm gold labeled proteins. For example, in this volume, each 1 μm length of membrane trace would represent an acceptance zone profile area of 0.04 μm^2 and this would equate to an LD of 25 gold particles per μm^2 for a signal intensity of one particle per μm of membrane of the 10 nm sized gold.

For membrane boundaries, the fraction of total labeled membrane was estimated stereologically using intersections with randomly superimposed test lines[157]. The fractional loss of images is then determined. With these relationships, a fractional loss of membrane traces was determined to be 0.91, which gives a correction factor (*K)* = 9.297[128,158].

Colocalization analysis

Following collection, images were convolved with a 3 x 3 median filtering kernel to minimize system noise. The contribution of unspecific staining was estimated in each image as the mean brightness value exhibited in the region of the cell nucleus plus one standard deviation. Background-corrected brightness values were then obtained by subtracting, pixel by pixel, this value from the original image. A region of interest was also interactively defined to restrict the analysis to a spatially confined area of the image covering the cell plasma membrane for each cell.

Image processing and analysis were performed with the ImagePro Plus image analysis software and using statistics-based colocalization routines within the application. Statistical analysis of the correlation of the intensity values of green and red pixels in a dual-channel image was performed using correlation coefficients that measure the strength of the linear relationship between two grey values of fluorescence intensity pixels of the image pairs. I evaluated the dependency of pixels in separate channel images by plotting the pixel grey

values of the images against each other within the cell outline. The results were displayed in a scatter plot with the intensity of a given pixel in the green image used as the x-coordinate and the intensity of the corresponding pixel in the red image as the y-coordinate. The slope reflects the relative stoichiometry of both fluorochromes, modulated by their relative detection amounts. A complete colocalization situation appears as a cloud centered around a line. The spread of this distribution with respect to the fitted line may be estimated by calculating the correlation coefficient, called Pearson's coefficient (PC).

References

1. Goldberg, A.L. Protein degradation and protection against misfolded or damaged proteins. *Nature* **426**, 895-899 (2003).

2. Schubert, U.*, et al.* Rapid degradation of a large fraction of newly synthesized proteins by proteasomes. *Nature* **404**, 770-774 (2000).

3. Esser, C., Alberti, S. & Hohfeld, J. Cooperation of molecular chaperones with the ubiquitin/proteasome system. *Biochimica et biophysica acta* **1695**, 171-188 (2004).

4. Lee, S. & Tsai, F.T. Molecular chaperones in protein quality control. *Journal of biochemistry and molecular biology* **38**, 259-265 (2005).

5. Liberek, K., Lewandowska, A. & Zietkiewicz, S. Chaperones in control of protein disaggregation. *The EMBO journal* **27**, 328-335 (2008).

6. Stefani, M. & Dobson, C.M. Protein aggregation and aggregate toxicity: new insights into protein folding, misfolding diseases and biological evolution. *Journal of Molecular Medicine (Berlin, Germany)* **81**, 678-699 (2003).

7. Gregersen, N. Protein misfolding disorders: pathogenesis and intervention. *Journal of inherited metabolic disease* **29**, 456-470 (2006).

8. Chaudhuri, T.K. & Paul, S. Protein-misfolding diseases and chaperone-based therapeutic approaches. *The FEBS journal* **273**, 1331-1349 (2006).

9. Rowe, S.M., Miller, S. & Sorscher, E.J. Cystic fibrosis. *The New England journal of medicine* **352**, 1992-2001 (2005).

10. Kulczycki, L.L., Kostuch, M. & Bellanti, J.A. A clinical perspective of cystic fibrosis and new genetic findings: relationship of CFTR mutations to genotype-phenotype manifestations. *American journal of medical genetics.Part A* **116A**, 262-267 (2003).

11. Turnbull, E.L., Rosser, M.F. & Cyr, D.M. The role of the UPS in cystic fibrosis. *BMC biochemistry* **8 Suppl 1**, S11 (2007).

12. Schellenberg, G.D. Early Alzheimer's disease genetics. *Journal of Alzheimer's disease : JAD* **9**, 367-372 (2006).

13. Duyao, M.*, et al.* Trinucleotide repeat length instability and age of onset in Huntington's disease. *Nature genetics* **4**, 387-392 (1993).

14. Cornett, J.*, et al.* Polyglutamine expansion of huntingtin impairs its nuclear export. *Nature genetics* **37**, 198-204 (2005).

15. Richards, R.I. Dynamic mutations: a decade of unstable expanded repeats in human genetic disease. *Human molecular genetics* **10**, 2187-2194 (2001).

16. Uversky, V.N. Neuropathology, biochemistry, and biophysics of alpha-synuclein aggregation. *Journal of neurochemistry* **103**, 17-37 (2007).

17. Konstantinova, I.M., Tsimokha, A.S. & Mittenberg, A.G. Role of proteasomes in cellular regulation. *International review of cell and molecular biology* **267**, 59-124 (2008).

18. Steiner, D.F. & Oyer, P.E. The Biosynthesis of Insulin and a Probable Precursor of Insulin by a Human Islet Cell Adenoma. *Proceedings of the National Academy of Sciences of the United States of America* **57**, 473-480 (1967).

19. Budihardjo, I., Oliver, H., Lutter, M., Luo, X. & Wang, X. Biochemical pathways of caspase activation during apoptosis. *Annual Review of Cell and Developmental Biology* **15**, 269-290 (1999).

20. Saleh, M. Caspase-1 builds a new barrier to infection. *Cell* **126**, 1028-1030 (2006).

21. Pickart, C.M. & Eddins, M.J. Ubiquitin: structures, functions, mechanisms. *Biochimica et biophysica acta* **1695**, 55-72 (2004).

22. Schwartz, D.C. & Hochstrasser, M. A superfamily of protein tags: ubiquitin, SUMO and related modifiers. *Trends in biochemical sciences* **28**, 321-328 (2003).

23. Li, W. & Ye, Y. Polyubiquitin chains: functions, structures, and mechanisms. *Cellular and molecular life sciences : CMLS* **65**, 2397-2406 (2008).

24. Haglund, K., Di Fiore, P.P. & Dikic, I. Distinct monoubiquitin signals in receptor endocytosis. *Trends Biochem Sci* **28**, 598-603 (2003).

25. Ikeda, F. & Dikic, I. Atypical ubiquitin chains: new molecular signals. 'Protein Modifications: Beyond the Usual Suspects' review series. *EMBO reports* **9**, 536-542 (2008).

26. Pickart, C.M. & Fushman, D. Polyubiquitin chains: polymeric protein signals. *Current opinion in chemical biology* **8**, 610-616 (2004).

27. Walz, J.*, et al.* 26S proteasome structure revealed by three-dimensional electron microscopy. *Journal of structural biology* **121**, 19-29 (1998).

28. Verma, R.*, et al.* Role of Rpn11 metalloprotease in deubiquitination and degradation by the 26S proteasome. *Science (New York, N.Y.)* **298**, 611-615 (2002).

29. Adams, J. The proteasome: structure, function, and role in the cell. *Cancer treatment reviews* **29 Suppl 1**, 3-9 (2003).

30. Fang, S. & Weissman, A.M. A field guide to ubiquitylation. *Cellular and molecular life sciences : CMLS* **61**, 1546-1561 (2004).

31. Ho, M.S., Tsai, P.I. & Chien, C.T. F-box proteins: the key to protein degradation. *Journal of Biomedical Science* **13**, 181-191 (2006).

32. Parry, G. & Estelle, M. Regulation of cullin-based ubiquitin ligases by the Nedd8/RUB ubiquitin-like proteins. *Seminars in cell & developmental biology* **15**, 221-229 (2004).

33. Murata, S., Minami, Y., Minami, M., Chiba, T. & Tanaka, K. CHIP is a chaperone-dependent E3 ligase that ubiquitylates unfolded protein. *EMBO reports* **2**, 1133-1138 (2001).

34. Mogk, A., Schmidt, R. & Bukau, B. The N-end rule pathway for regulated proteolysis: prokaryotic and eukaryotic strategies. *Trends in cell biology* **17**, 165-172 (2007).

35. Meusser, B., Hirsch, C., Jarosch, E. & Sommer, T. ERAD: the long road to destruction. *Nature cell biology* **7**, 766-772 (2005).

36. Romisch, K. Endoplasmic reticulum-associated degradation. *Annual Review of Cell and Developmental Biology* **21**, 435-456 (2005).

37. Nishikawa, S., Brodsky, J.L. & Nakatsukasa, K. Roles of molecular chaperones in endoplasmic reticulum (ER) quality control and ER-associated degradation (ERAD). *Journal of Biochemistry* **137**, 551-555 (2005).

38. Carvalho, P., Goder, V. & Rapoport, T.A. Distinct ubiquitin-ligase complexes define convergent pathways for the degradation of ER proteins. *Cell* **126**, 361-373 (2006).

39. Ruddock, L.W. & Molinari, M. N-glycan processing in ER quality control. *Journal of cell science* **119**, 4373-4380 (2006).

40. Nakatsukasa, K. & Brodsky, J.L. The recognition and retrotranslocation of misfolded proteins from the endoplasmic reticulum. *Traffic* **9**, 861-870 (2008).

41. Ye, Y., Meyer, H.H. & Rapoport, T.A. Function of the p97-Ufd1-Npl4 complex in retrotranslocation from the ER to the cytosol: dual recognition of nonubiquitinated polypeptide segments and polyubiquitin chains. *The Journal of cell biology* **162**, 71-84 (2003).

42. Ye, Y., Meyer, H.H. & Rapoport, T.A. The AAA ATPase Cdc48/p97 and its partners transport proteins from the ER into the cytosol. *Nature* **414**, 652-656 (2001).

43. Carlson, E.J., Pitonzo, D. & Skach, W.R. p97 functions as an auxiliary factor to facilitate TM domain extraction during CFTR ER-associated degradation. *The EMBO journal* **25**, 4557-4566 (2006).

44. Lee, R.J.*, et al.* Uncoupling retro-translocation and degradation in the ER-associated degradation of a soluble protein. *The EMBO journal* **23**, 2206-2215 (2004).

45. Mayer, T.U., Braun, T. & Jentsch, S. Role of the proteasome in membrane extraction of a short-lived ER-transmembrane protein. *The EMBO journal* **17**, 3251-3257 (1998).

46. Oberdorf, J., Carlson, E.J. & Skach, W.R. Uncoupling proteasome peptidase and ATPase activities results in cytosolic release of an ER polytopic protein. *Journal of cell science* **119**, 303-313 (2006).

47. Braun, B.C*., et al.* The base of the proteasome regulatory particle exhibits chaperone-like activity. *Nature cell biology* **1**, 221-226 (1999).

48. Enenkel, C., Lehmann, A. & Kloetzel, P.M. Subcellular distribution of proteasomes implicates a major location of protein degradation in the nuclear envelope-ER network in yeast. *The EMBO journal* **17**, 6144-6154 (1998).

49. Frydman, J. Folding of newly translated proteins in vivo: the role of molecular chaperones. *Annual Review of Biochemistry* **70**, 603-647 (2001).

50. McClellan, A.J., Scott, M.D. & Frydman, J. Folding and quality control of the VHL tumor suppressor proceed through distinct chaperone pathways. *Cell* **121**, 739-748 (2005).

51. Park, S.H*., et al.* The cytoplasmic Hsp70 chaperone machinery subjects misfolded and endoplasmic reticulum import-incompetent proteins to degradation via the ubiquitin-proteasome system. *Molecular biology of the cell* **18**, 153-165 (2007).

52. Metzger, M.B., Maurer, M.J., Dancy, B.M. & Michaelis, S. Degradation of a cytosolic protein requires endoplasmic reticulum-associated degradation machinery. *The Journal of biological chemistry* **283**, 32302-32316 (2008).

53. Ravid, T., Kreft, S.G. & Hochstrasser, M. Membrane and soluble substrates of the Doa10 ubiquitin ligase are degraded by distinct pathways. *The EMBO journal* **25**, 533-543 (2006).

54. Kurz, T., Terman, A., Gustafsson, B. & Brunk, U.T. Lysosomes in iron metabolism, ageing and apoptosis. *Histochemistry and cell biology* **129**, 389-406 (2008).

55. Luzio, J.P., Pryor, P.R. & Bright, N.A. Lysosomes: fusion and function. *Nature reviews.Molecular cell biology* **8**, 622-632 (2007).

56. Ding, W.X. & Yin, X.M. Sorting, recognition and activation of the misfolded protein degradation pathways through macroautophagy and the proteasome. *Autophagy* **4**, 141-150 (2008).

57. Cecconi, F. & Levine, B. The role of autophagy in mammalian development: cell makeover rather than cell death. *Developmental cell* **15**, 344-357 (2008).

58. Vyas, J.M., Van der Veen, A.G. & Ploegh, H.L. The known unknowns of antigen processing and presentation. *Nature reviews.Immunology* **8**, 607-618 (2008).

59. Uttenweiler, A. & Mayer, A. Microautophagy in the yeast Saccharomyces cerevisiae. *Methods in molecular biology (Clifton, N.J.)* **445**, 245-259 (2008).

60. Muller, O.*, et al.* Autophagic tubes: vacuolar invaginations involved in lateral membrane sorting and inverse vesicle budding. *The Journal of cell biology* **151**, 519-528 (2000).

61. Majeski, A.E. & Dice, J.F. Mechanisms of chaperone-mediated autophagy. *The international journal of biochemistry & cell biology* **36**, 2435-2444 (2004).

62. Cuervo, A.M. & Dice, J.F. A receptor for the selective uptake and degradation of proteins by lysosomes. *Science (New York, N.Y.)* **273**, 501-503 (1996).

63. Dice, J.F. Chaperone-mediated autophagy. *Autophagy* **3**, 295-299 (2007).

64. Noda, T., Suzuki, K. & Ohsumi, Y. Yeast autophagosomes: de novo formation of a membrane structure. *Trends in cell biology* **12**, 231-235 (2002).

65. Suzuki, K. & Ohsumi, Y. Molecular machinery of autophagosome formation in yeast, Saccharomyces cerevisiae. *FEBS letters* **581**, 2156-2161 (2007).

66. Kabeya, Y.*, et al.* LC3, a mammalian homologue of yeast Apg8p, is localized in autophagosome membranes after processing. *The EMBO journal* **19**, 5720-5728 (2000).

67. Tanida, I., Ueno, T. & Kominami, E. LC3 conjugation system in mammalian autophagy. *The international journal of biochemistry & cell biology* **36**, 2503-2518 (2004).

68. Mizushima, N., Yoshimori, T. & Ohsumi, Y. Role of the Apg12 conjugation system in mammalian autophagy. *The international journal of biochemistry & cell biology* **35**, 553-561 (2003).

69. Mizushima, N.*, et al.* Mouse Apg16L, a novel WD-repeat protein, targets to the autophagic isolation membrane with the Apg12-Apg5 conjugate. *Journal of cell science* **116**, 1679-1688 (2003).

70. Yoshimori, T. & Noda, T. Toward unraveling membrane biogenesis in mammalian autophagy. *Current opinion in cell biology* **20**, 401-407 (2008).

71. Yorimitsu, T. & Klionsky, D.J. Autophagy: molecular machinery for self-eating. *Cell death and differentiation* **12 Suppl 2**, 1542-1552 (2005).

72. Kihara, A., Kabeya, Y., Ohsumi, Y. & Yoshimori, T. Beclin-phosphatidylinositol 3-kinase complex functions at the trans-Golgi network. *EMBO reports* **2**, 330-335 (2001).

73. Juhasz, G. & Neufeld, T.P. Autophagy: a forty-year search for a missing membrane source. *PLoS biology* **4**, e36 (2006).

74. Pankiv, S.*, et al.* p62/SQSTM1 binds directly to Atg8/LC3 to facilitate degradation of ubiquitinated protein aggregates by autophagy. *The Journal of biological chemistry* **282**, 24131-24145 (2007).

75. Kopito, R.R. Aggresomes, inclusion bodies and protein aggregation. *Trends in cell biology* **10**, 524-530 (2000).

76. Johnston, J.A., Ward, C.L. & Kopito, R.R. Aggresomes: a cellular response to misfolded proteins. *J Cell Biol* **143**, 1883-1898 (1998).

77. Kaganovich, D., Kopito, R. & Frydman, J. Misfolded proteins partition between two distinct quality control compartments. *Nature* **454**, 1088-1095 (2008).

78. M, L.G., Jr.*, et al.* N-acetyltransferase phenotype and risk in urinary bladder cancer: approaches in molecular epidemiology. Preliminary results in Sweden and Denmark. *Environ Health Perspect* **29**, 71-79 (1979).

79. Garcia-Closas, M.*, et al.* NAT2 slow acetylation, GSTM1 null genotype, and risk of bladder cancer: results from the Spanish Bladder Cancer Study and meta-analyses. *Lancet* **366**, 649-659 (2005).

80. Terreni, L., Calabrese, E., Calella, A.M., Forloni, G. & Mariani, C. New mutation (R42P) of the parkin gene in the ubiquitinlike domain associated with parkinsonism. *Neurology* **56**, 463-466 (2001).

81. Kitada, T.*, et al.* Mutations in the parkin gene cause autosomal recessive juvenile parkinsonism. *Nature* **392**, 605-608 (1998).

82. Butcher, N.J., Arulpragasam, A. & Minchin, R.F. Proteasomal degradation of N-acetyltransferase 1 is prevented by acetylation of the active site cysteine: a mechanism for the slow acetylator phenotype and substrate-dependent down-regulation. *The Journal of biological chemistry* **279**, 22131-22137 (2004).

83. Evans, D.A. N-acetyltransferase. *Pharmacol Ther* **42**, 157-234 (1989).

84. Weber, W.W. & Hein, D.W. N-acetylation pharmacogenetics. *Pharmacol Rev* **37**, 25-79 (1985).

85. Riddle, B. & Jencks, W.P. Acetyl-coenzyme A: arylamine N-acetyltransferase. Role of the acetyl-enzyme intermediate and the effects of substituents on the rate. *J Biol Chem* **246**, 3250-3258 (1971).

86. Hughes, H.B. On the metabolic fate of isoniazid. *J Pharmacol Exp Ther* **109**, 444-452 (1953).

87. Minchin, R.F. Acetylation of p-aminobenzoylglutamate, a folic acid catabolite, by recombinant human arylamine N-acetyltransferase and U937 cells. *Biochem J* **307 (Pt 1)**, 1-3 (1995).

88. Upton, A.*, et al.* Placental arylamine N-acetyltransferase type 1: potential contributory source of urinary folate catabolite p-acetamidobenzoylglutamate during pregnancy. *Biochim Biophys Acta* **1524**, 143-148 (2000).

89. Hein, D.W.*, et al.* Acetyltransferases and susceptibility to chemicals. *Toxicol Lett* **64-65 Spec No**, 123-130 (1992).

90. Vineis, P.*, et al.* Genetically based N-acetyltransferase metabolic polymorphism and low-level environmental exposure to carcinogens. *Nature* **369**, 154-156 (1994).

91. Hanna, P.E. N-acetyltransferases, O-acetyltransferases, and N,O-acetyltransferases: enzymology and bioactivation. *Adv Pharmacol* **27**, 401-430 (1994).

92. Yu, M.C.*, et al.* Acetylator phenotype, aminobiphenyl-hemoglobin adduct levels, and bladder cancer risk in white, black, and Asian men in Los Angeles, California. *J Natl Cancer Inst* **86**, 712-716 (1994).

93. Gu, J., Liang, D., Wang, Y., Lu, C. & Wu, X. Effects of N-acetyl transferase 1 and 2 polymorphisms on bladder cancer risk in Caucasians. *Mutat Res* **581**, 97-104 (2005).

94. Filiadis, I.F.*, et al.* Genotypes of N-acetyltransferase-2 and risk of bladder cancer: a case-control study. *J Urol* **161**, 1672-1675 (1999).

95. Okkels, H., Sigsgaard, T., Wolf, H. & Autrup, H. Arylamine N-acetyltransferase 1 (NAT1) and 2 (NAT2) polymorphisms in susceptibility to bladder cancer: the influence of smoking. *Cancer Epidemiol Biomarkers Prev* **6**, 225-231 (1997).

96. Brockmoller, J., Cascorbi, I., Kerb, R. & Roots, I. Combined analysis of inherited polymorphisms in arylamine N-acetyltransferase 2, glutathione S-transferases M1 and T1, microsomal epoxide hydrolase, and cytochrome P450 enzymes as modulators of bladder cancer risk. *Cancer Res* **56**, 3915-3925 (1996).

97. Hein, D.W.*, et al.* Molecular genetics and epidemiology of the NAT1 and NAT2 acetylation polymorphisms. *Cancer Epidemiol Biomarkers Prev* **9**, 29-42 (2000).

98. Hein, D.W. Molecular genetics and function of NAT1 and NAT2: role in aromatic amine metabolism and carcinogenesis. *Mutat Res* **506-507**, 65-77 (2002).

99. Sinclair, J.C., Sandy, J., Delgoda, R., Sim, E. & Noble, M.E. Structure of arylamine N-acetyltransferase reveals a catalytic triad. *Nat Struct Biol* **7**, 560-564 (2000).

100. Sandy, J.*, et al.* The structure of arylamine N-acetyltransferase from Mycobacterium smegmatis--an enzyme which inactivates the anti-tubercular drug, isoniazid. *J Mol Biol* **318**, 1071-1083 (2002).

101. Wang, H.*, et al.* Overexpression, purification, and characterization of recombinant human arylamine N-acetyltransferase 1. *Protein J.* **24**, 65-75 (2005).

102. Wang, H., Liu, L., Hanna, P.E. & Wagner, C.R. The Catalytic Mechanism of Hamster Arylamine N-Acetyltransferase 2. *Biochemistry* **44**, 11295-11306 (2005).

103. Sticha, K.R., Sieg, C.A., Bergstrom, C.P., Hanna, P.E. & Wagner, C.R. Overexpression and large-scale purification of recombinant hamster polymorphic arylamine N-acetyltransferase as a dihydrofolate reductase fusion protein. *Protein Expr Purif* **10**, 141-153 (1997).

104. Treier, M., Staszewski, L.M. & Bohmann, D. Ubiquitin-dependent c-Jun degradation in vivo is mediated by the delta domain. *Cell* **78**, 787-798 (1994).

105. Matsuo, H.*, et al.* Identification by NMR Spectroscopy of Residues at Contact Surfaces in Large, Slowly Exchanging Macromolecular Complexes. *J. Am. Chem. Soc.* **121**, 9903-9904 (1999).

106. Kawamura, A.*, et al.* Eukaryotic arylamine N-acetyltransferase Investigation of substrate specificity by high-throughput screening. *Biochem Pharmacol* **69**, 347-359 (2005).

107. Wang, H., Vath, G.M., Gleason, K.J., Hanna, P.E. & Wagner, C.R. Probing the mechanism of hamster arylamine N-acetyltransferase 2 acetylation by active site modification, site-directed mutagenesis, and pre-steady state and steady state kinetic studies. *Biochemistry* **43**, 8234-8246 (2004).

108. Simons, K.T., Bonneau, R., Ruczinski, I. & Baker, D. Ab initio protein structure prediction of CASP III targets using ROSETTA. *Proteins* **Suppl 3**, 171-176 (1999).

109. Wu, H.*, et al.* Structural basis of substrate-binding specificity of human arylamine N-acetyltransferases. *The Journal of biological chemistry* **282**, 30189-30197 (2007).

110. Zang, Y., Zhao, S., Doll, M.A., States, J.C. & Hein, D.W. The T341C (Ile114Thr) polymorphism of N-acetyltransferase 2 yields slow acetylator phenotype by enhanced protein degradation. *Pharmacogenetics* **14**, 717-723 (2004).

111. Hampton, R.Y. ER-associated degradation in protein quality control and cellular regulation. *Current opinion in cell biology* **14**, 476-482 (2002).

112. Klionsky, D.J. & Emr, S.D. Autophagy as a regulated pathway of cellular degradation. *Science (New York, N.Y.)* **290**, 1717-1721 (2000).

113. Fortun, J., Dunn, W.A., Jr., Joy, S., Li, J. & Notterpek, L. Emerging role for autophagy in the removal of aggresomes in Schwann cells. *The Journal of neuroscience : the official journal of the Society for Neuroscience* **23**, 10672-10680 (2003).

114. Perlmutter, D.H. The role of autophagy in alpha-1-antitrypsin deficiency: a specific cellular response in genetic diseases associated with aggregation-prone proteins. *Autophagy* **2**, 258-263 (2006).

115. Teckman, J.H. & Perlmutter, D.H. Retention of mutant alpha(1)-antitrypsin Z in endoplasmic reticulum is associated with an autophagic response. *Am J Physiol Gastrointest Liver Physiol* **279**, G961-974 (2000).

116. Fujita, E.*, et al.* Two endoplasmic reticulum-associated degradation (ERAD) systems for the novel variant of the mutant dysferlin: ubiquitin/proteasome ERAD(I) and autophagy/lysosome ERAD(II). *Human molecular genetics* **16**, 618-629 (2007).

117. Yorimitsu, T. & Klionsky, D.J. Eating the endoplasmic reticulum: quality control by autophagy. *Trends Cell Biol* **17**, 279-285 (2007).

118. Yorimitsu, T., Nair, U., Yang, Z. & Klionsky, D.J. Endoplasmic reticulum stress triggers autophagy. *The Journal of biological chemistry* **281**, 30299-30304 (2006).

119. Liu, F.*, et al.* Arylamine N-acetyltransferase aggregation and constitutive ubiquitylation. *Journal of Molecular Biology* **361**, 482-492 (2006).

120. Verhoef, L.G., Lindsten, K., Masucci, M.G. & Dantuma, N.P. Aggregate formation inhibits proteasomal degradation of polyglutamine proteins. *Hum Mol Genet* **11**, 2689-2700 (2002).

121. Johnston, J.A., Illing, M.E. & Kopito, R.R. Cytoplasmic dynein/dynactin mediates the assembly of aggresomes. *Cell Motil Cytoskeleton* **53**, 26-38 (2002).

122. Depierre, J., Dallner, G. & Maddy, A.H. Biochemical Analysis of Membranes. in *Biochemical Analysis of Membranes* (ed. Anonymous) 79-131 (John Wiley, New York, 1976).

123. Hamilton, R.L., Moorehouse, A., Lear, S.R., Wong, J.S. & Erickson, S.K. A rapid calcium precipitation method of recovering large amounts of highly pure hepatocyte rough endoplasmic reticulum. *J Lipid Res* **40**, 1140-1147 (1999).

124. Sunaga, K., Takahashi, H., Chuang, D.M. & Ishitani, R. Glyceraldehyde-3-phosphate dehydrogenase is over-expressed during apoptotic death of neuronal cultures and is recognized by a monoclonal antibody against amyloid plaques from Alzheimer's brain. *Neurosci Lett* **200**, 133-136 (1995).

125. Cumming, R.C. & Schubert, D. Amyloid-beta induces disulfide bonding and aggregation of GAPDH in Alzheimer's disease. *FASEB J* **19**, 2060-2062 (2005).

126. Shepshelovich, J.*, et al.* Protein synthesis inhibitors and the chemical chaperone TMAO reverse endoplasmic reticulum perturbation induced by overexpression of the iodide transporter pendrin. *J Cell Sci* **118**, 1577-1586 (2005).

127. Mimnaugh, E.G., Xu, W., Vos, M., Yuan, X. & Neckers, L. Endoplasmic reticulum vacuolization and valosin-containing protein relocalization result from simultaneous hsp90 inhibition by geldanamycin and proteasome inhibition by velcade. *Mol Cancer Res* **4**, 667-681 (2006).

128. Mayhew, T.M. & Lucocq, J.M. Quantifying immunogold labelling patterns of cellular compartments when they comprise mixtures of membranes (surface-occupying) and organelles (volume-occupying). *Histochemistry and cell biology* **129**, 367-378 (2008).

129. Plemper, R.K., Deak, P.M., Otto, R.T. & Wolf, D.H. Re-entering the translocon from the lumenal side of the endoplasmic reticulum. Studies on mutated carboxypeptidase yscY species. *FEBS Lett* **443**, 241-245 (1999).

130. Milger, K.*, et al.* Cellular uptake of fatty acids driven by the ER-localized acyl-CoA synthetase FATP4. *J Cell Sci* **119**, 4678-4688 (2006).

131. Lieblich, J.M., Weintraub, B.D., Rosen, S.W., Chou, J.Y. & Robinson, J.C. HeLa cells secrete alpha subunit of glycoprotein tropic hormones. *Nature* **260**, 530-532 (1976).

132. Wojcik, C.*, et al.* Valosin-containing protein (p97) is a regulator of endoplasmic reticulum stress and of the degradation of N-end rule and ubiquitin-fusion degradation pathway substrates in mammalian cells. *Mol Biol Cell* **17**, 4606-4618 (2006).

133. Ogata, M.*, et al.* Autophagy is activated for cell survival after endoplasmic reticulum stress. *Mol Cell Biol* **26**, 9220-9231 (2006).

134. Kouroku, Y.*, et al.* ER stress (PERK/eIF2alpha phosphorylation) mediates the polyglutamine-induced LC3 conversion, an essential step for autophagy formation. *Cell death and differentiation* **14**, 230-239 (2007).

135. Ngosuwan, J., Wang, N.M., Fung, K.L. & Chirico, W.J. Roles of cytosolic Hsp70 and Hsp40 molecular chaperones in post-translational translocation of presecretory proteins into the endoplasmic reticulum. *J Biol Chem* **278**, 7034-7042 (2003).

136. Chirico, W.J., Waters, M.G. & Blobel, G. 70K heat shock related proteins stimulate protein translocation into microsomes. *Nature* **332**, 805-810 (1988).

137. Abell, B.M., Rabu, C., Leznicki, P., Young, J.C. & High, S. Post-translational integration of tail-anchored proteins is facilitated by defined molecular chaperones. *Journal of cell science* **120**, 1743-1751 (2007).

138. Plath, K. & Rapoport, T.A. Spontaneous release of cytosolic proteins from posttranslational substrates before their transport into the endoplasmic reticulum. *J Cell Biol* **151**, 167-178 (2000).

139. Zimmermann, R. The role of molecular chaperones in protein transport into the mammalian endoplasmic reticulum. *Biol Chem* **379**, 275-282 (1998).

140. Shimura, H.*, et al.* Familial Parkinson disease gene product, parkin, is a ubiquitin-protein ligase. *Nature genetics* **25**, 302-305 (2000).

141. Takahashi, R. & Imai, Y. Pael receptor, endoplasmic reticulum stress, and Parkinson's disease. *Journal of neurology* **250 Suppl 3**, III25-29 (2003).

142. Henn, I.H., Gostner, J.M., Lackner, P., Tatzelt, J. & Winklhofer, K.F. Pathogenic mutations inactivate parkin by distinct mechanisms. *Journal of neurochemistry* **92**, 114-122 (2005).

143. Safadi, S.S. & Shaw, G.S. A disease state mutation unfolds the parkin ubiquitin-like domain. *Biochemistry* **46**, 14162-14169 (2007).

144. Kubo, S.I.*, et al.* Parkin is associated with cellular vesicles. *Journal of neurochemistry* **78**, 42-54 (2001).

145. Jensen, L.D., Vinther-Jensen, T., Kahns, S., Sundbye, S. & Jensen, P.H. Cellular parkin mutants are soluble under non-stress conditions. *Neuroreport* **17**, 1205-1208 (2006).

146. Mayer, M.P. & Bukau, B. Hsp70 chaperones: cellular functions and molecular mechanism. *Cellular and molecular life sciences : CMLS* **62**, 670-684 (2005).

147. Bernales, S., McDonald, K.L. & Walter, P. Autophagy counterbalances endoplasmic reticulum expansion during the unfolded protein response. *PLoS biology* **4**, e423 (2006).

148. Noda, T. & Farquhar, M.G. A non-autophagic pathway for diversion of ER secretory proteins to lysosomes. *The Journal of cell biology* **119**, 85-97 (1992).

149. Umebayashi, K.*, et al.* Accumulation of misfolded protein aggregates leads to the formation of russell body-like dilated endoplasmic reticulum in yeast. *Yeast (Chichester, England)* **13**, 1009-1020 (1997).

150. Gatti, G., Podini, P. & Meldolesi, J. Overexpression of calsequestrin in L6 myoblasts: formation of endoplasmic reticulum subdomains and their evolution into discrete vacuoles where aggregates of the protein are specifically accumulated. *Molecular biology of the cell* **8**, 1789-1803 (1997).

151. Nishitoh, H.*, et al.* ASK1 is essential for endoplasmic reticulum stress-induced neuronal cell death triggered by expanded polyglutamine repeats. *Genes & development* **16**, 1345-1355 (2002).

152. Kouroku, Y.*, et al.* Polyglutamine aggregates stimulate ER stress signals and caspase-12 activation. *Human molecular genetics* **11**, 1505-1515 (2002).

153. Brodsky, J.L. Translocation of proteins across the endoplasmic reticulum membrane. *Int Rev Cytol* **178**, 277-328 (1998).

154. Kamhi-Nesher, S.*, et al.* A novel quality control compartment derived from the endoplasmic reticulum. *Mol Biol Cell* **12**, 1711-1723 (2001).

155. Ethen, C.M., Reilly, C., Feng, X., Olsen, T.W. & Ferrington, D.A. The proteome of central and peripheral retina with progression of age-related macular degeneration. *Invest Ophthalmol Vis Sci* **47**, 2280-2290 (2006).

156. Mayhew, T.M., Lucocq, J.M. & Griffiths, G. Relative labelling index: a novel stereological approach to test for non-random immunogold labelling of organelles and membranes on transmission electron microscopy thin sections. *J Microsc* **205**, 153-164 (2002).

157. Mayhew, T.M., Reith, A., Reith, A. & Mayhew, T.M. Practical ways to correct cytomembrane surface densities for the loss of membrane images that results from oblique sectioning. in *Stereology and morphometry in electron microscopy. Problems and solutions* (ed. Anonymous) 99-110 (Hemisphere, New York, 1988).

158. Mayhew, T.M. & Lucocq, J.M. Developments in cell biology for quantitative immunoelectron microscopy based on thin sections: a review. *Histochem Cell Biol* **130**, 299-313 (2008).